Project Report
EO-1-5

EO-1 Advanced Land Imager:

Dark Current and Noise Characterization and Anomalous Detectors

J.A. Mendenhall

Lincoln Laboratory
Massachusetts Institute of Technology
Lexington, Massachusetts

7 May 2001

Prepared for the National Aeronautics and Space Administration
under Air Force Contract F19628-00-C0002.

ABSTRACT

The dark current and noise characteristics of the Earth Observing-1 Advanced Land Imager measured during ground calibration at MIT Lincoln Laboratory are presented. Data were collected for the nominal focal plane operating temperature of 220 K as well as supplemental operating temperatures (215 and 225 K). Dark current baseline values are provided, and noise characterization includes the evaluation of white, coherent, low frequency, and high frequency components. Finally, anomalous detectors, characterized by unusual dark current, noise, gain, or cross-talk properties are investigated.

ACKNOWLEDGMENTS

The author wishes to thank Dr. Donald Lencioni, Dr. David Hearn, and Mr. Edward Wack of Lincoln Laboratory for valuable discussions and insights pertaining to dark current and noise analysis.

TABLE OF CONTENTS

LIST OF FIGURES

LIST OF FIGURES (Continued)

LIST OF FIGURES (Continued)

LIST OF TABLES

1 INTRODUCTION

This document provides a review of three key Advanced Land Imager (ALI) instrument [1–5] performance parameters: dark current, noise, and anomalous detectors. The dark current and noise of the ALI are closely coupled. The dark current defines the background level for each detector, and frame-to-frame fluctuations of this current is a major contributor to the noise of the instrument.* As a result, both the dark current and noise characterization of the ALI will be covered in Section 2 of this document. Results obtained while operating the focal plane at the nominal integration times (4.05 ms for multispectral bands and 1.35 ms for the panchromatic band) and at 215, 220, and 225 K will be provided. It should also be noted that all results are referenced to the 12-bit system the ALI employs.

This document also provides a review of anomalous detectors of the instrument in Section 3. These detectors have been selected based on unusual dark current and noise characteristics, as well as gain and cross-talk peculiarities. The behavior of anomalous detectors should be carefully considered when selecting targets of small spatial extent or scientifically assessing the quality of particular scenes.

* All SWIR detectors have a transient effect associated with the initial data collected following the focal plane turn-on. As a result, the first ten frames from all data sets have been excluded from dark current and noise analysis

2 DARK CURRENT AND NOISE CHARACTERIZATION

2.1 Dark Current

The ALI dark current is a measure of the background level of each detector. It is a combination of thermally excited electrons within the detector and the gain of the associated electronics. The dark current for each detector of every band has been calculated as the mean of 512 multispectral and 1536 panchromatic frames (2 seconds). The dark current levels calculated from data collected during calibration at MIT Lincoln Laboratory are provided in Figures 1-6. Dark current values depicted in Figures 1 and 2, Figures 3 and 4, and Figures 5 and 6 were obtained when the focal plane was maintained at 215 K, 220 K, and 225 K respectively. In all cases, expected detector to detector and Sensor Chip Assembly to Sensor Chip Assembly (SCA to SCA) variations are present. Five of the six ALI inoperable detectors, defined in Section 3, are clearly evident in the dark current data and are listed in Table 1. Nine ALI detectors have been identified as having excessive dark current (>1.25 times the mean dark current for that band and SCA) and are listed in Table 2. The observed large dark current offsets between odd and even detectors on SCA 4 band 2 and SCA 3 band 3 are the result of two 'leaky' detectors. Detector 1149 on band 2 and detector 864 on band 3 have significant cross-talk with neighboring odd and even detectors respectively. As a result, even under dark conditions, over 300 digital number (DN) units (out of 4096) of induced signal are present on the corrupted detectors. This effect is covered in more detail elsewhere [6]. Finally, bands 5p, 5, and 7 exhibit large increases in dark current centered on detector 1200. These regions of enhanced dark current, otherwise referred to as 'hot spots', are stable (Section 2.2.3) and repeatable (Section 2.3), and may be accounted for by using normal dark current subtraction techniques.

To investigate the effects of temperature on dark current generation, data collected when the focal plane was at 215 and 225 K have been subtracted from values obtained when the focal plane was at 220 K. These results are depicted in Figures 7-10. For the VNIR multispectral and panchromatic bands, definite clumping of dark current shifts is evident at the SCA level. Additionally, SCA 2 is most sensitive to temperature, with an average dark current change of > 4 DN. The SWIR bands are the most sensitive to the thermal environment and have up to 200 DN shifts per 5 K and the gradual dark current shift from detector 1 to detector 1280 for all three SWIR bands suggests a slight thermal gradient exists across the focal plane.

The mean and standard deviation of the dark current distributions have been defined as figures of merit (FOM). These FOM are used to compare ALI dark current values obtained from data sets collected during different operational scenarios or time periods (e.g., to track performance during various phases of integration and testing or throughout the EO-1 mission). Figures of merit have been calculated while the focal plane was held at 215, 220, and 225 K for each band and each SCA. Additionally, even and odd detectors are treated separately to isolate rows with largely differing dark current values. SCA 4 is divided into four sections for the SWIR bands (5p, 5, 7) in an effort to track dark current changes near the hot spot in this region of the focal plane. Finally, figures of merit for the Panchromatic band have been divided according to tri-read components and odd and even detectors. All baseline figures of merit values are provided in Table 3.

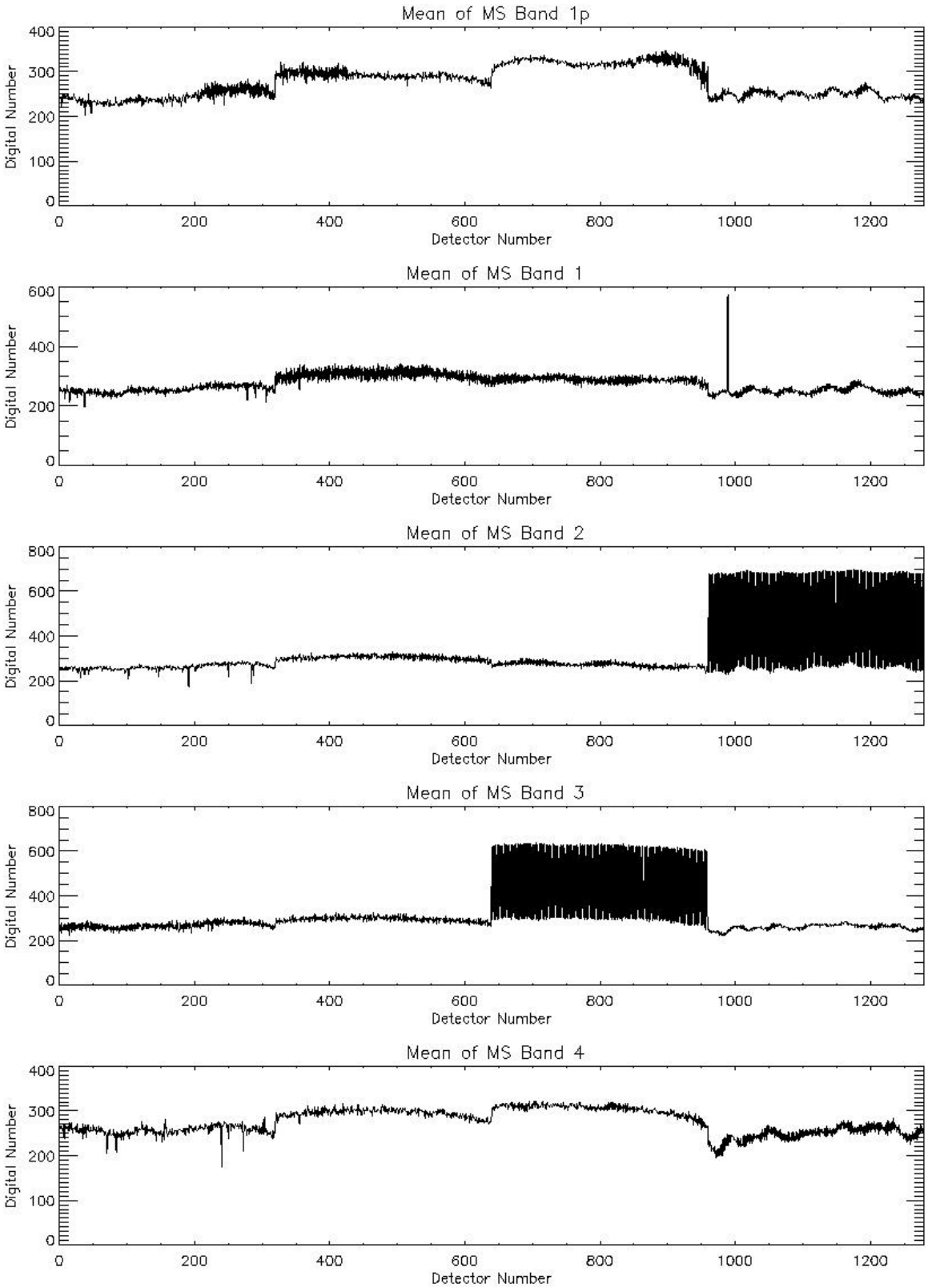

Figure 1: Band 1p, 1, 2, 3, 4 dark current values at 215 K.

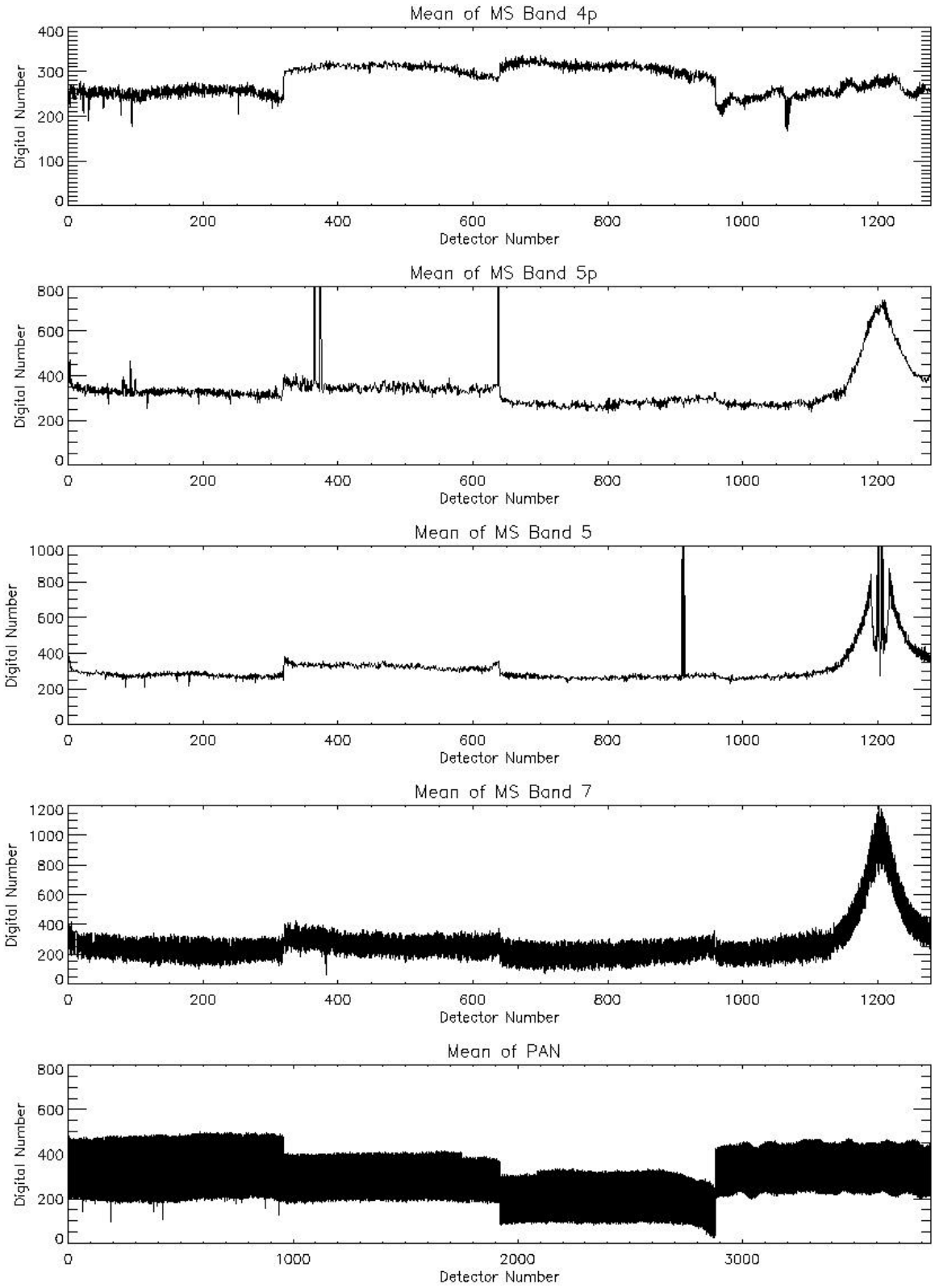

Figure 2: Band 4p, 5p, 5, 7 and pan band dark current values at 215 K.

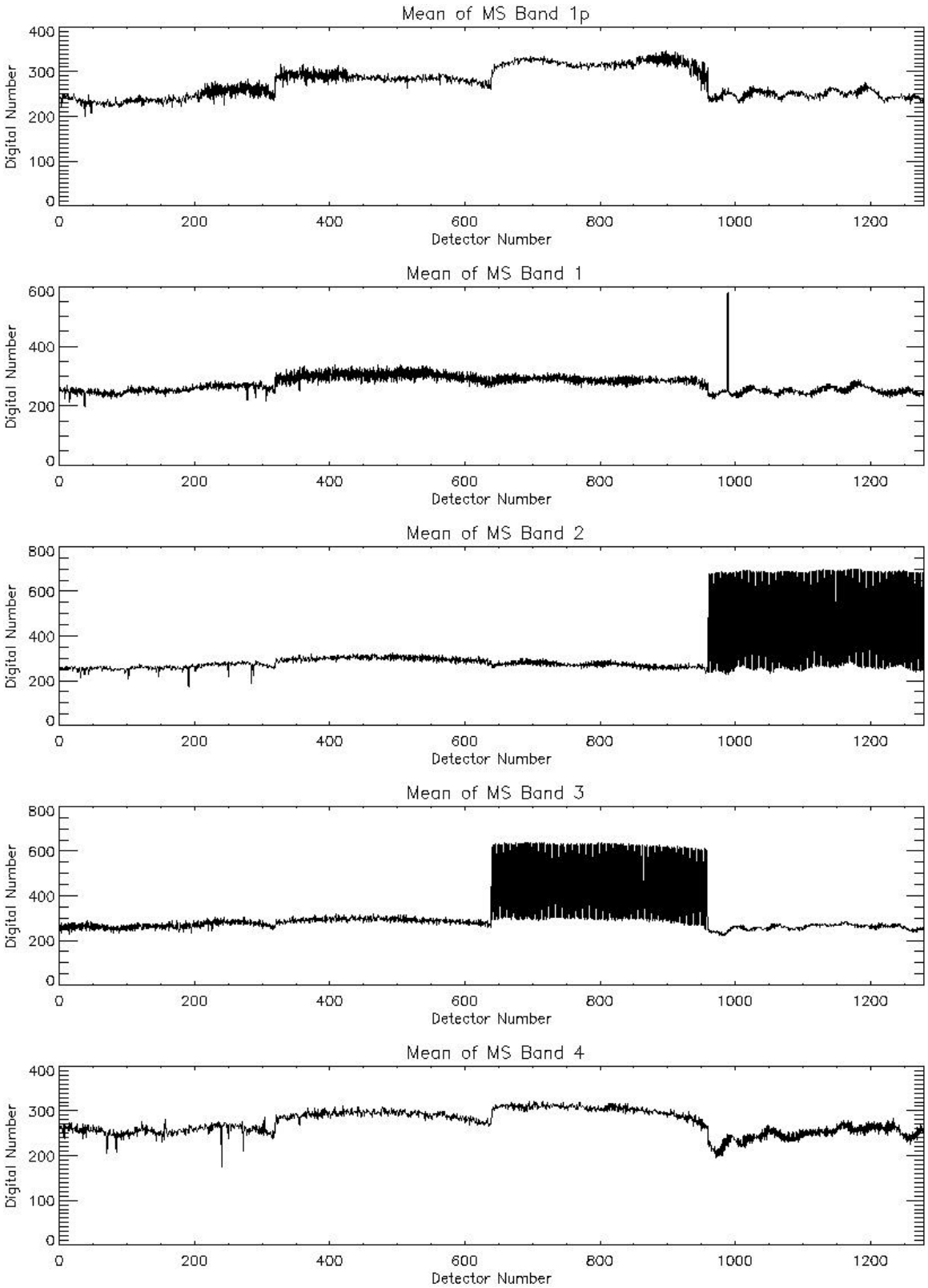

Figure 3: Band 1p, 1, 2, 3, 4 dark current values at 220 K.

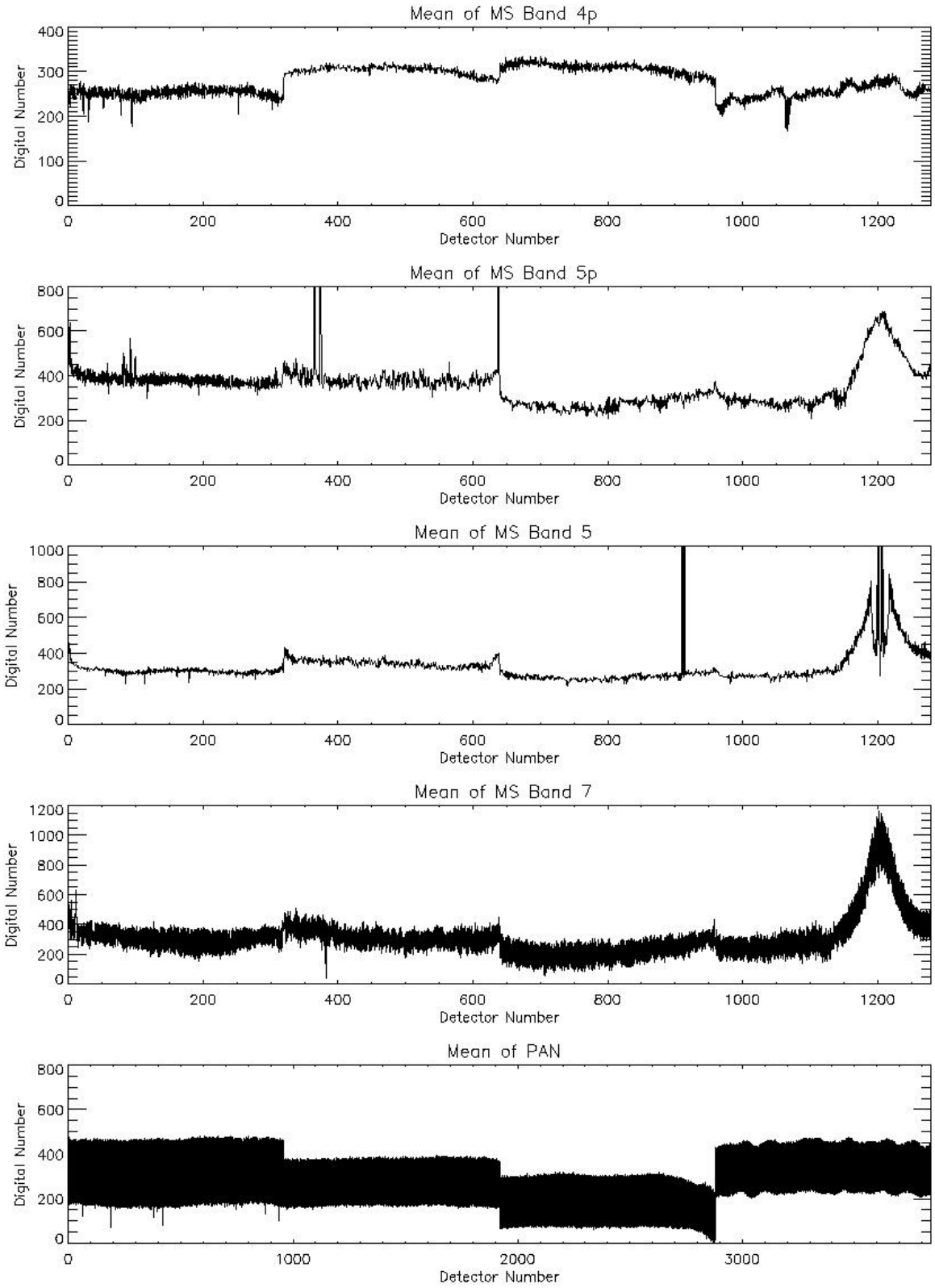

Figure 4: Band 4p, 5p, 5, 7 and pan band dark current values at 220 K.

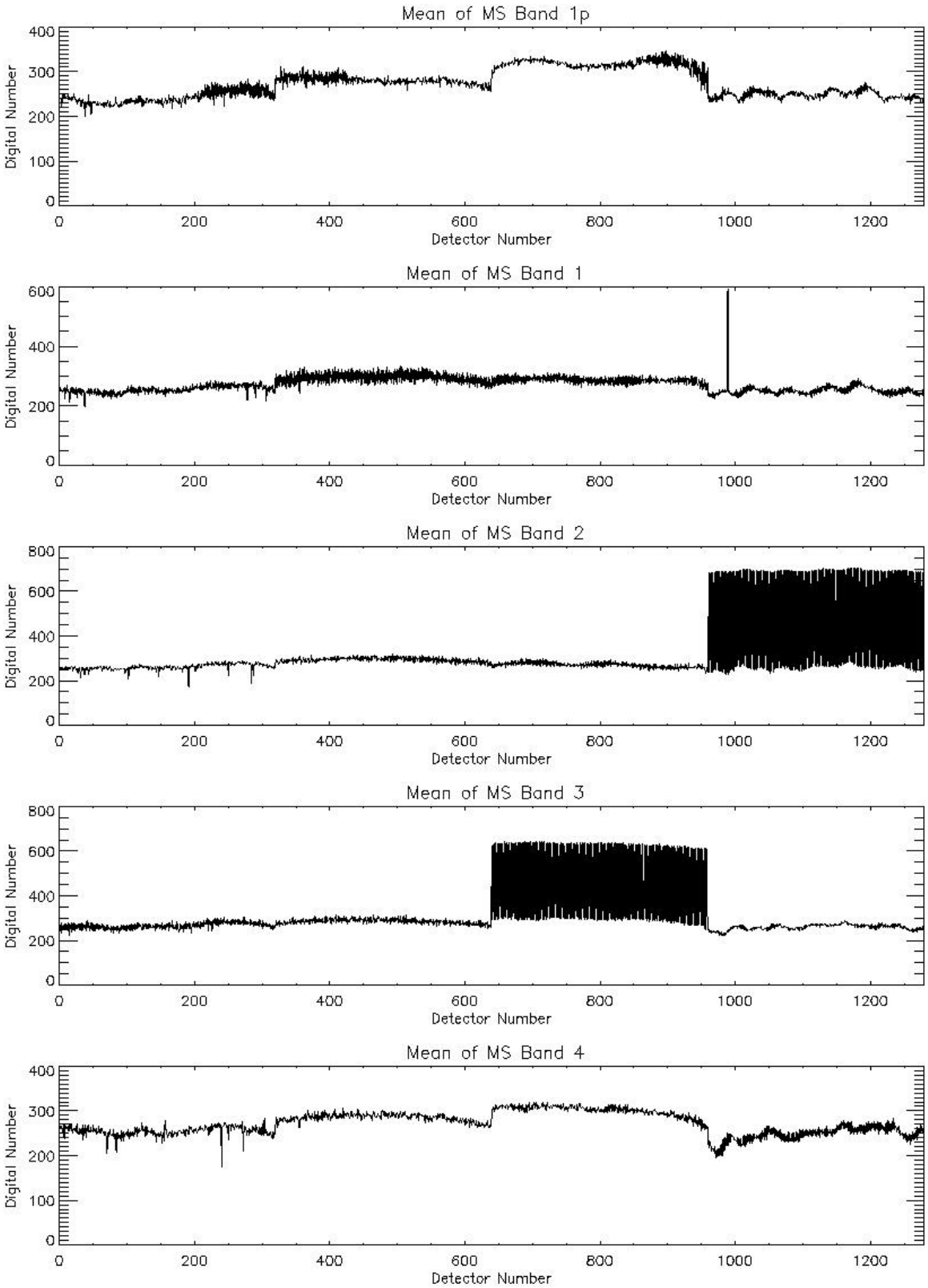

Figure 5: Band 1p, 1, 2, 3, 4 dark current values at 225 K.

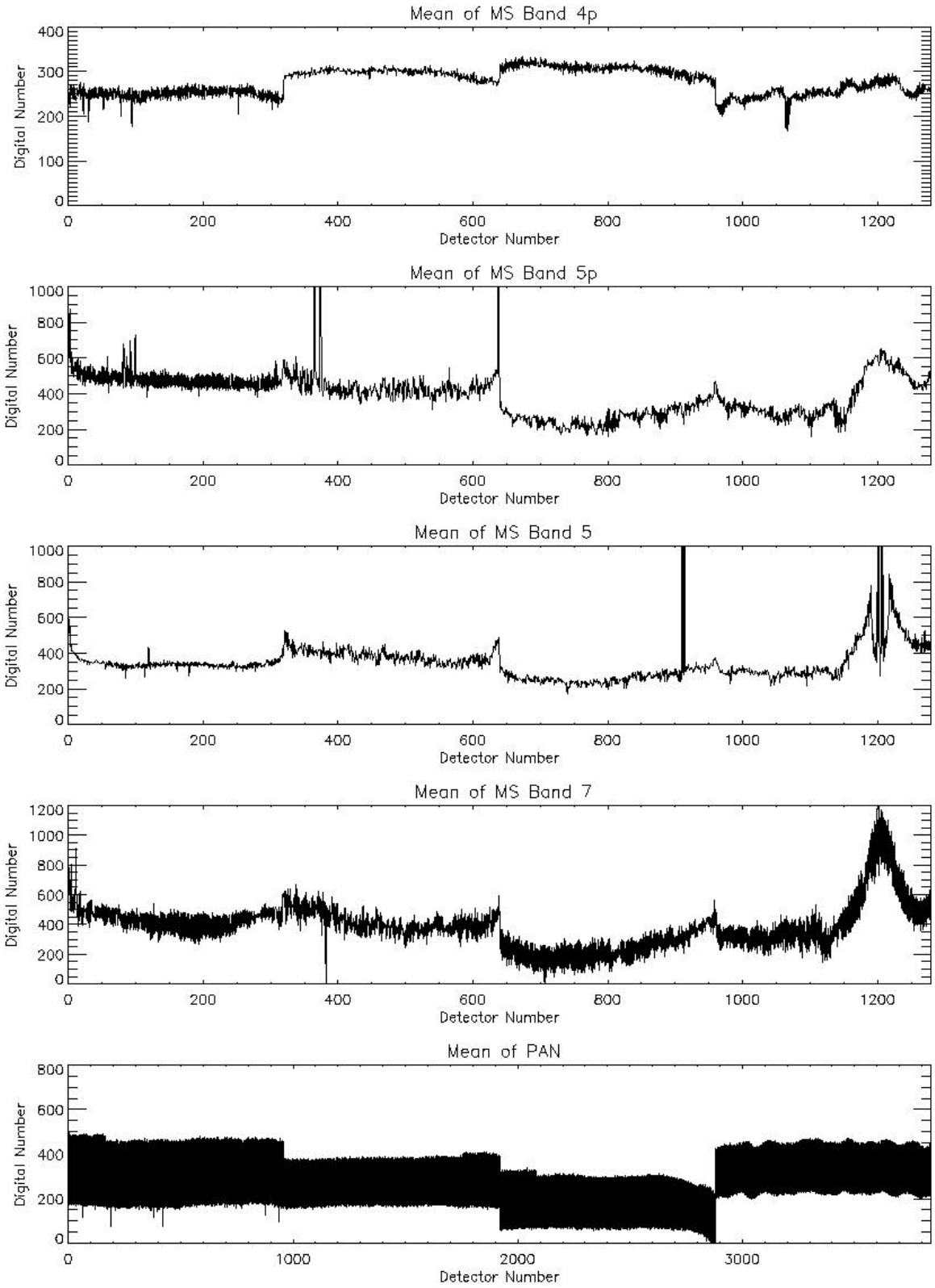

Figure 6: Band 4p, 5p, 5, 7 and pan band dark current values at 225 K.

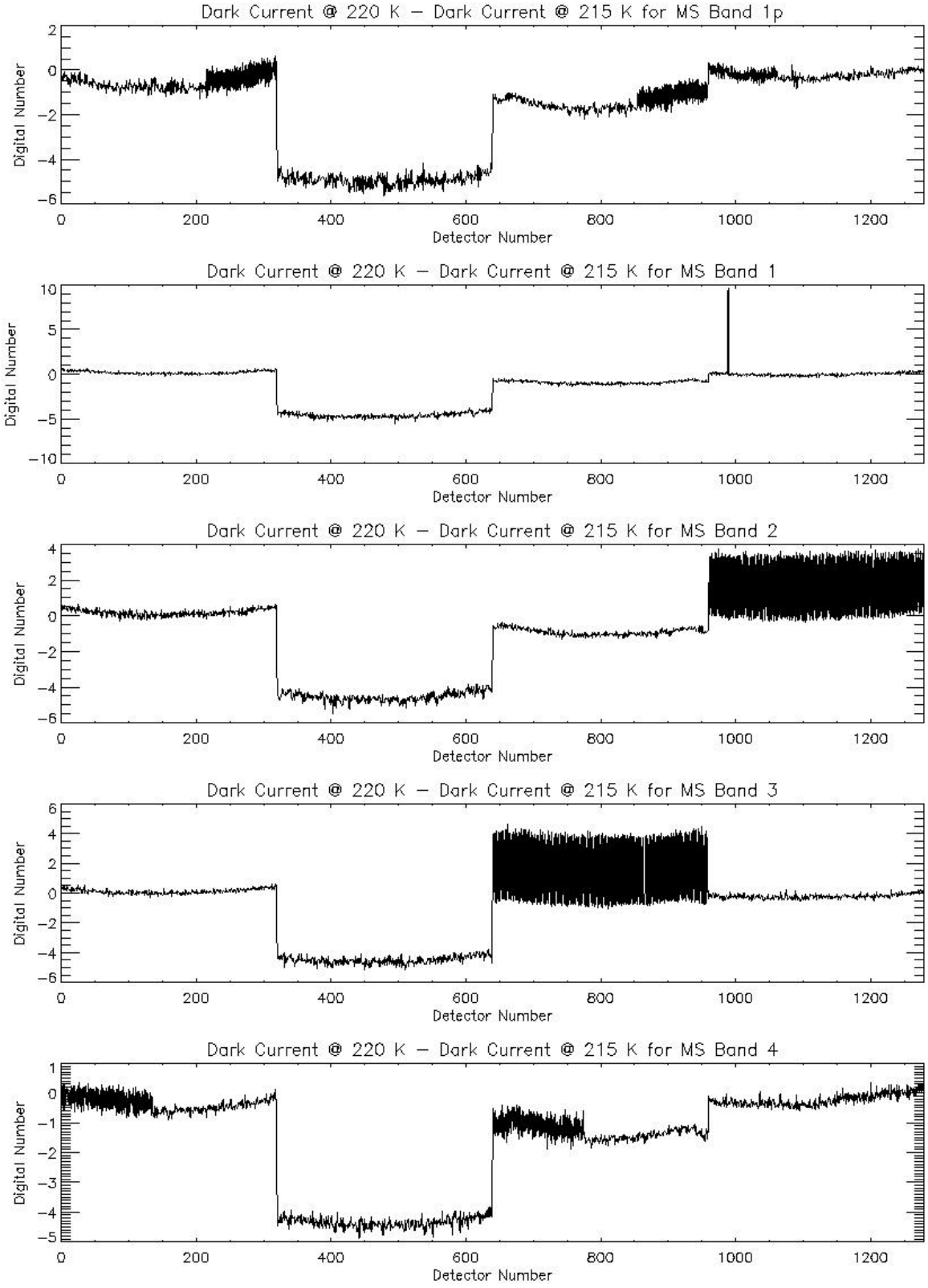

Figure 7: Band 1p, 1, 2, 3, 4 dark current differences between 220 K and 215 K.

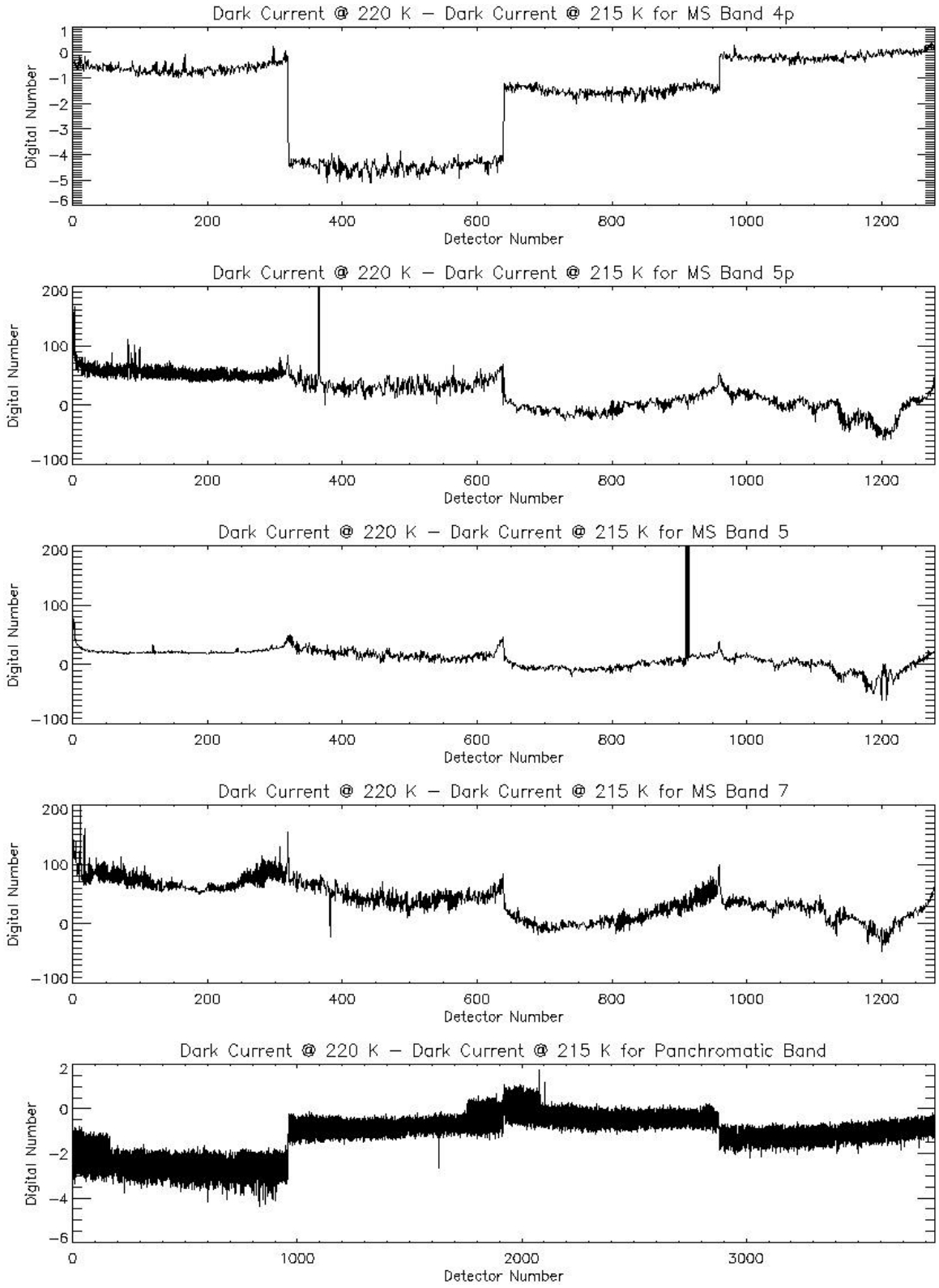

Figure 8: Band 4p, 5p, 5, 7 and pan band dark current differences between 220 K and 215 K.

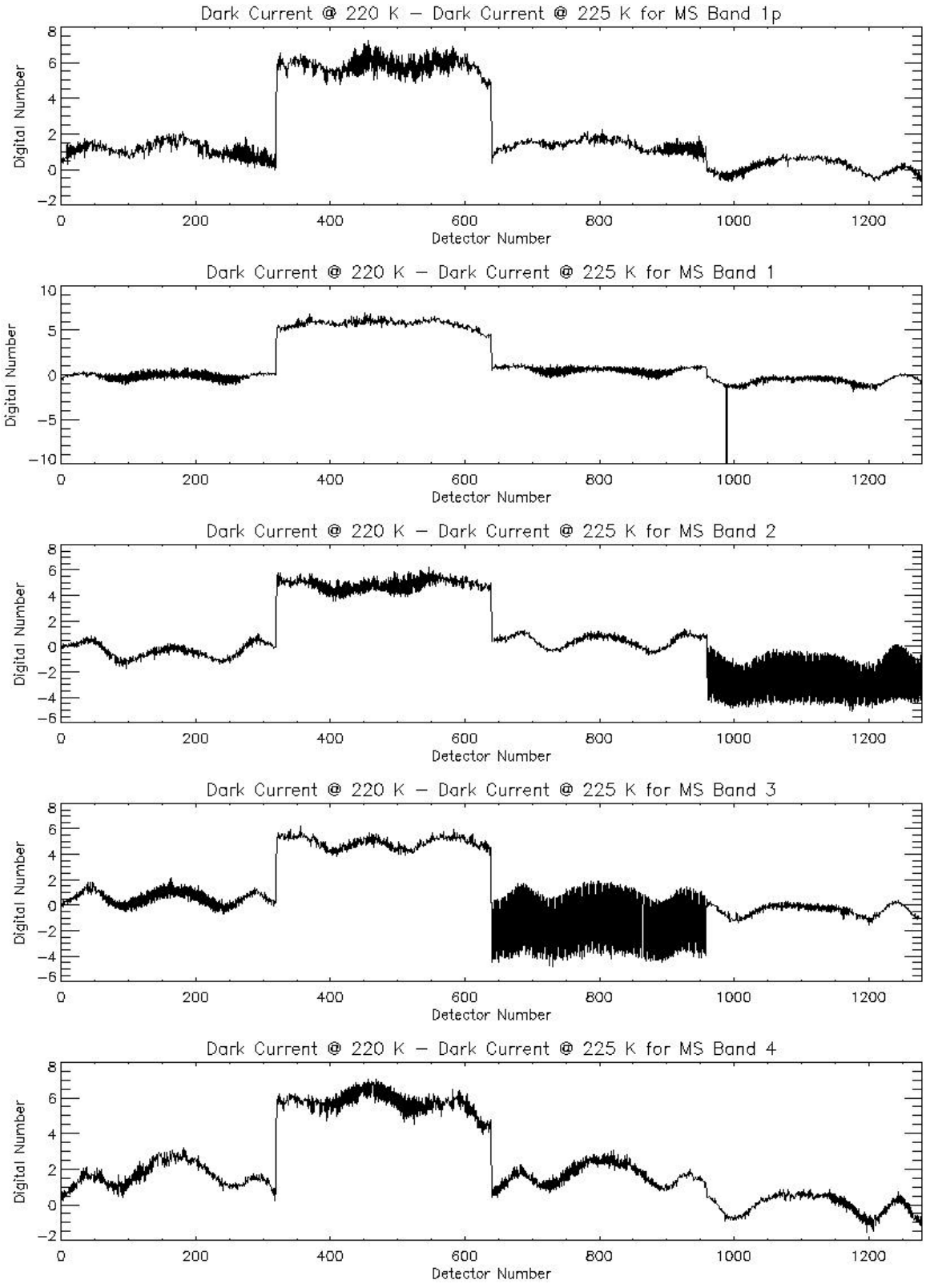

Figure 9: Band 1p, 1, 2, 3, 4 dark current differences between 220 K and 225 K.

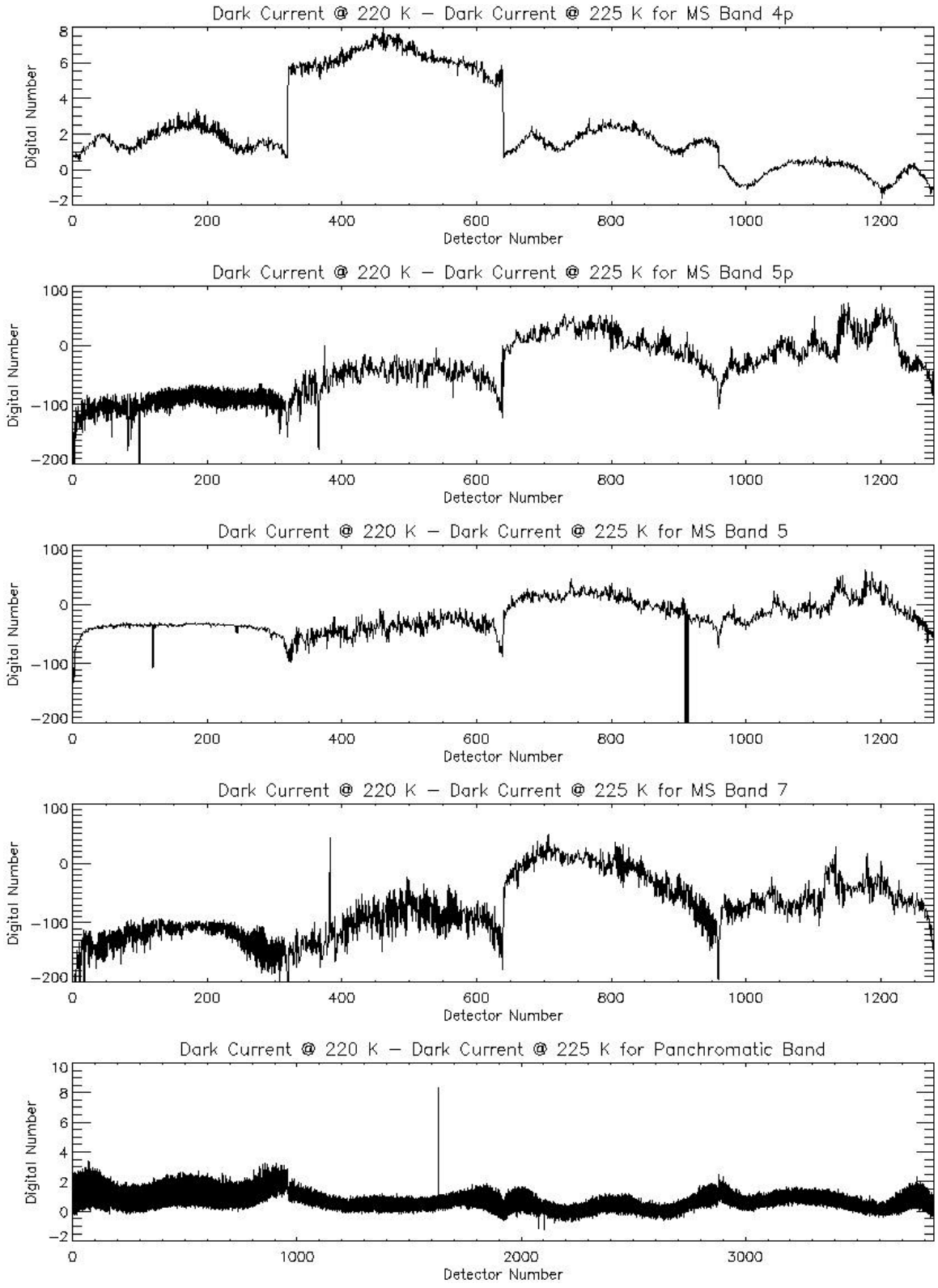

Figure 10: Band 4p, 5p, 5, 7 and pan band dark current differences between 220 K and 225 K.

Table 1: Inoperable Detectors with Marked Dark Current.

Band	Detector	Comment
5p	374	HOT
5p	638	HOT
5	1202	HOT
5	1204	HOT
5	1206	HOT

Table 2: Detectors with Marked Dark Current.

Band	Detector	Comment
1	989	--
5p	365	Excessive noise
5p	374	Excessive noise, Inoperable detector
5p	638	Excessive noise, Inoperable detector
5	911	Excessive noise
5	913	Excessive noise
5	1202	Excessive noise, Inoperable detector
5	1204	Inoperable detector
5	1206	Excessive noise, Inoperable detector

Table 3: Band and SCA Dark Current Baseline Figures of Merit

Band	SCA	T = 215 K		T = 220 K		T = 225 K	
		Mean (DN)	Standard Deviation (DN)	Mean (DN)	Standard Deviation (DN)	Mean (DN)	Standard Deviation (DN)
1P	1E	238.6	9.4	238.0	9.4	236.7	9.4
1P	1O	248.4	16.7	248.0	17.1	247.0	17.4
1P	2E	294.9	11.2	290.1	11.3	283.8	11.3
1P	2O	287.3	5.9	282.6	5.9	277.0	5.9
1P	3E	317.3	11.6	315.7	11.6	314.3	11.6
1P	3O	323.2	10.7	321.9	10.9	320.7	11.0
1P	4E	251.8	9.0	251.6	9.0	251.5	9.0
1P	4O	246.3	8.0	246.1	8.0	245.9	7.9
1	1E	248.1	10.8	248.2	10.8	248.0	10.8
1	1O	261.6	12.4	261.8	12.3	262.2	12.4
1	2E	322.6	10.4	318.2	10.3	312.5	10.0
1	2O	289.4	9.5	285.0	9.4	279.1	9.2
1	3E	278.6	7.1	277.7	7.1	276.9	7.1
1	3O	298.3	6.7	297.3	6.7	297.0	6.7
1	4E	257.1	10.8	257.0	10.8	257.9	11.0
1	4O	246.0	27.8	246.1	28.5	246.7	29.3
2	1E	259.3	13.1	259.5	13.1	260.0	13.1
2	1O	262.6	15.1	262.7	15.1	262.9	15.1
2	2E	296.4	8.6	292.0	8.5	287.4	8.7
2	2O	310.5	8.5	306.0	8.4	300.7	8.3

2	3E	264.6	7.8	263.6	7.8	263.3	7.6
2	3O	278.7	11.1	277.8	11.2	277.3	11.1
2	4E	257.4	11.4	257.4	11.4	258.1	11.5
2	4O	683.3	11.9	686.7	11.9	691.1	12.0
3	1E	256.7	11.5	256.9	11.5	256.6	11.6
3	1O	277.3	11.6	277.3	11.6	276.5	11.7
3	2E	287.9	8.9	283.8	8.8	278.6	8.8
3	2O	302.4	9.6	298.0	9.5	293.2	9.7
3	3E	621.4	15.0	625.2	15.2	629.1	15.5
3	3O	294.0	10.8	293.4	10.8	292.3	10.8
3	4E	261.8	12.2	261.6	12.2	261.8	12.2
3	4O	256.5	11.9	256.3	11.9	256.9	11.9
4	1E	258.9	13.0	258.6	13.0	257.2	13.1
4	1O	254.8	9.0	254.3	9.0	252.5	9.0
4	2E	296.7	9.4	292.5	9.3	286.3	9.0
4	2O	293.5	7.9	289.4	7.9	283.8	7.7
4	3E	301.1	12.4	299.9	12.6	298.5	12.7
4	3O	306.5	10.5	305.0	10.4	303.3	10.2
4	4E	255.6	14.9	255.3	14.9	255.3	14.9
4	4O	240.6	14.6	240.4	14.7	240.6	14.8
4P	1E	242.1	11.3	241.5	11.3	239.7	11.1
4P	1O	263.2	7.6	262.6	7.5	260.9	7.4
4P	2E	304.9	10.0	300.6	10.0	294.4	9.5
4P	2O	309.1	9.1	304.8	9.0	298.3	8.5
4P	3E	302.4	11.4	301.0	11.4	299.3	11.2
4P	3O	316.1	10.6	314.5	10.6	312.8	10.5
4P	4E	259.0	20.7	258.9	20.8	259.1	20.9
4P	4O	247.0	15.4	246.8	15.4	247.0	15.5
5P	1E	339.6	22.1	405.9	33.1	519.7	49.0
5P	1O	316.0	14.7	361.7	20.6	443.9	36.8
5P	2E	350.6	19.6	385.9	30.3	441.3	53.0
5P	2O	342.8	14.7	377.6	23.9	426.6	40.6
5P	3E	283.1	15.2	283.8	27.1	279.1	51.0
5P	3O	272.2	15.6	269.8	28.0	259.9	52.3
5P	4EQ1	267.4	11.7	282.7	20.8	311.4	39.5
5P	4EQ2	266.8	11.7	263.4	17.6	259.8	30.1
5P	4EQ3	430.0	143.5	403.8	134.5	372.5	133.2
5P	4EQ4	521.4	129.6	509.7	104.1	512.5	70.0
5P	4OQ1	278.6	8.8	301.1	17.3	341.3	33.6
5P	4OQ2	281.2	11.6	285.4	15.9	296.5	27.0
5P	4OQ3	439.5	122.1	426.5	112.7	418.6	108.2
5P	4OQ4	512.7	113.7	510.5	89.3	526.8	60.1
5	1E	284.8	14.0	307.7	19.7	348.1	31.1
5	1O	271.5	17.3	293.5	19.8	332.8	27.9
5	2E	328.1	14.7	347.9	22.9	393.3	39.2
5	2O	324.1	15.1	340.0	22.2	375.9	37.9
5	3E	261.4	8.0	261.2	14.6	258.0	30.0
5	3O	272.1	10.6	272.1	17.6	269.4	34.9
5	4EQ1	265.6	10.0	276.3	12.8	299.6	21.7
5	4EQ2	280.2	12.6	281.4	15.3	287.2	23.5
5	4EQ3	462.9	142.8	441.0	133.3	418.8	129.4
5	4EQ4	541.3	163.2	535.8	146.4	552.6	132.7
5	4OQ1	258.2	6.8	270.0	9.1	295.0	16.6

5	4OQ2	270.1	11.9	272.4	15.0	279.8	23.5
5	4OQ3	423.0	126.6	406.4	117.7	390.8	113.3
5	4OQ4	467.9	104.5	465.6	93.8	481.8	85.8
7	1E	317.1	20.5	382.3	30.4	494.2	49.4
7	1O	151.1	27.7	235.7	50.6	378.6	76.7
7	2E	187.3	26.6	242.3	39.6	358.7	66.1
7	2O	348.0	24.2	389.1	38.8	474.1	69.7
7	3E	293.1	14.6	300.1	29.4	308.6	59.8
7	3O	120.0	23.3	140.2	45.4	169.9	86.9
7	4EQ1	126.5	10.5	164.5	17.9	245.7	36.8
7	4EQ2	150.8	16.2	181.2	20.9	250.0	36.0
7	4EQ3	365.6	177.2	371.1	169.5	410.2	173.5
7	4EQ4	468.5	194.1	483.0	176.7	552.0	162.9
7	4OQ1	289.0	10.0	318.4	13.2	380.2	25.1
7	4OQ2	331.7	21.3	359.6	26.6	422.9	40.7
7	4OQ3	602.2	242.5	599.1	233.1	626.7	239.2
7	4OQ4	717.6	260.4	726.7	236.7	790.7	217.6
PAN	1ET1	463.9	7	465.7	7.1	463.5	6.9
PAN	1ET2	477.4	9.3	479.2	9.3	477	9.5
PAN	1ET3	463.8	11	465.3	11	464	10.9
PAN	1OT1	173.4	11.8	176.6	11.9	171.2	11.7
PAN	1OT2	194.2	12	197.2	11.9	191.8	12.2
PAN	1OT3	173.4	12	175.9	12	171.5	12
PAN	2ET1	171.2	5.6	172.4	5.6	170	5.8
PAN	2ET2	192.8	5.8	193.8	5.8	191.6	6.7
PAN	2ET3	170.8	5.8	171.5	5.8	169.9	6
PAN	2OT1	382	10.3	381.8	10.3	381.9	10.3
PAN	2OT2	396	10	396.2	9.9	395.6	10.4
PAN	2OT3	378.2	5.9	378.5	5.9	378	6.1
PAN	3ET1	295.9	16.4	295.8	16.4	296.1	16.6
PAN	3ET2	311.6	16.6	311.3	16.6	311.4	17
PAN	3ET3	295.9	20.5	295.4	20.4	296.2	20.5
PAN	3OT1	73.2	12.9	74	12.9	72.3	13.2
PAN	3OT2	91.2	13.1	91.9	13.1	90	13.6
PAN	3OT3	67.1	13.2	67.5	13.2	66.6	13.5
PAN	4ET1	224.7	9	226.3	9	223.7	9.2
PAN	4ET2	227.9	9	229.5	9	226.7	9.1
PAN	4ET3	222.5	9	224.5	9	221.3	9.2
PAN	4OT1	448	10.6	448.7	10.6	448.1	10.7
PAN	4OT2	450.7	10.7	451.4	10.7	450.5	10.7
PAN	4OT3	446.3	10.2	447.3	10.2	446.1	10.3

E = Even numbered detectors
O = Odd numbered detectors
Q1 = Detectors 959:1039
Q2 = Detectors 1040:1119
Q3 = Detectors 1120:1199
Q4 = Detectors 1200:1279
T1 = Tri-read #1
T2 = Tri-read #2
T3 = Tri-read #3

2.2 Noise

The overall noise of the ALI is a combination of random, coherent, and pseudo-random fluctuations (PRF) in a detector's dark current value. For a standard Earth scene, the effects of these noise sources will be varied. The random or white noise component will establish the overall noise floor on a detector-to-detector basis. Coherent or pick-up noise will manifest itself as recognizable rippling or patterns in an otherwise 'clean' image. Pseudo-random or drifting dark current could affect the quality of an image on a frame-by-frame (high frequency) basis and as a function of time (low frequency) during an observation. Each of these sources will be discussed, and their contributions noted.

2.2.1 Random Fluctuations

The random or white noise of the ALI has been calculated for each detector as the standard deviation of dark current data collected over 500 multispectral and 1500 panchromatic frames (~2 seconds). Results from these calculations are provided in Figures 11-16. Noise values depicted in Figures 11 and 12, Figures 13 and 14, and Figures 15 and 16 were obtained when the focal plane was maintained at 215 K, 220 K, and 225 K, respectively. The mean of white noise values is ≤ 1.2 DN for all bands and all sensor chip assemblies for all focal plane operating temperatures. Detectors with white noise values greater than three times the mean noise value for each sensor chip assembly or detectors with zero white noise, have been flagged as unusual. Fifteen ALI detectors have more than three times the average white noise values for all three focal plane operating temperatures and are listed in Table 4. All but one of these detectors are SWIR detectors and are associated with high dark current and/or high pseudo-random noise.

White noise values obtained when the focal plane was at 215 and 225 K have been subtracted from values obtained when the focal plane was at 220 K. These results are depicted in Figures 17-20. In all cases, the standard deviation of the differences is < 0.1 DN. This indicates very similar white noise characteristics of the focal plane when operating between 215 and 225 K.

The mean and standard deviation of the white noise data have been defined as figures of merit. The baseline figures of merit values are provided in Table 5.

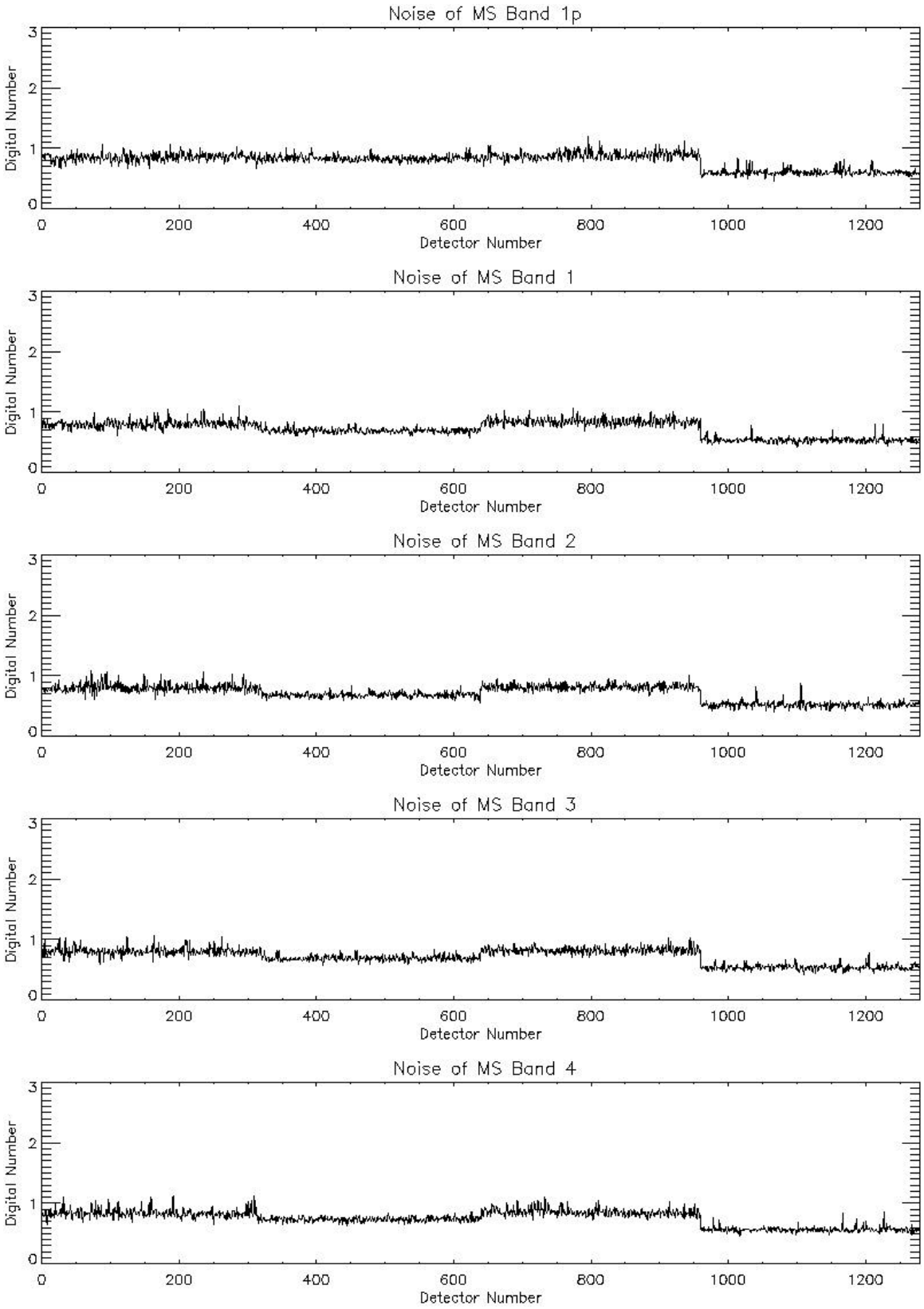

Figure 11: Band 1p, 1, 2, 3, 4 noise values at 215 K.

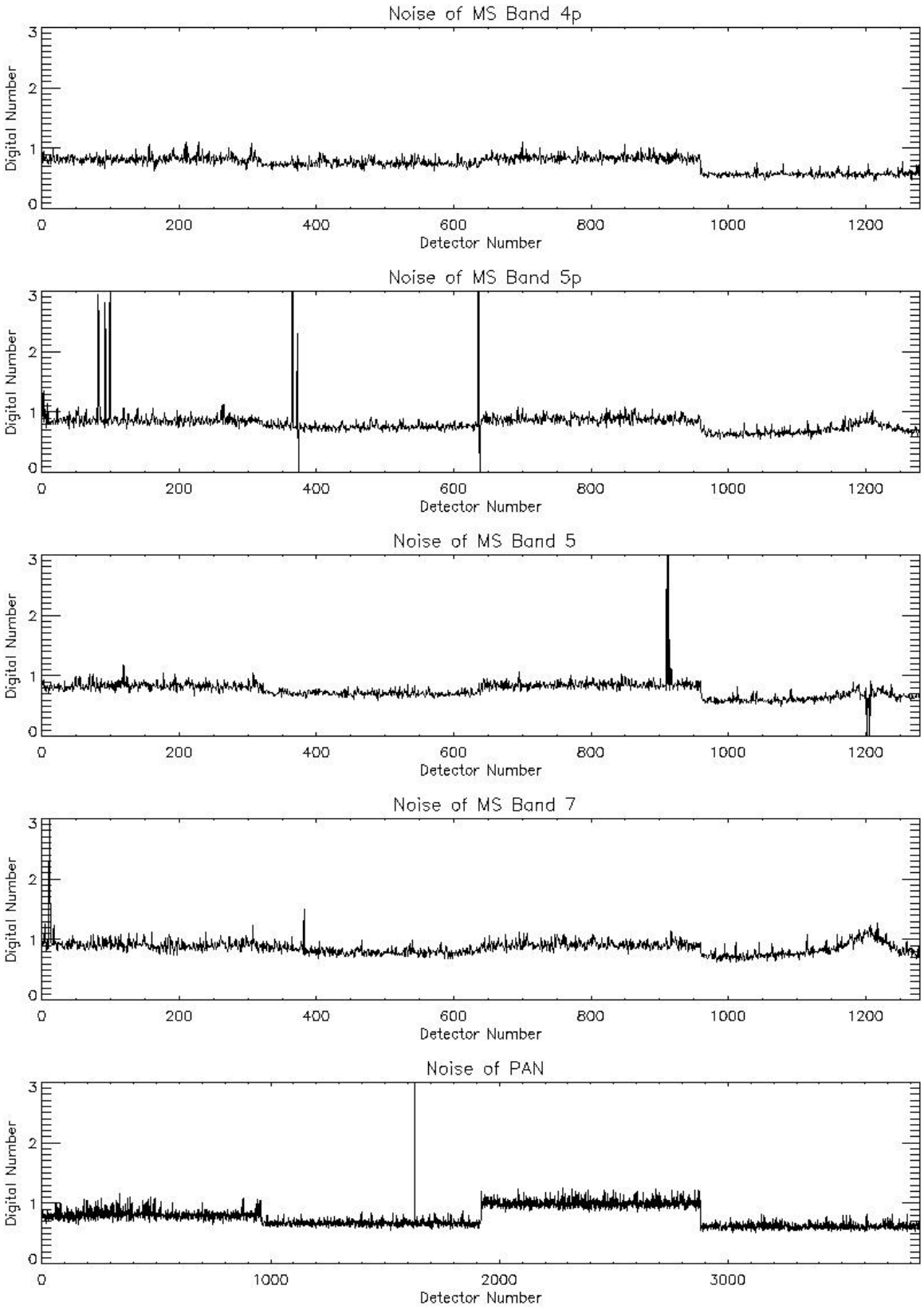

Figure 12: Band 4p, 5p, 5, 7 and pan band noise values at 215 K.

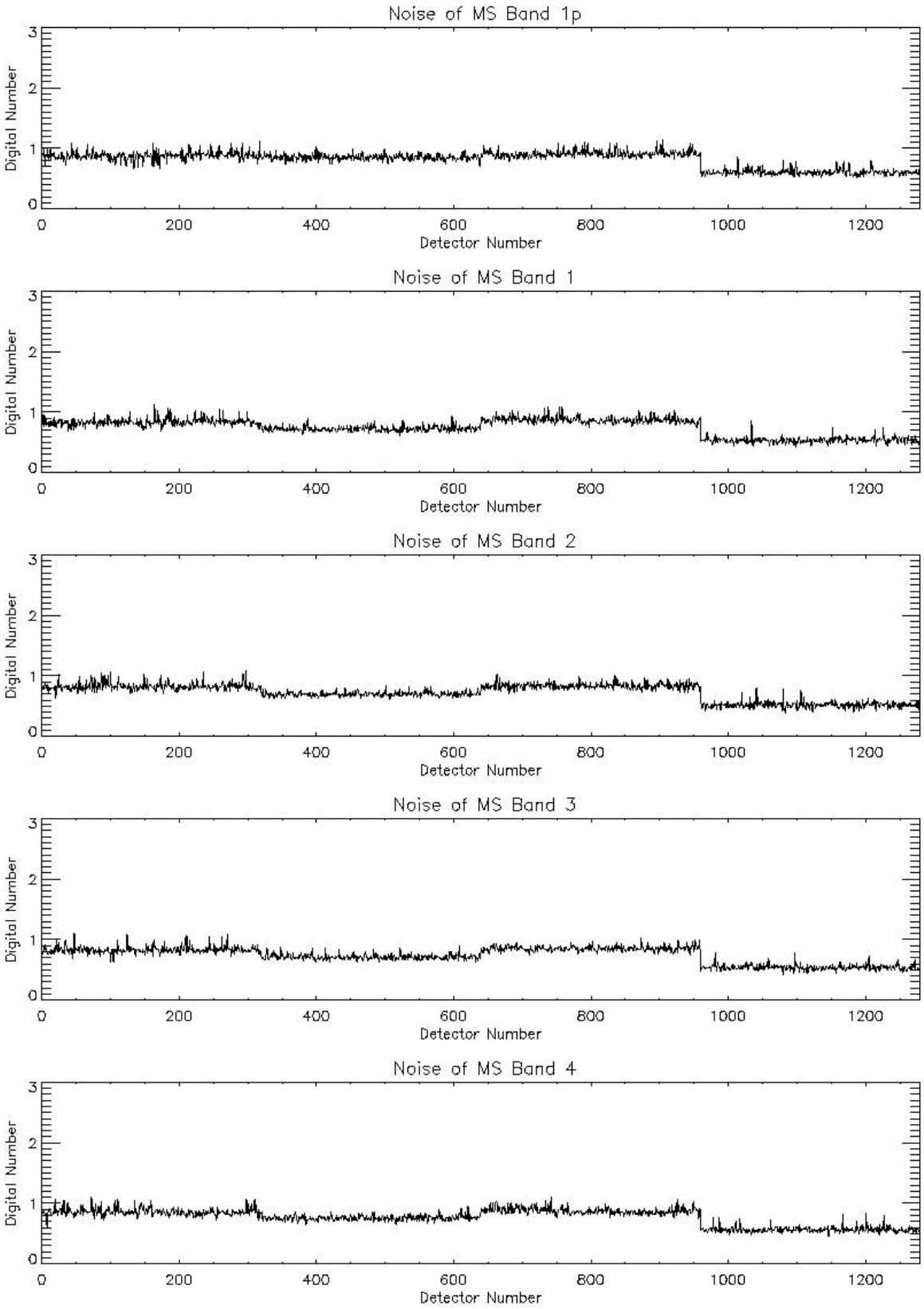

Figure 13: Band 1p, 1, 2, 3, 4 noise values at 220 K.

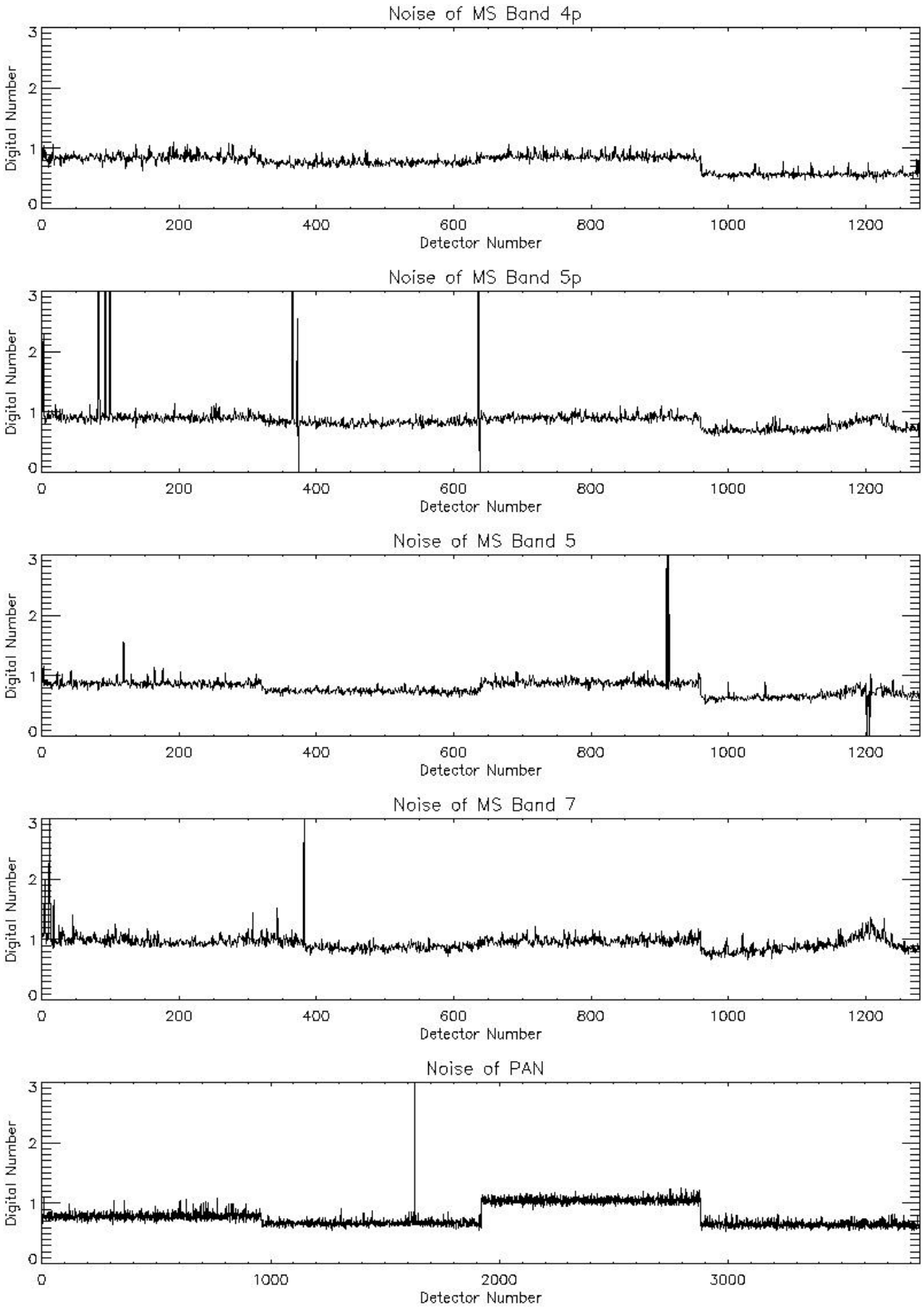

Figure 14: Band 4p, 5p, 5, 7 and pan band noise values at 220 K.

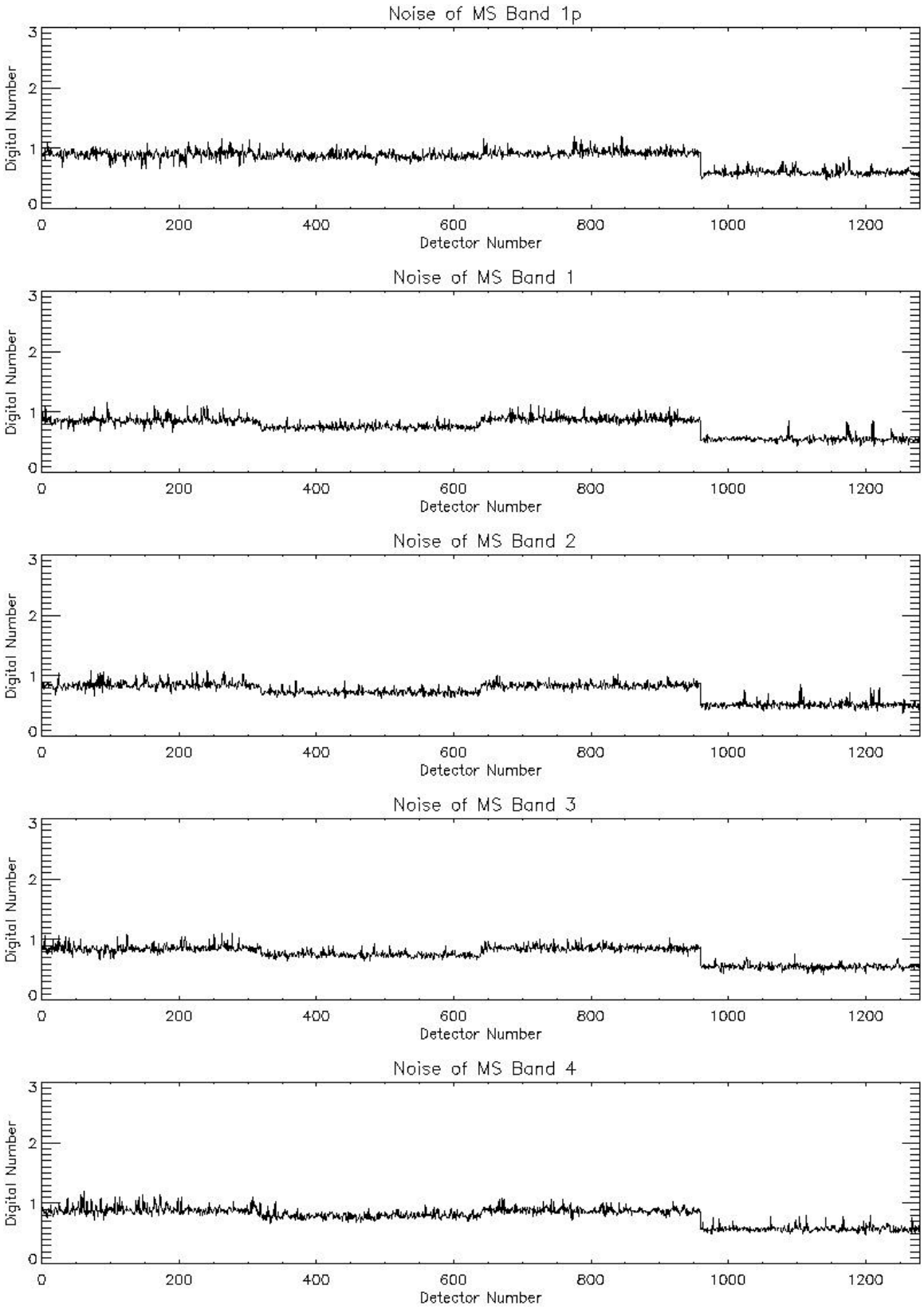

Figure 15: Band 1p, 1, 2, 3, 4 noise values at 225 K.

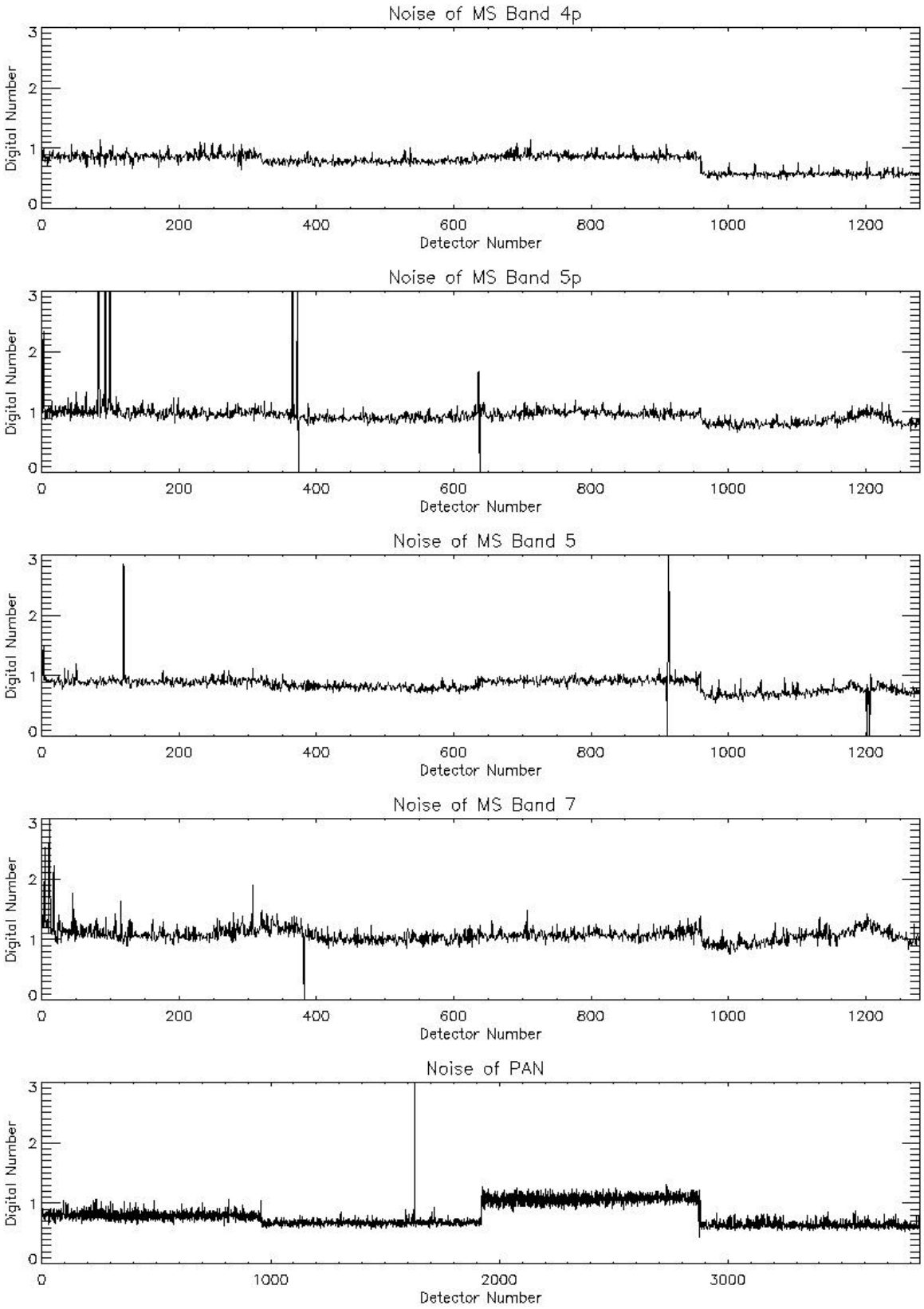

Figure 16: Band 4p, 5p, 5, 7 and pan band noise values at 225 K.

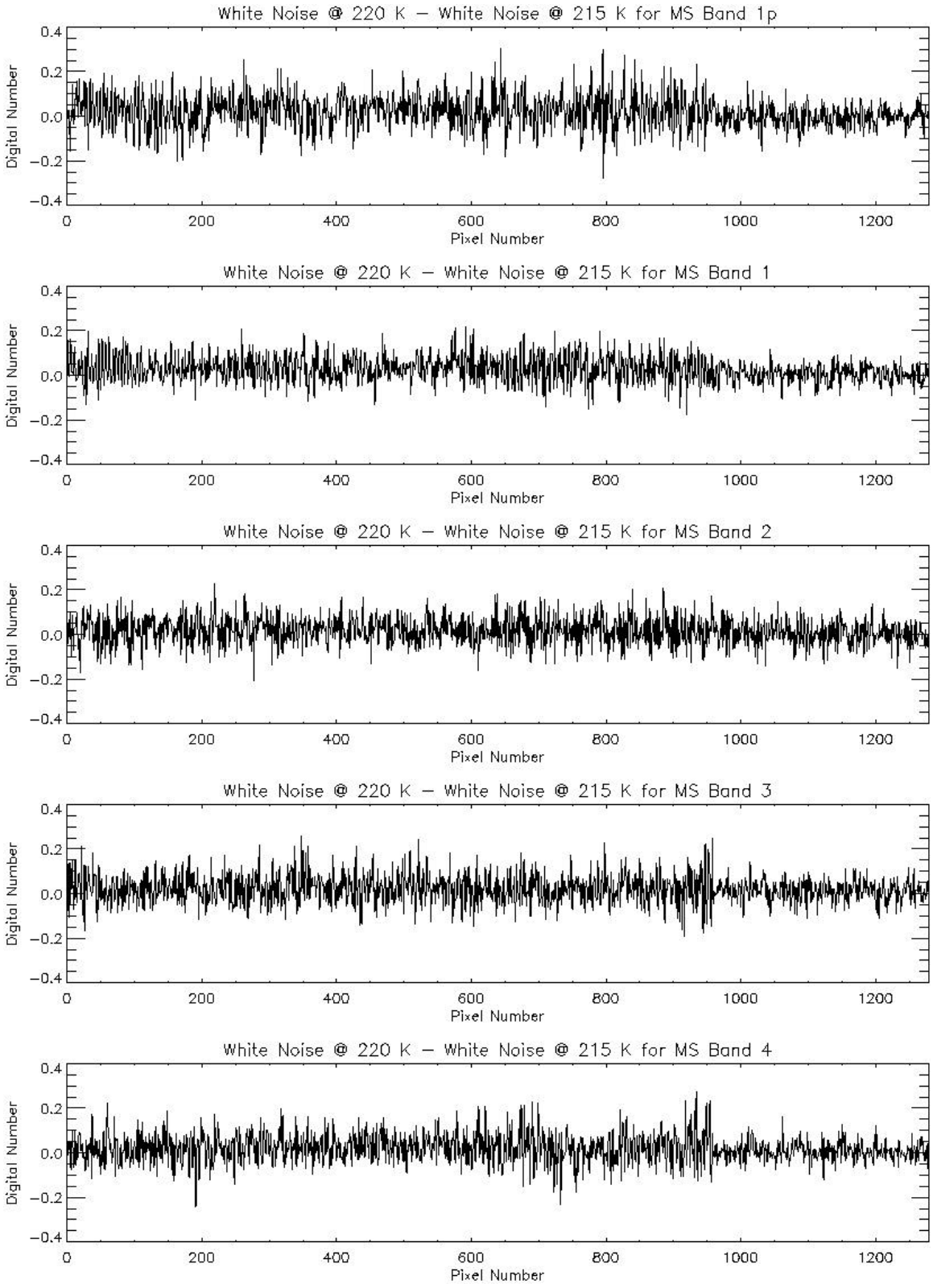

Figure 17: Detector noise differences for bands 1p, 1, 2, 3, 4 between 220 K and 215 K.

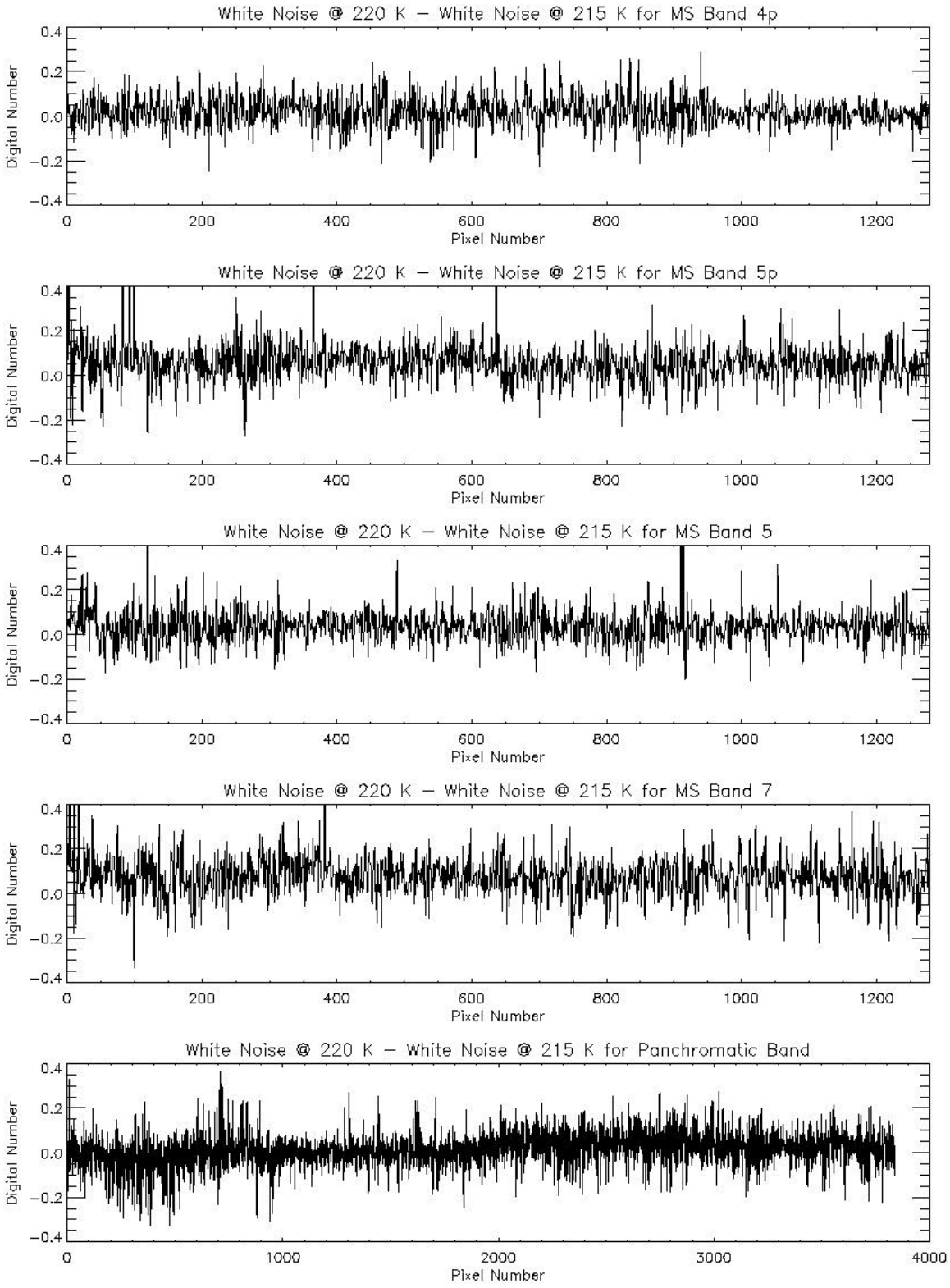

Figure 18: Detector noise differences for bands 4p, 5p, 5, 7 and pan bands between 220 K and 215 K.

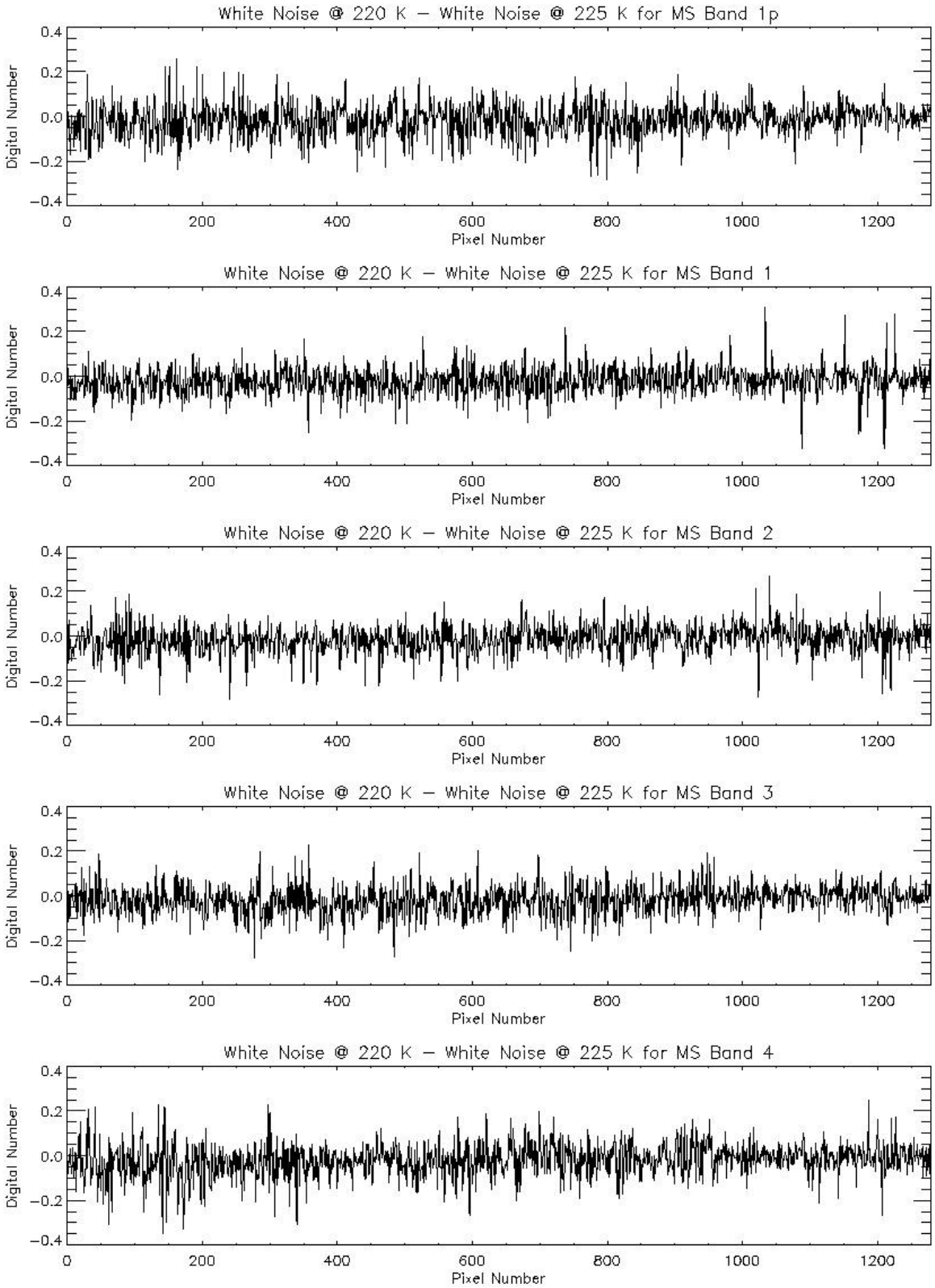

Figure 19: Detector noise differences for bands 1p, 1, 2, 3, 4 between 220 K and 225 K.

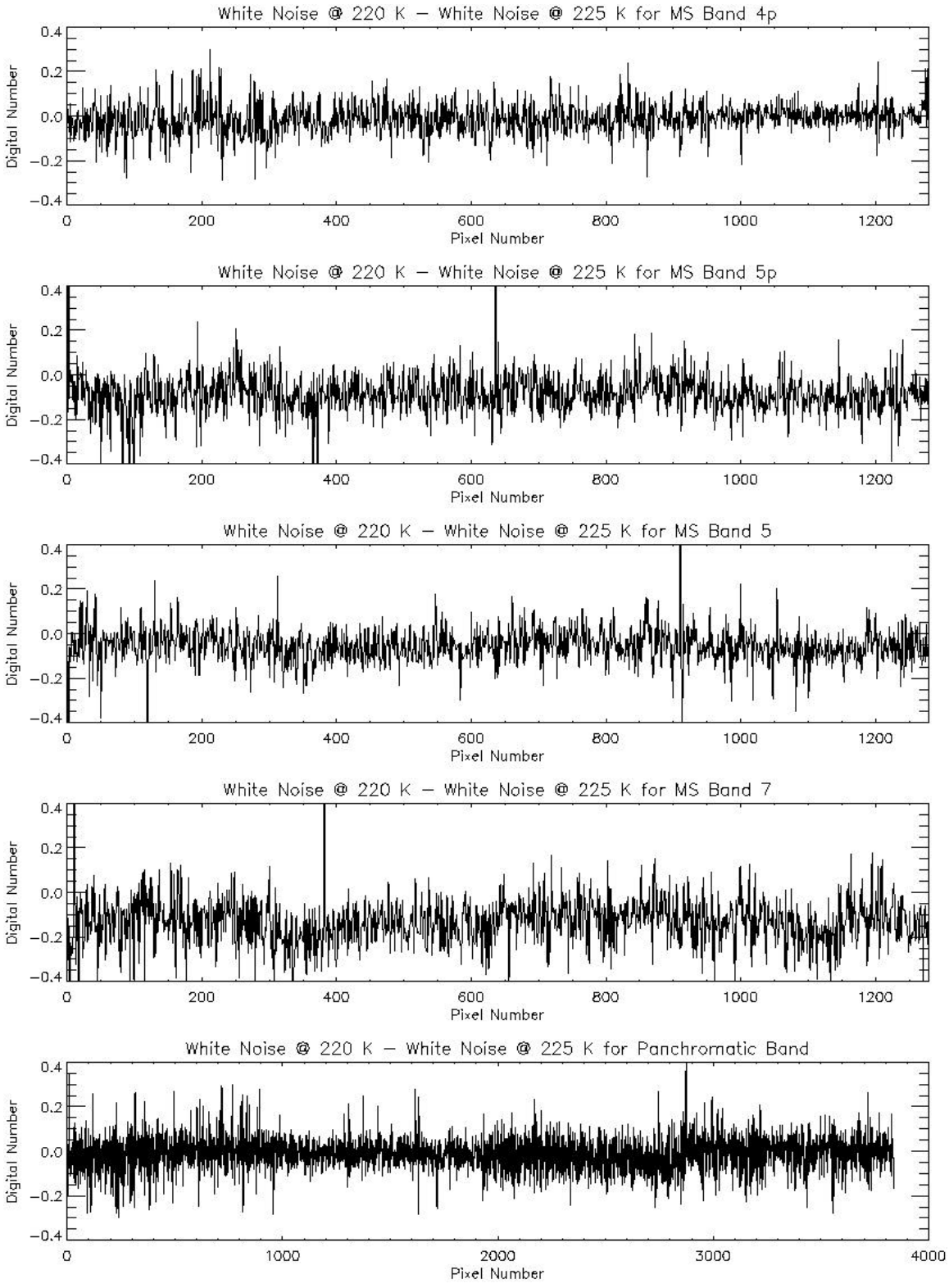

Figure 20: Detector noise differences for bands 4p, 5p, 5, 7 and pan band between 220 K and 225 K.

Table 4: Detectors with Marked Random or White Noise

Band	Detector	Comment
5p	82	--
5p	92	--
5p	99	--
5p	365	Excess dark current
5p	372	--
5p	374	Excess dark current , Inoperable
5p	636	Noise value <3x mean with FPA @ 225 K
5p	638	Excess dark current, Inoperable
5	911	Excess dark current
5	913	Excess dark current
5	1202	Excess dark current , Inoperable
5	1206	Excess dark current , Inoperable
7	11	--
7	382	--
Pan	1631	--

Table 5: Band and SCA White Noise Baseline Figures of Merit

Band	Sensor Chip Assembly	Mean (DN)	Standard Deviation (DN)
1p	1	0.88	0.07
1p	2	0.86	0.05
1p	3	0.91	0.06
1p	4	0.60	0.05
1	1	0.83	0.07
1	2	0.73	0.04
1	3	0.87	0.06
1	4	0.54	0.05
2	1	0.82	0.07
2	2	0.70	0.04
2	3	0.84	0.05
2	4	0.53	0.05
3	1	0.83	0.07
3	2	0.72	0.05
3	3	0.85	0.05
3	4	0.55	0.05
4	1	0.86	0.07
4	2	0.77	0.04
4	3	0.88	0.06
4	4	0.57	0.05
4p	1	0.85	0.07
4p	2	0.78	0.05
4p	3	0.87	0.06
4p	4	0.58	0.05
5p	1	0.92	0.06

5p	2	0.83	0.05
5p	3	0.92	0.05
5p	4	0.75	0.08
5	1	0.87	0.06
5	2	0.75	0.04
5	3	0.89	0.05
5	4	0.67	0.07
7	1	0.99	0.08
7	2	0.90	0.08
7	3	0.98	0.07
7	4	0.90	0.12
Pan	1	0.80	0.05
Pan	2	0.67	0.03
Pan	3	1.05	0.04
Pan	4	0.64	0.04

2.2.2 Coherent Fluctuations

Coherent noise is often identified as recognizable patterns in reconstructed dark current images or images of scenes with little spatial fluctuation. This type of noise may be introduced by 'pick-up' of external motor or equipment noise near sensitive electronics and may be most effectively avoided through proper instrument grounding and shielding.

The contribution that coherent noise makes to the overall noise of the instrument has been quantified using Fourier analysis. Initially, the mean dark current is calculated for each detector during a 226-frame period. A five-second dark image is then 'flattened' by subtracting the mean dark levels of each detector from each frame. This will remove any detector-to-detector dark current variations, while preserving any coherent noise in the data. Once the image is flattened, a two-dimensional Fourier transform is then performed and the magnitudes in both cycles/detector and cycles/second are plotted.

Examples of a flattened Band 1p image and its corresponding Fourier transform magnitude image are provided in Figures 21 and 22, respectively. The flattened image has been scaled to the ± 2 DN levels in order to magnify any obvious coherent noise. The contribution of each coherent component identified in the magnitude image to the overall image noise has been calculated as the integrated power density of a given component divided by the integrated power density of the entire image. This may be expressed analytically as

$$P_{i,b} = \frac{\sqrt{\int_{r1}^{r2}\int_{c1}^{c2} M_b^2 \, drdc}}{\sqrt{\int\int M_b^2 \, drdc}}$$

Here, $P_{i,b}$ is percent of the noise contributed by component i of Band b, M is the magnitude image of Band b, and $r1$, $r2$, $c1$ and $c2$ are the integration limits for the component in question. The noise contribution of this component in digital numbers may be calculated as the product of the standard deviation of the image (N) and the percent contribution of the component ($P_{i,b}$) or $N_{i,b} = P_{i,b} * N$. Finally, the combined effect of all coherent contributions to the noise of an image may be obtained by summing the contributions of individual components ($N_{i,b}$) in quadrature. Applying these calculations to the Band 1p image, a peak contribution of 19.3% or 0.16 DN to the overall noise of the image and a combined coherent noise effect of 49% is obtained. Although these contributions appear large, each component is spread over 10-30 cycles/second, and the combination of several components at differing frequencies results in images with no recognizable coherent patterns.

To demonstrate the effects of a known coherent source, a sine wave with a one-half digital number amplitude and 63 pixel period was added to the Band 1p dark image, and the Fourier analysis repeated. The 'noisy' flattened image and corresponding Fourier magnitude image are provided in Figures 23 and 24, respectively. Two clear enhancements are correctly noted on the magnitude image at 0.016 cycles/detector and 3.59 cycles/second. These enhancements correspond to a 27.5% or 0.25 DN contribution to the overall noise of the image. Furthermore, this component is highly concentrated in the frequency domain, resulting in the obvious coherent pattern in the image.

Following the analysis outlined above, magnitude images for Bands 1-7 and the Panchromatic Band are provided in Figures 25-33. The upper limits of coherent noise contributions are listed in Table 6. Approximately 50% of the noise for all bands may be accounted for by coherent noise. However, these contributions are made of numerous broad–frequency components, resulting in no recognizable patterns for any of the flattened dark images.

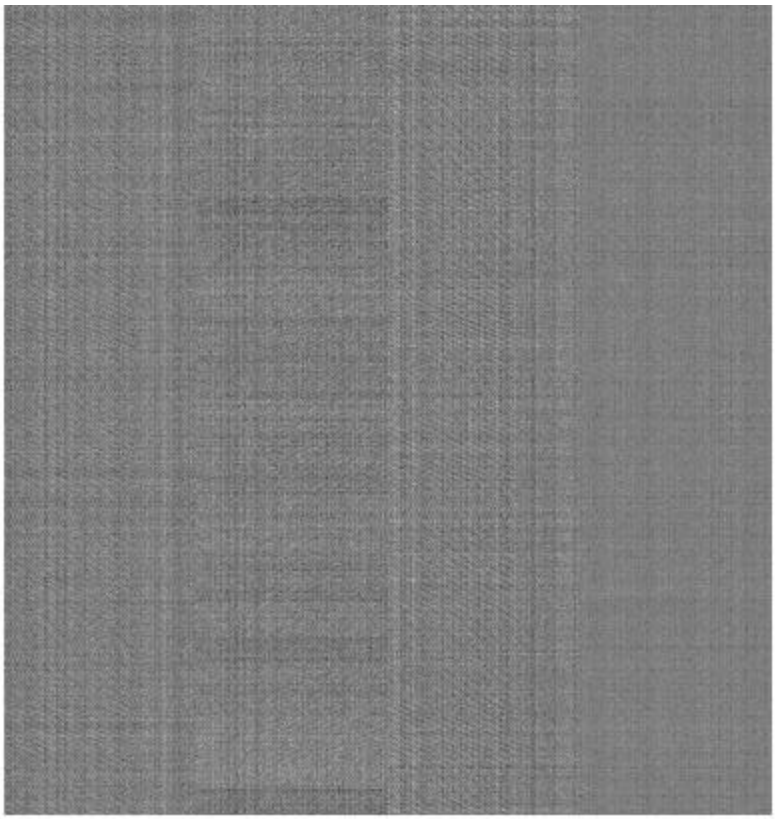

Figure 21: Band 1p flattened dark image.

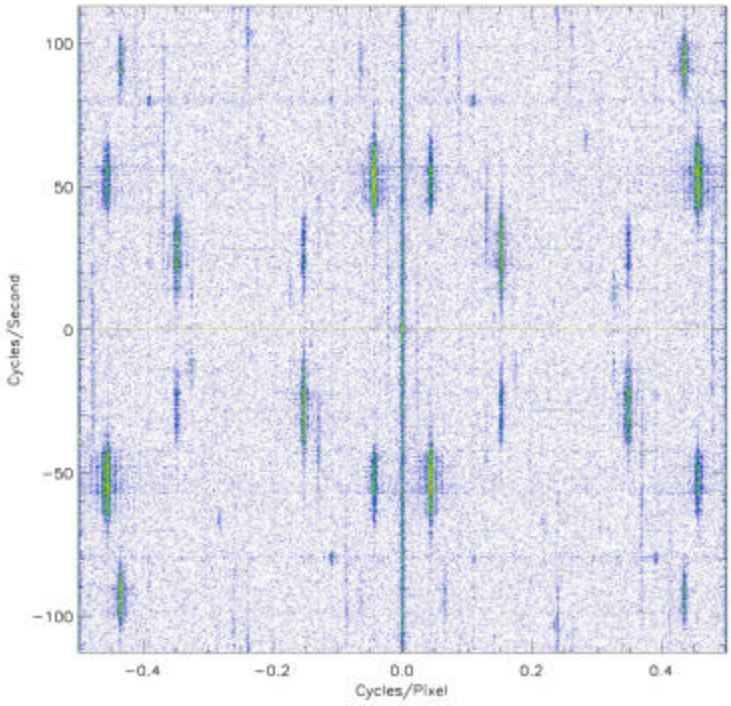

Figure 22: Fourier transform of a Band 1p flat field.

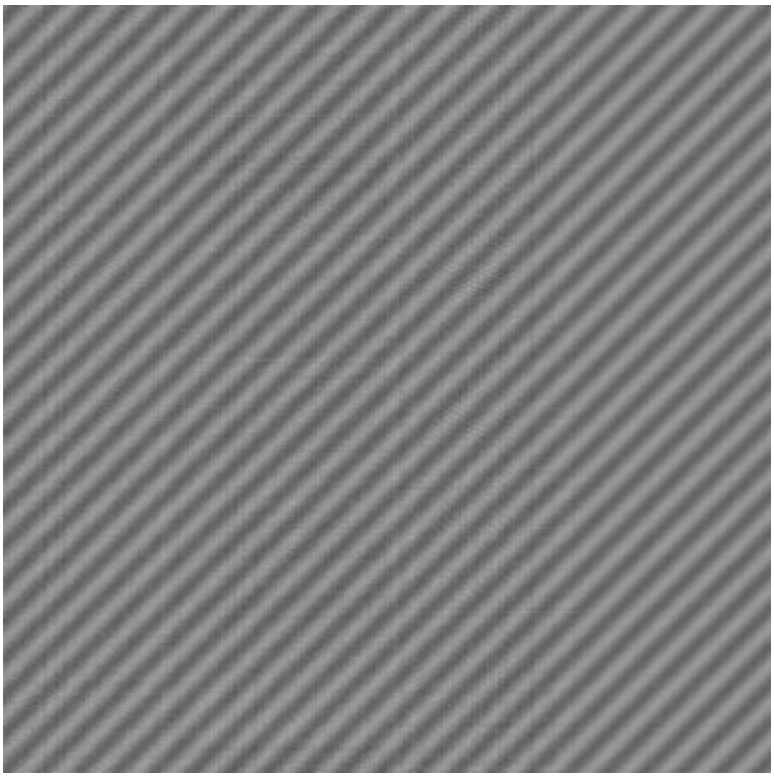

Figure 23: Band 1p flattened dark image after a one-half DN sine wave was added.

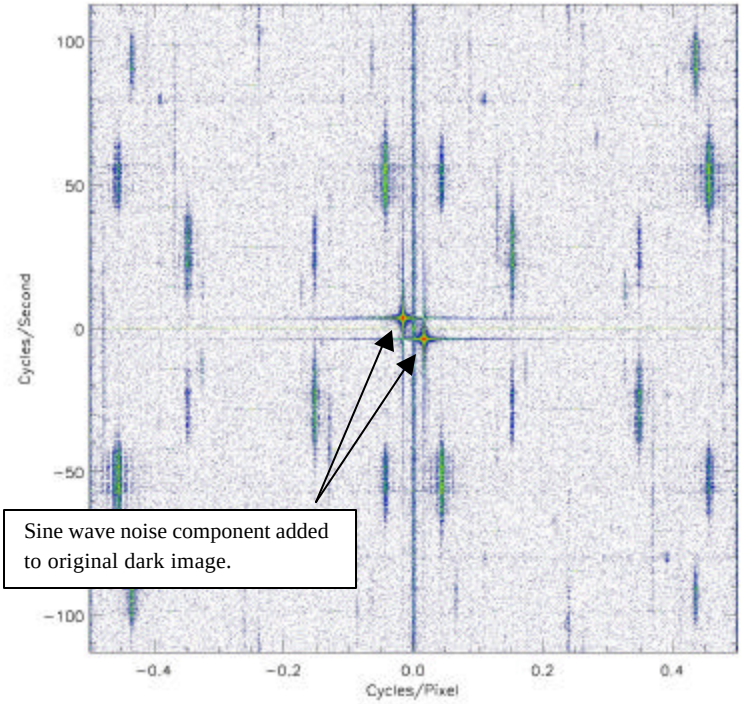

Figure 24: Fourier transform of a Band 1p flat field after a one-half DN sine wave was added.

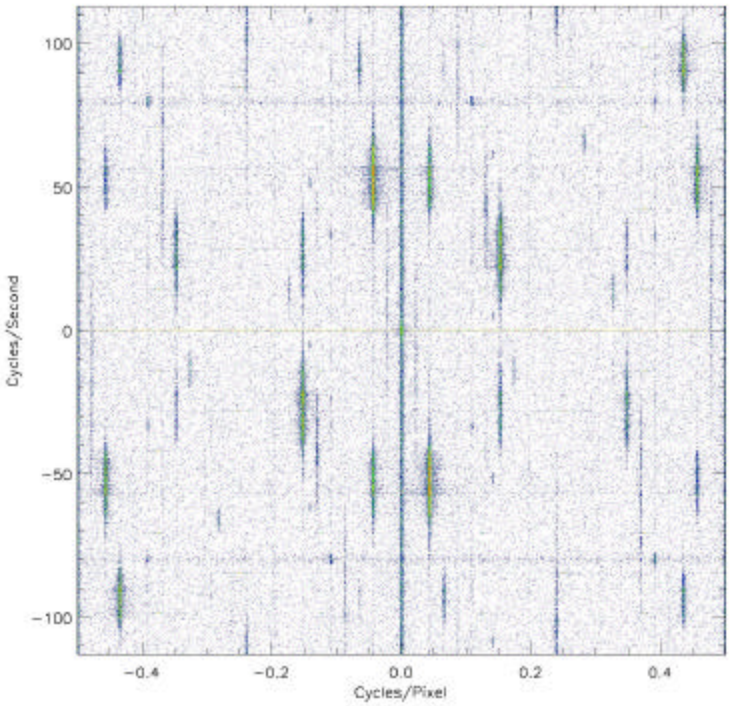

Figure 25: Fourier transform of a Band 1 flat field.

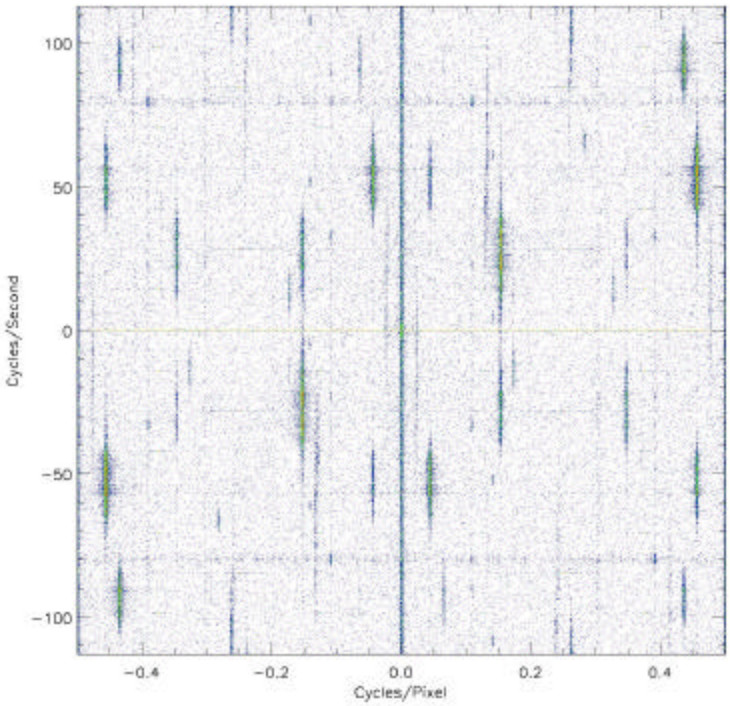

Figure 26: Fourier transform of a Band 2 flat field.

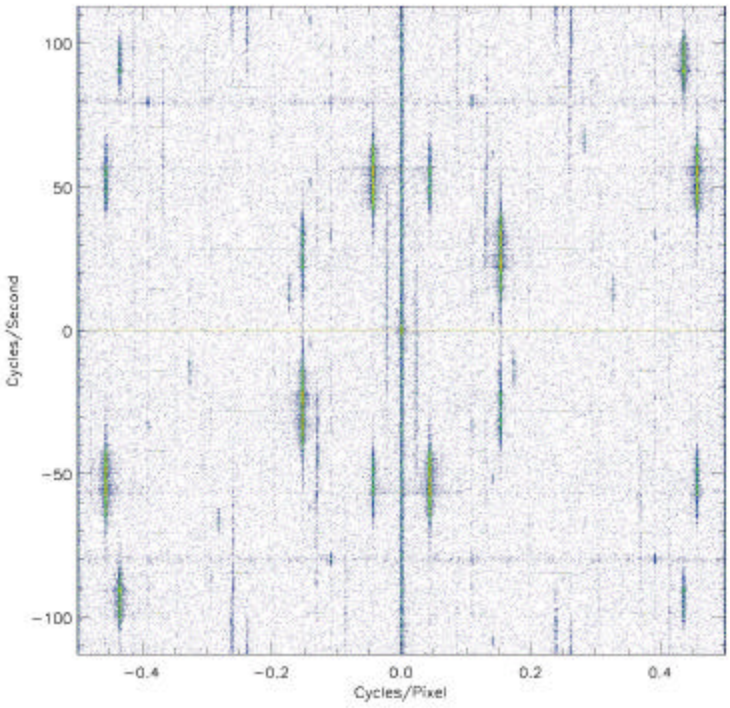

Figure 27: Fourier transform of a Band 3 flat field.

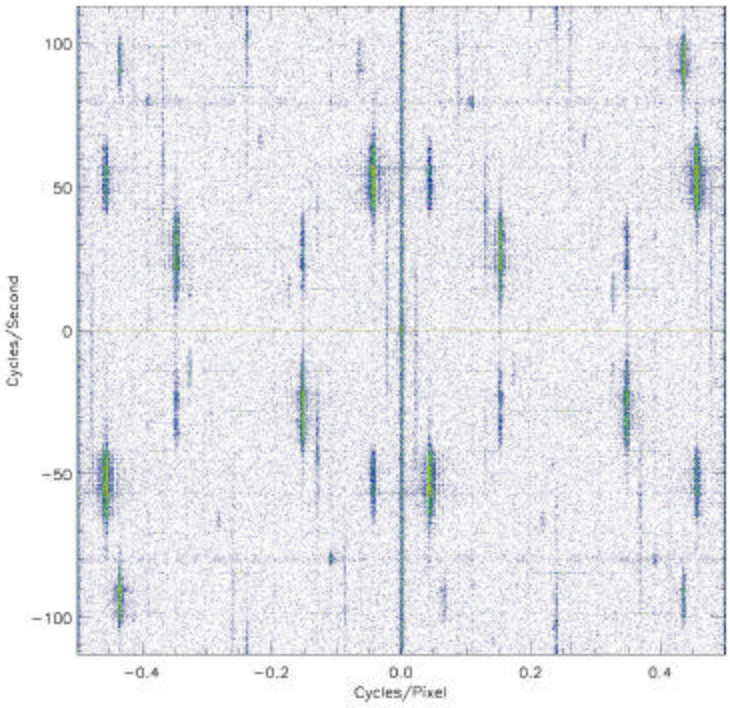

Figure 28: Fourier transform of a Band 4 flat field.

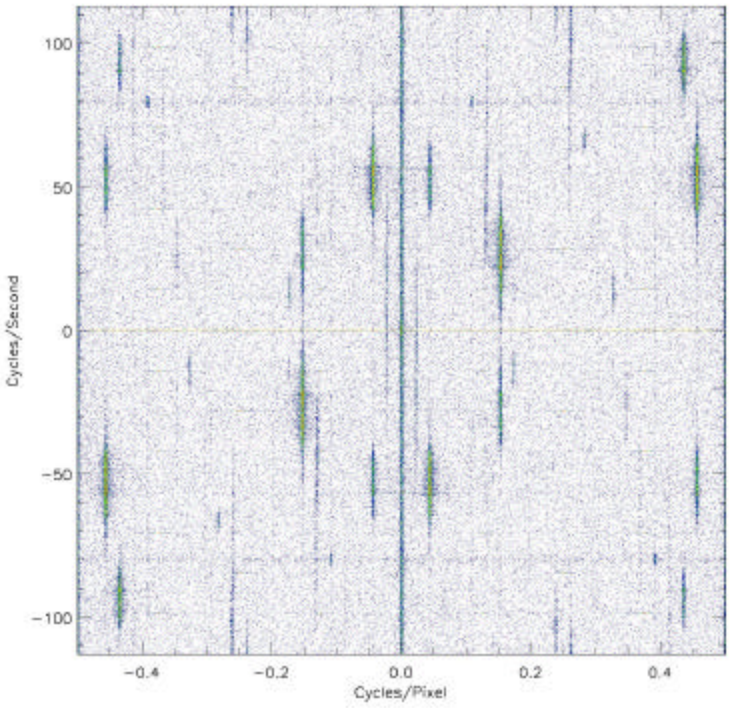

Figure 29: Fourier transform of a Band 4p flat field.

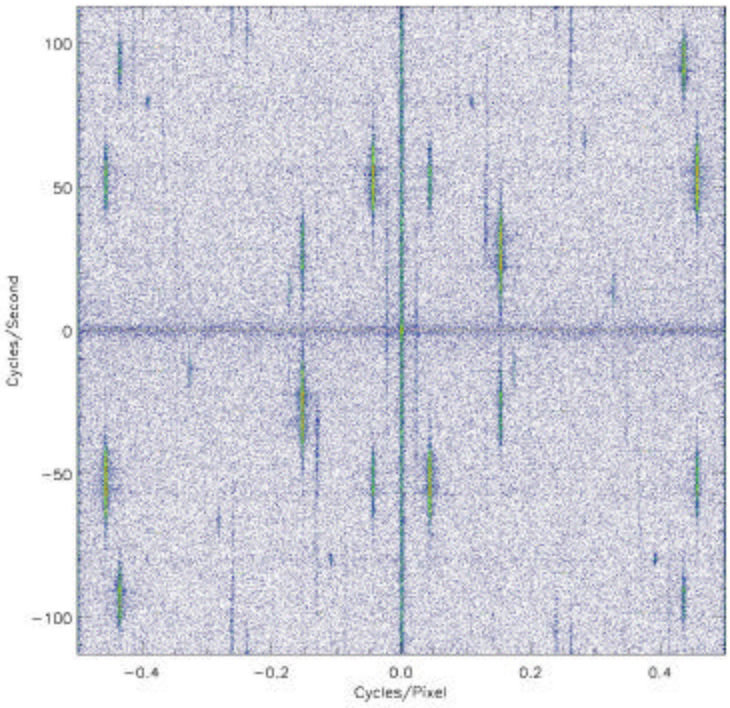

Figure 30: Fourier transform of a Band 5p flat field.

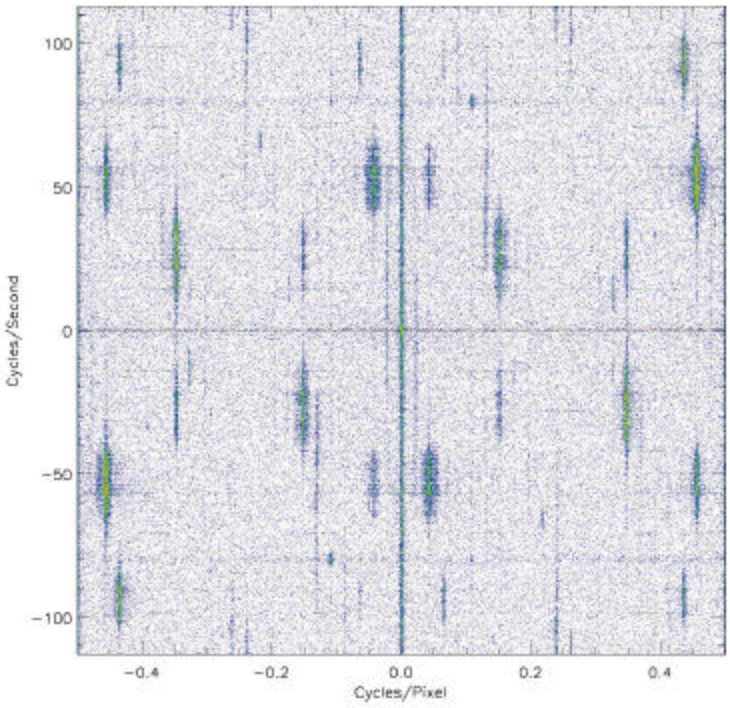

Figure 31: Fourier transform of a Band 5 flat field.

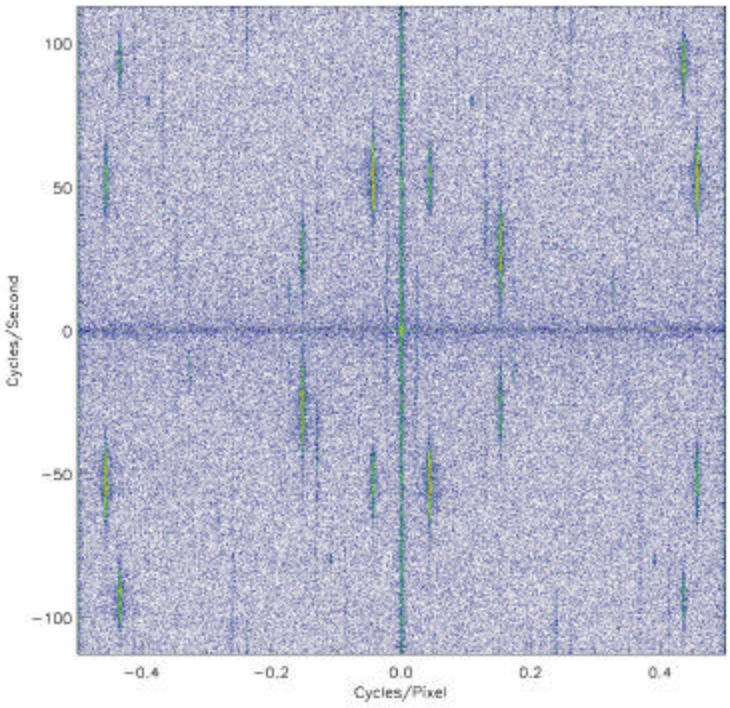

Figure 32: Fourier transform of a Band 7 flat field.

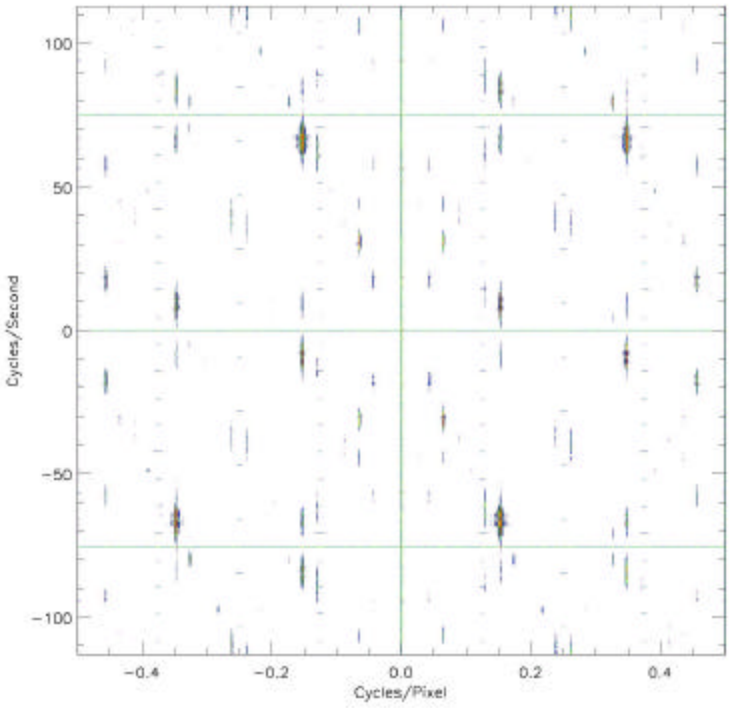

Figure 33: Fourier transform of a Panchromatic Band flat field.

Table 6: Coherent Noise Analysis Results.

Band	Maximum Coherent Noise Contributor (% of Total Noise)	Combined Coherent Noise Effect (% of Total Noise)	Combined Coherent Noise Effect (Digital Number)
1p	19.3	49.0	0.40
1	26.4	56.1	0.42
2	23.4	55.6	0.41
3	19.6	56.8	0.42
4	21.0	50.7	0.39
4p	20.0	54.0	0.42
5p	17.4	47.8	0.42
5	23.4	45.3	0.37
7	16.4	43.4	0.42
Pan	21.0	53.0	0.60

2.2.3 Pseudo-random Fluctuations

The third component of instrument noise is pseudo-random in nature. Pseudo-random noise in the Advanced Land Imager is composed of low frequency or slow drift (<0.03 Hz or for periods greater than 30 seconds) and high frequency (>0.03 Hz or for periods less than 30 seconds) components.

A low frequency pseudo-random fluctuation (LFPRF) manifests itself as gradual dark current drifting over time. During flight operations, one-second dark scenes will be collected prior to and just after the nadir-

looking Earth scene. The first dark scene will be used to generate dark current maps for the subsequent Earth scene. The second dark scene will be used to track each detector's dark current drift to ensure proper background normalization. If a LFPRF is detected for a specific detector, linear interpolation of the two dark current reference values will be used to correct the Earth scene on a frame-by-frame basis for that detector.

A high frequency fluctuation manifests itself as a rapid, pseudo-random dark current variation throughout a data collection period. Unfortunately, due to the rapidly changing dark current values observed during high frequency pseudo-random fluctuations (HFPRF), the noise contribution from these detectors cannot be directly compensated for in the Earth scene. The influence of this high frequency term in the time domain will result in the addition of fluctuations in the earth scene dark current that cannot be compensated. As a result, when analyzing earth scenes with regions exhibiting low-level spatial fluctuations, one should be cognizant of any detectors marked as having noted HFPRF noise, such that interesting scientific results are not the result of misinterpretation of this effect. It is also recommended that long dark current scenes be collected periodically on orbit (2-4 weeks) to assess the HFPRF as a function of time.

Characterization of the ALI low and high frequency pseudo-random noise component for a 40-second period has been performed while the focal plane was maintained at 215 and 220 K. For each band, candidate detectors were selected if their noise values exceed 1.5 DN. Seventeen detectors were selected in this manner when the focal plane was operating at 220 K. Eleven detectors were selected when the focal plane was maintained at 215 K. For each candidate, a Fourier transform was performed, and the magnitude and power spectrum were derived. A Fourier analysis of a typical, low-noise detector (Band 5p, detector 6) is provided in Figure 34 as a baseline for comparison. Table 7 lists the candidate detectors, and Figures 35-45 present the results of the Fourier analysis with the focal plane temperature at 215 K. Table 8 lists the candidate detectors, and Figures 46-62 present the results of the Fourier analysis with the focal plane temperature at 220 K.

As expected, the spectral distribution for the reference detector is flat, indicating that random fluctuations dominate this detector's dark current over the 40-second period. Six noted deviations occur at 14.1, 28.2, 42.3, 70.6, 98.9, 113.0 Hz. The latter five are higher harmonics of 14.1 Hz. At these frequencies, the magnitude of the Fourier transform rises to > 3.0 DN/ Hz.

The magnitude data for all candidate detectors have been fit to the following function in an effort to quantify their characteristics

$$M_P = A_0(1. + (A_1 / f)^{A_2}).$$

Here, M_P is the magnitude obtained from the Fourier analysis, f is the channel frequency, A_0 is the magnitude offset, A1 is the knee frequency, and A_2 is the slope of the low frequency component. Initially, the fitted knee frequencies were unphysically high due to a non-zero slope in the magnitude data above 40 Hz. To account for this, magnitude data above 40 Hz was fit to a linear function. All data were then normalized to remove the slope and the data were refit to the above function. Results from this analysis, including factors used to normalize the magnitude data, are provided in Tables 7 and 8.

It should be noted that all seventeen detectors with suspected pseudo-random noise are SWIR detectors. Detectors listed in Table 7 (215 K) are also a subset of detectors listed in Table 8 (220 K), indicative of improved thermal stability with colder temperature.

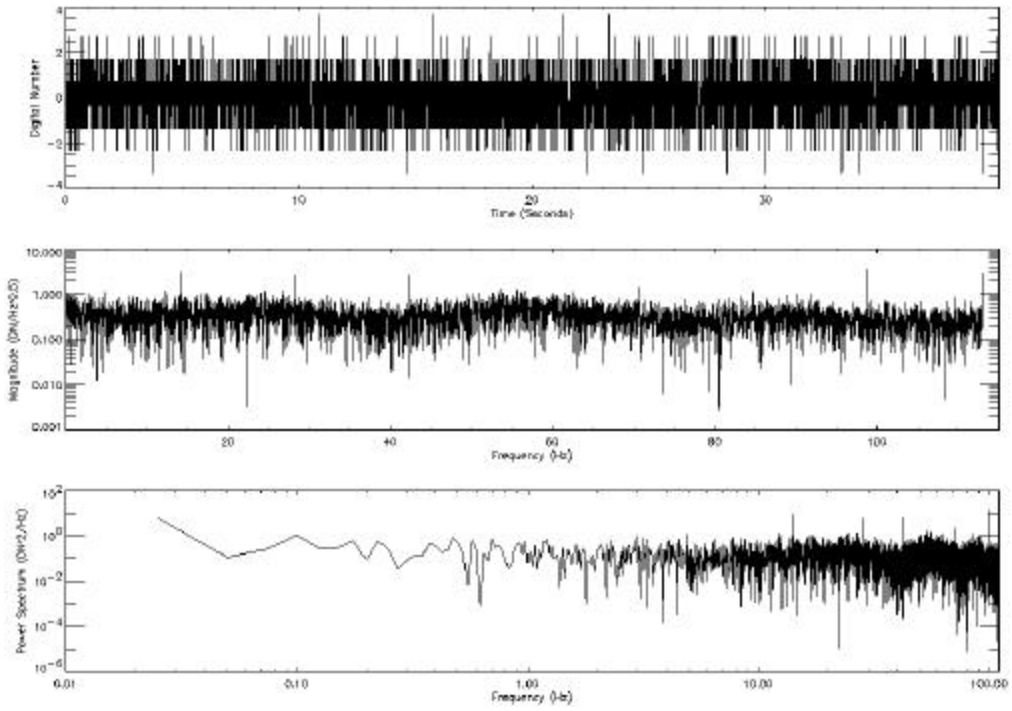

Figure 34: Baseline Fourier analysis for Band 5p, detector 6 (T=220 K).

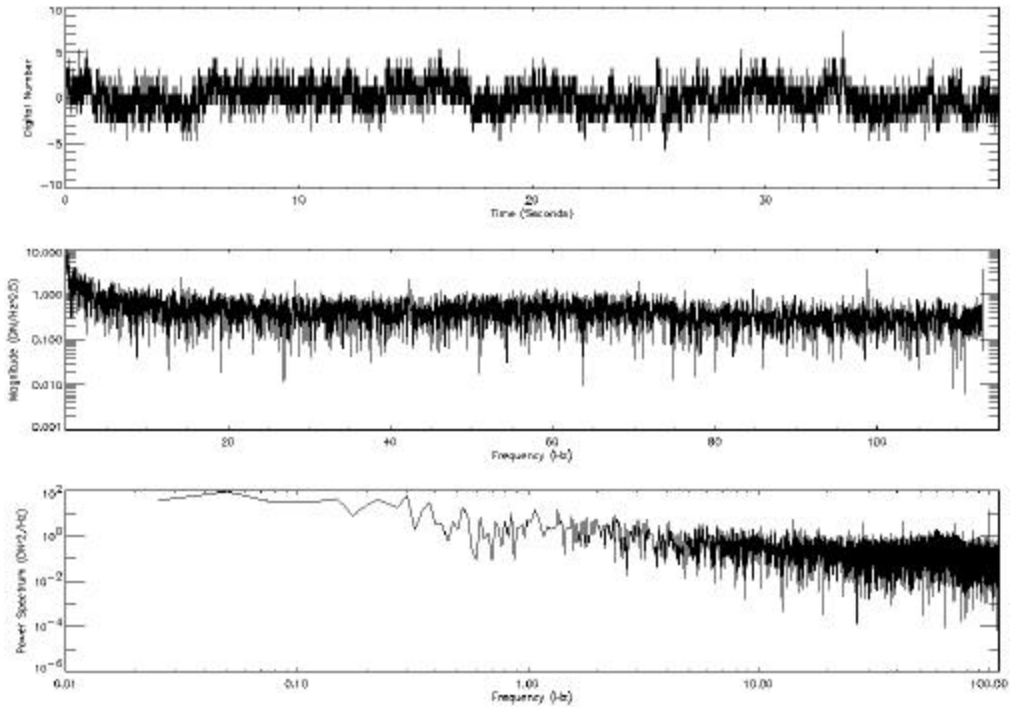

Figure 35: Fourier analysis of Band 5p, detector 2 (T=215 K).

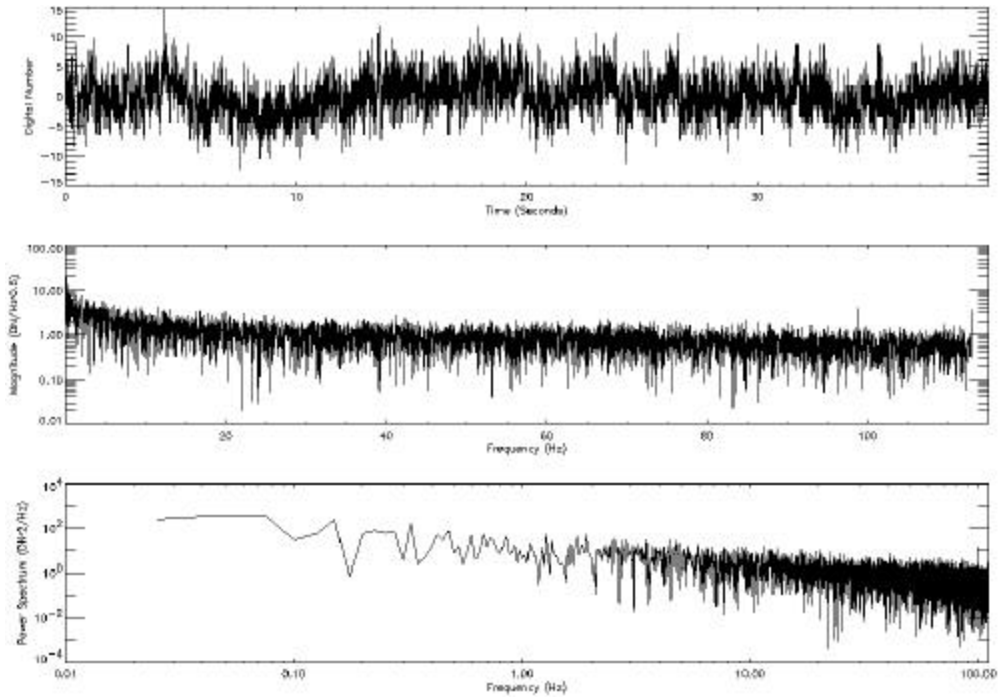

Figure 36: Fourier analysis of Band 5p, detector 82 (T=215 K).

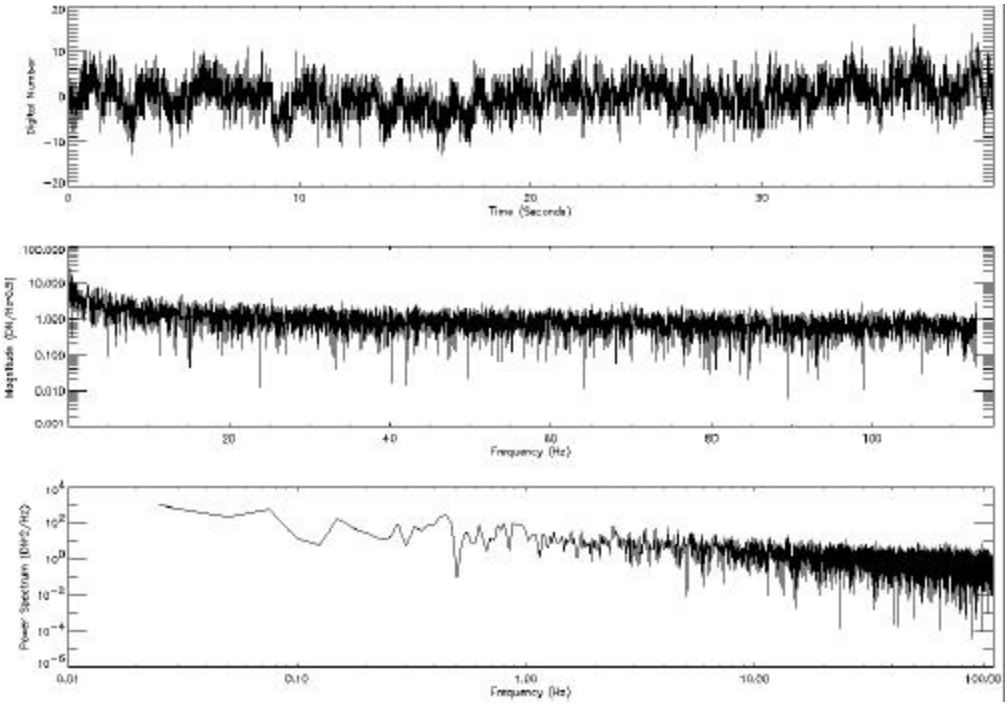

Figure 37: Fourier analysis of Band 5p, detector 92 (T=215 K).

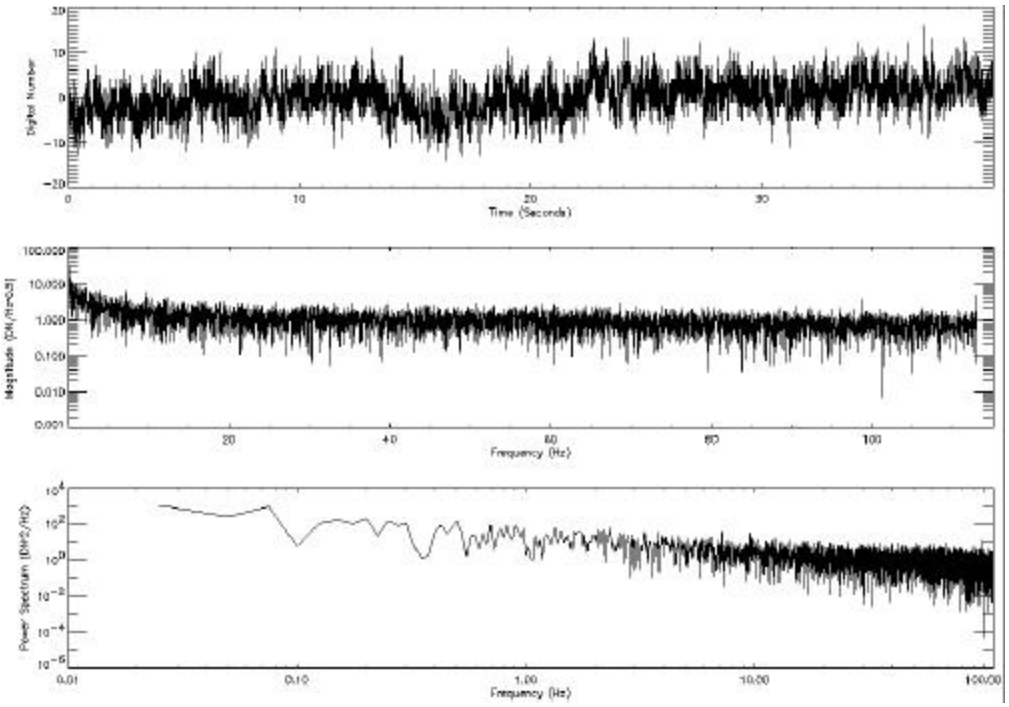

Figure 38: Fourier analysis of Band 5p, detector 99 (T=215 K).

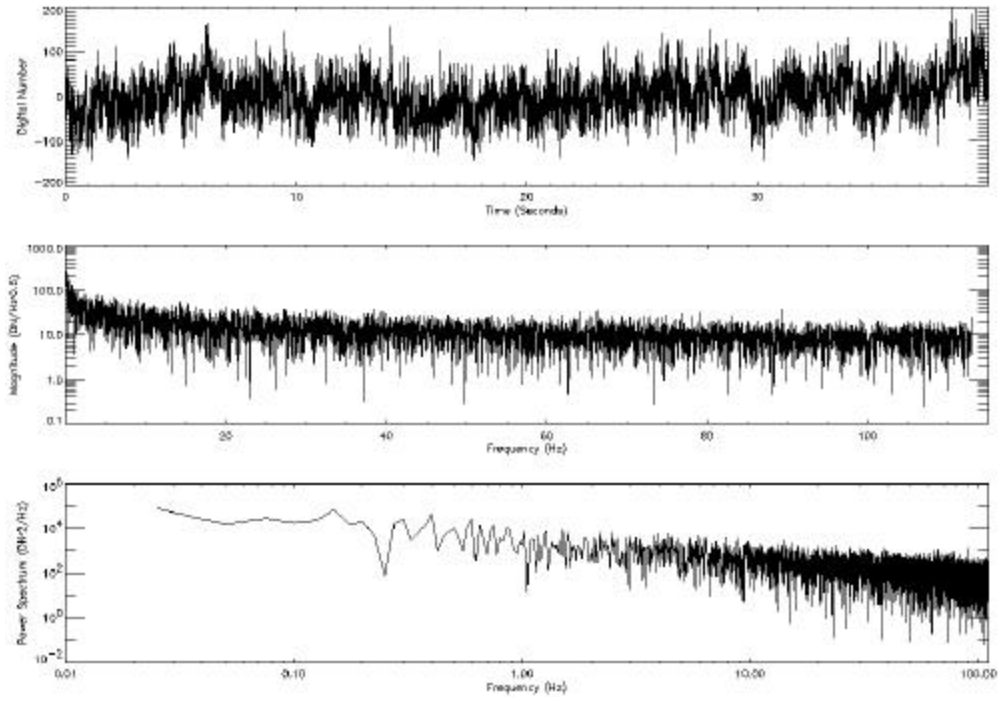

Figure 39: Fourier analysis of Band 5p, detector 365 (T=215 K).

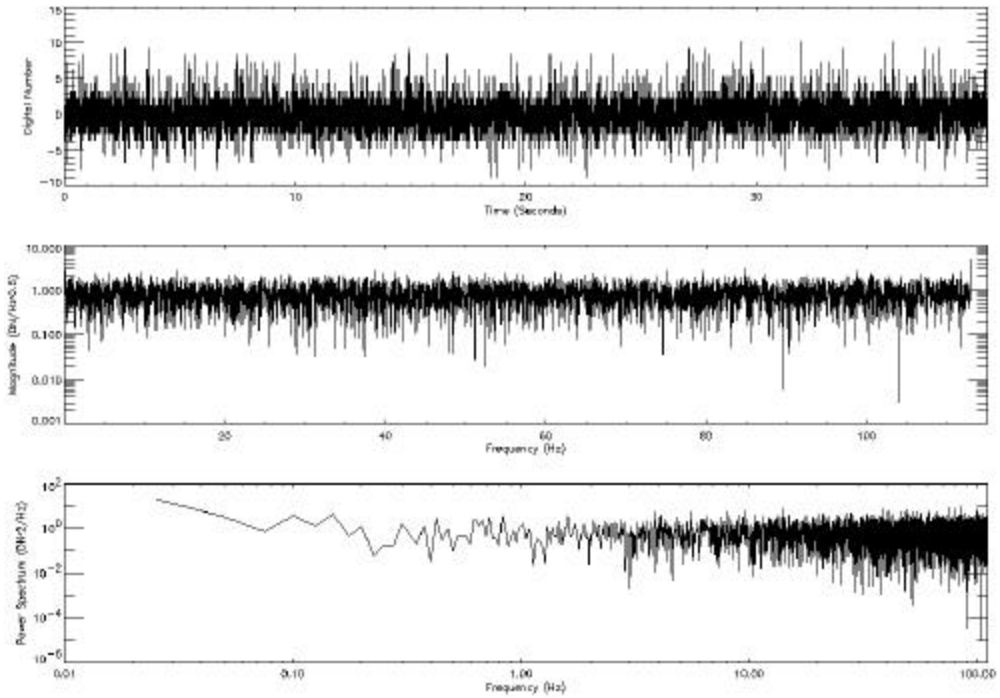

Figure 40: Fourier analysis of Band 5p, detector 372 (T=215 K).

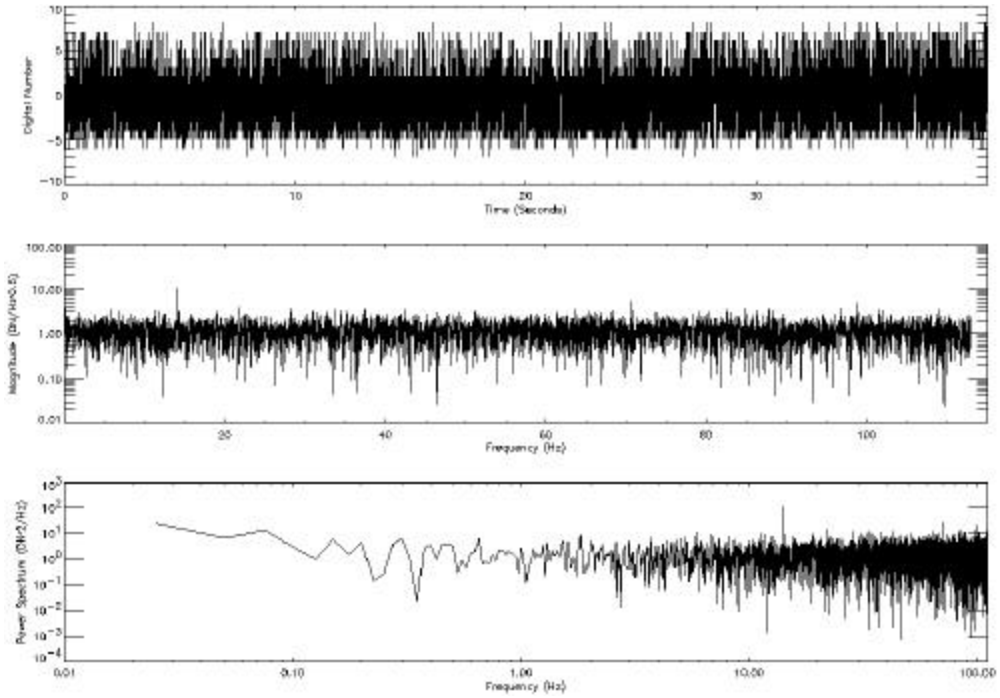

Figure 41: Fourier analysis of Band 5p, detector 636 (T=215 K).

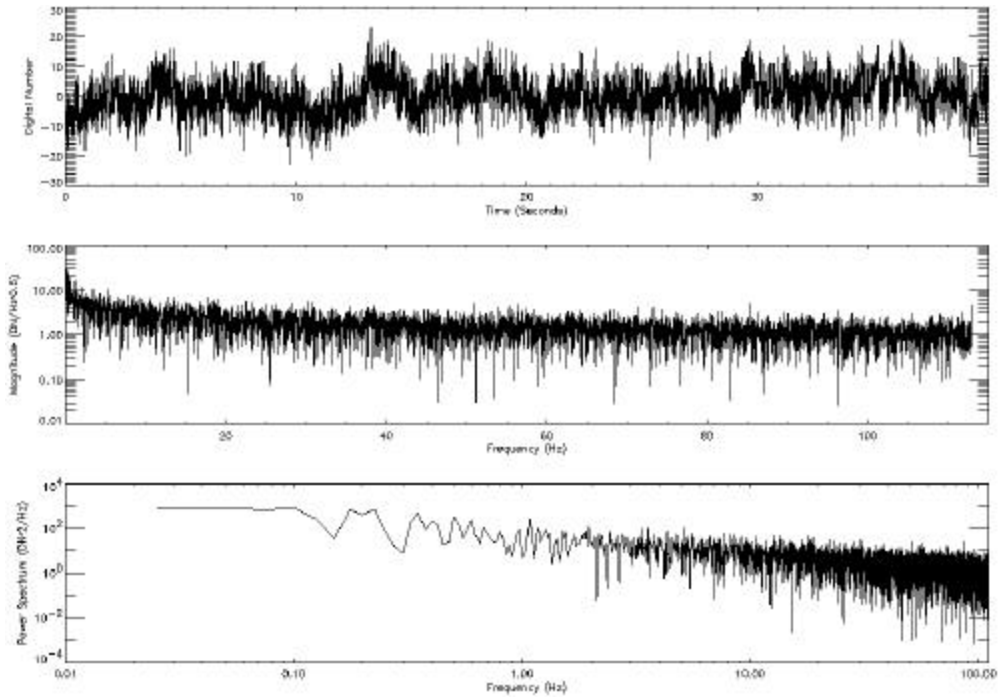

Figure 42: Fourier analysis of Band 5, detector 911 (T=215 K).

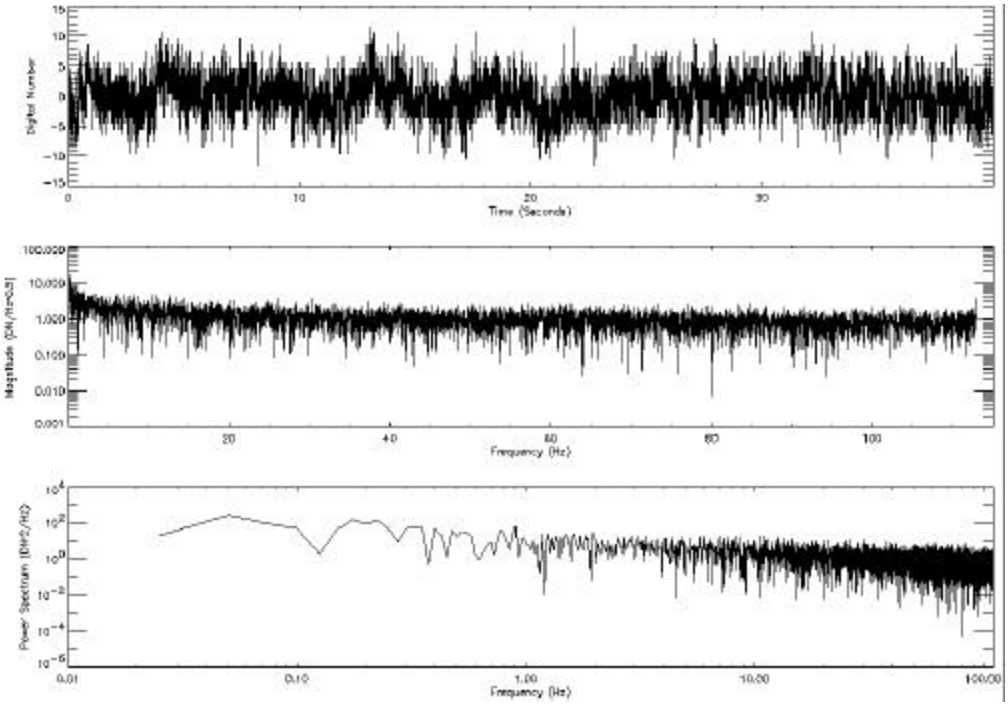

Figure 43: Fourier analysis of Band 5, detector 913 (T=215 K).

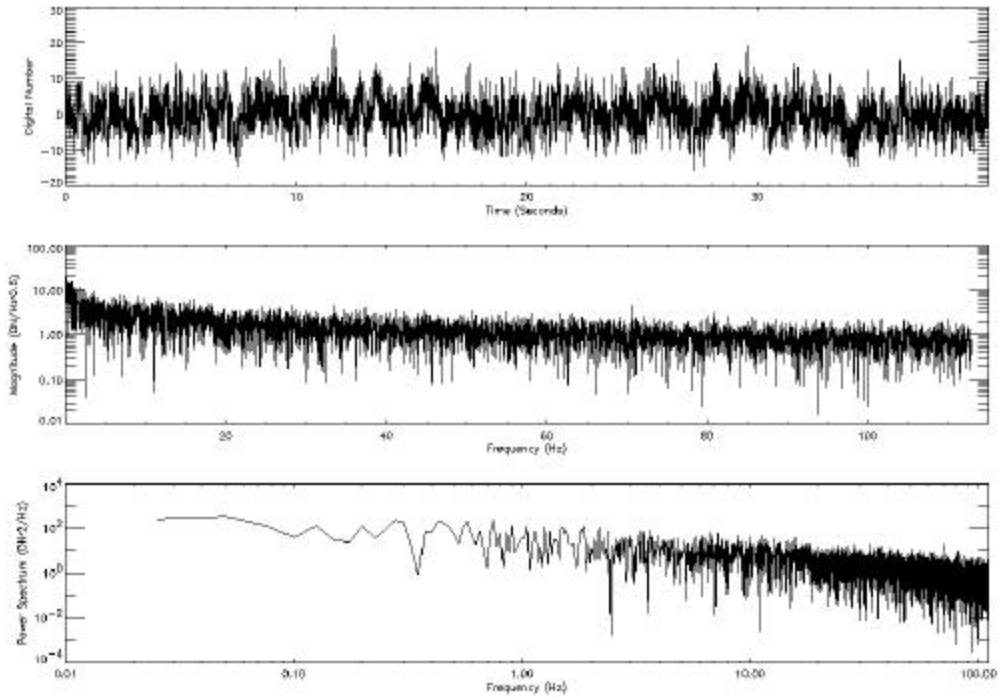

Figure 44: Fourier analysis of Band 7, detector 11 (T=215 K).

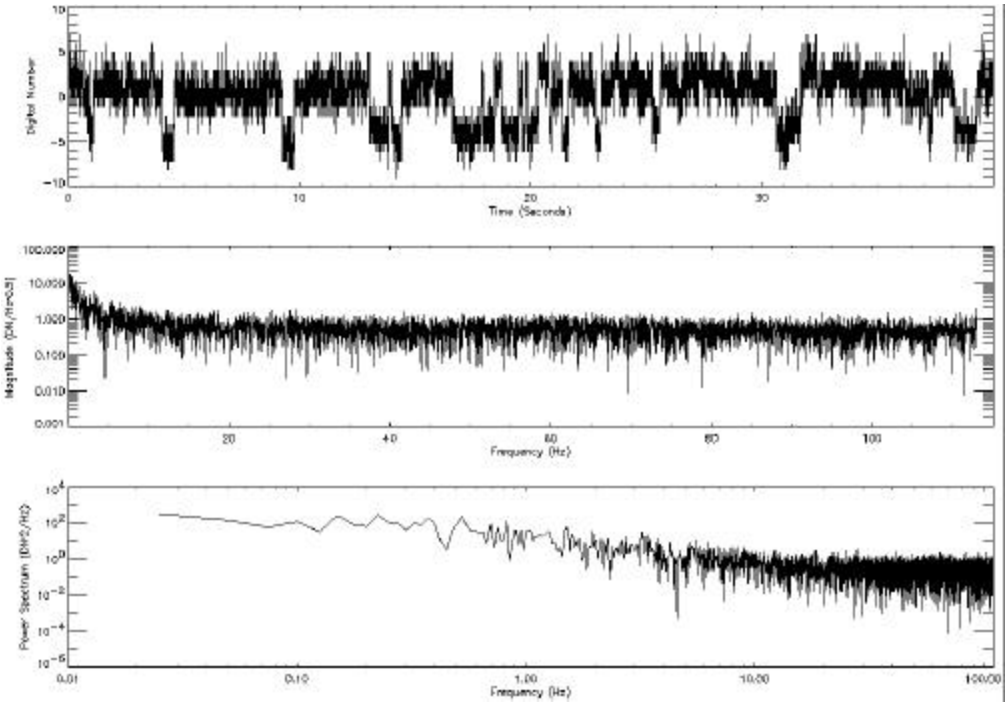

Figure 45: Fourier analysis of Band 7, detector 382 (T=215 K).

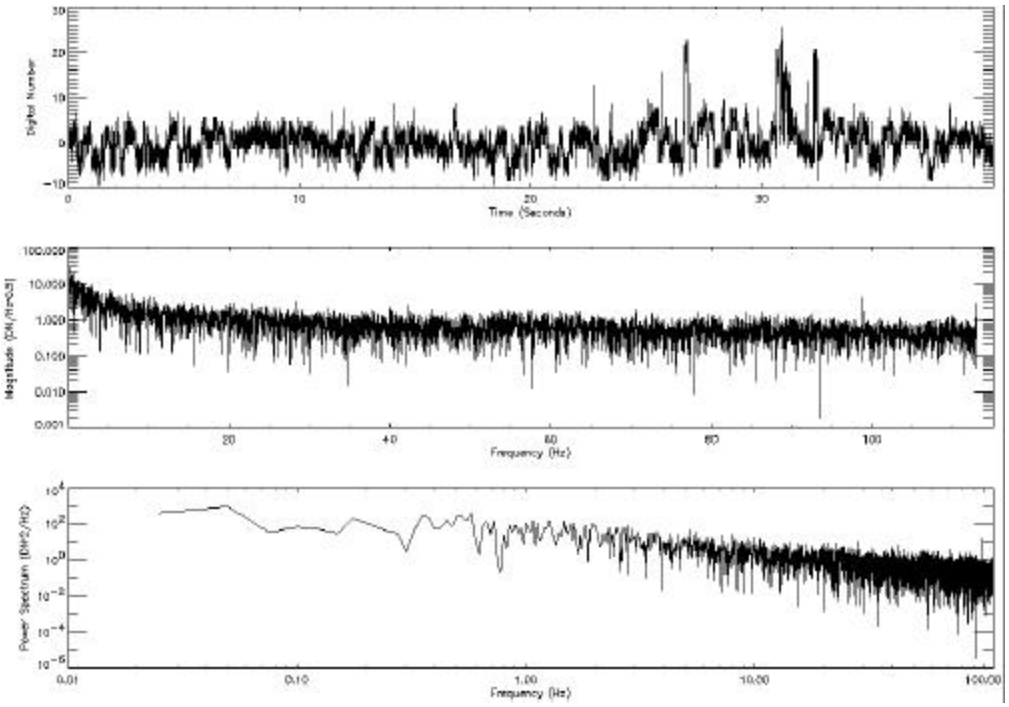

Figure 46: Fourier analysis of Band 5p, detector 2 (T=220 K).

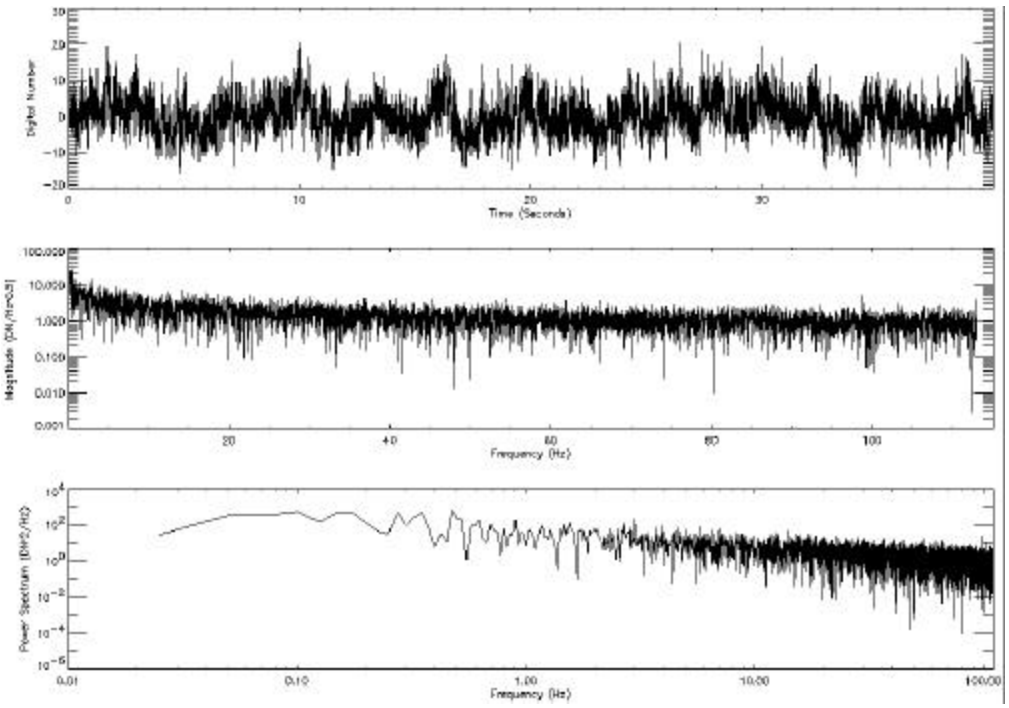

Figure 47: Fourier analysis of Band 5p, detector 82 (T=220 K).

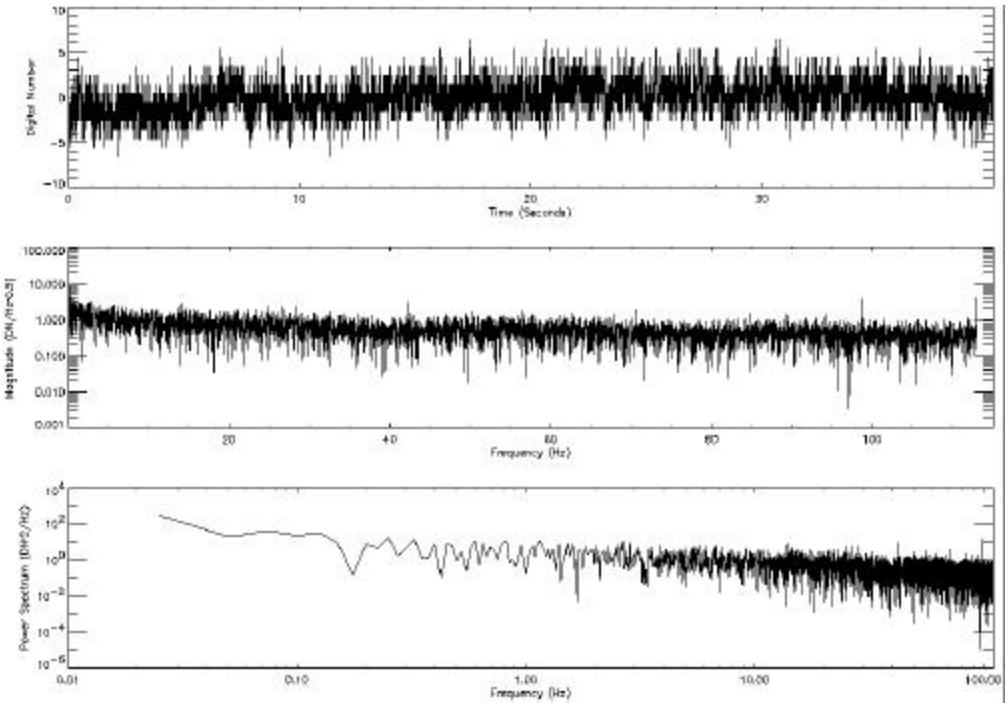

Figure 48: Fourier analysis of Band 5p, detector 83 (T=220 K).

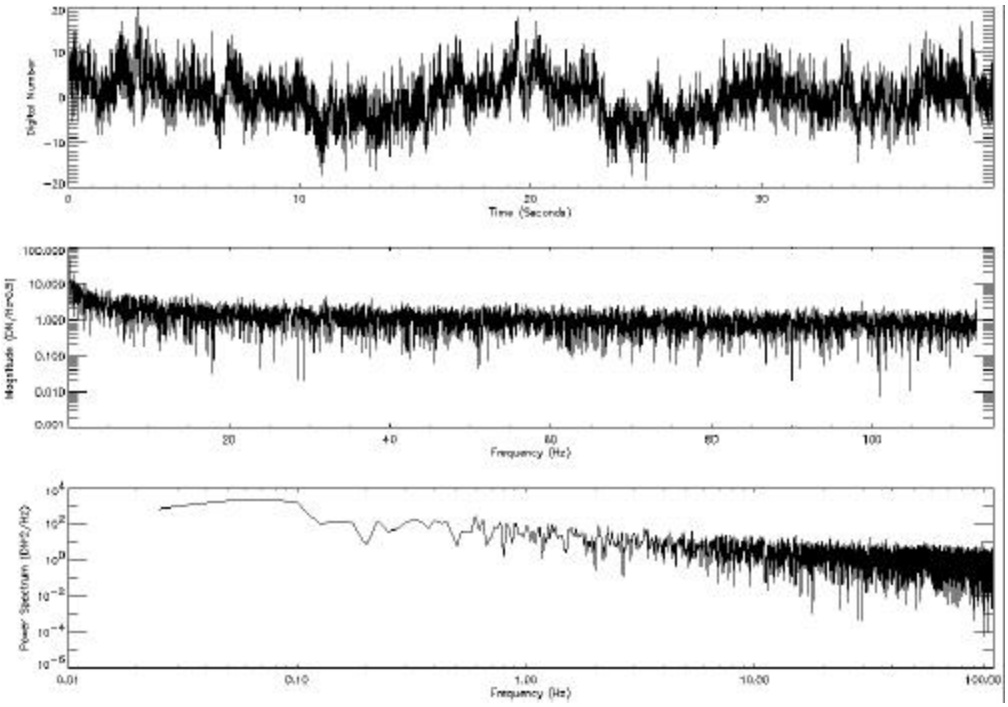

Figure 49: Fourier analysis of Band 5p, detector 92 (T=220 K).

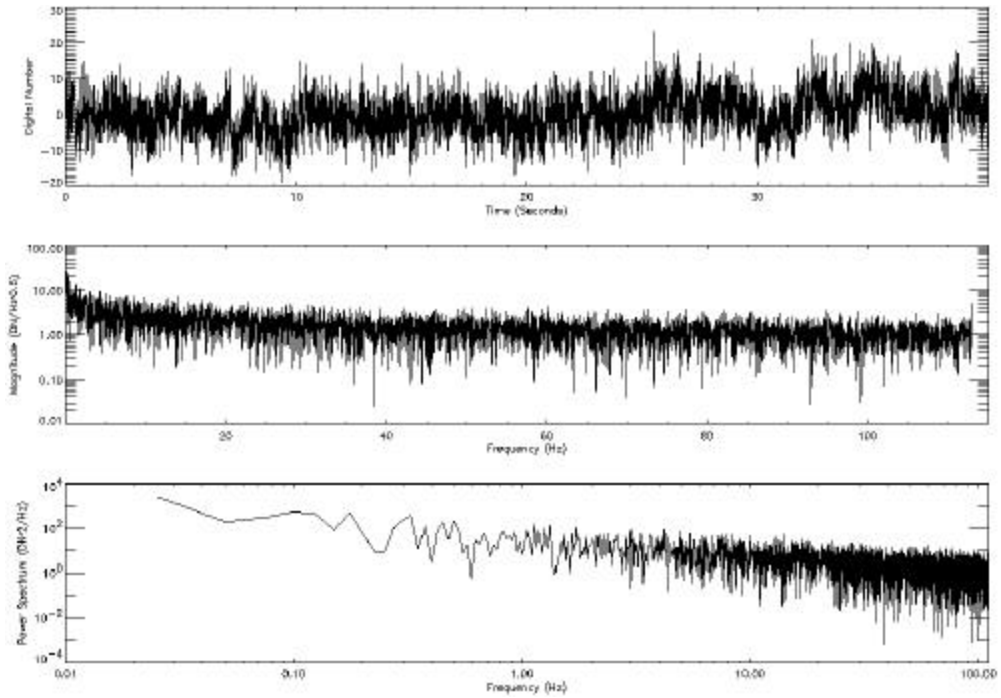

Figure 50: Fourier analysis of Band 5p, detector 99 (T=220 K).

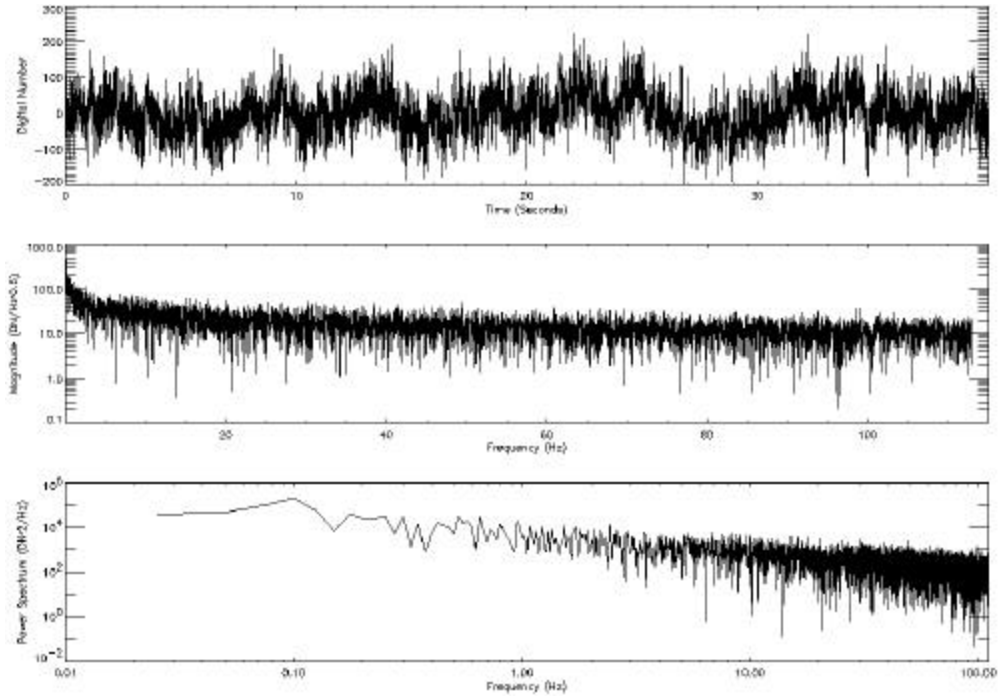

Figure 51: Fourier analysis of Band 5p, detector 365 (T=220 K).

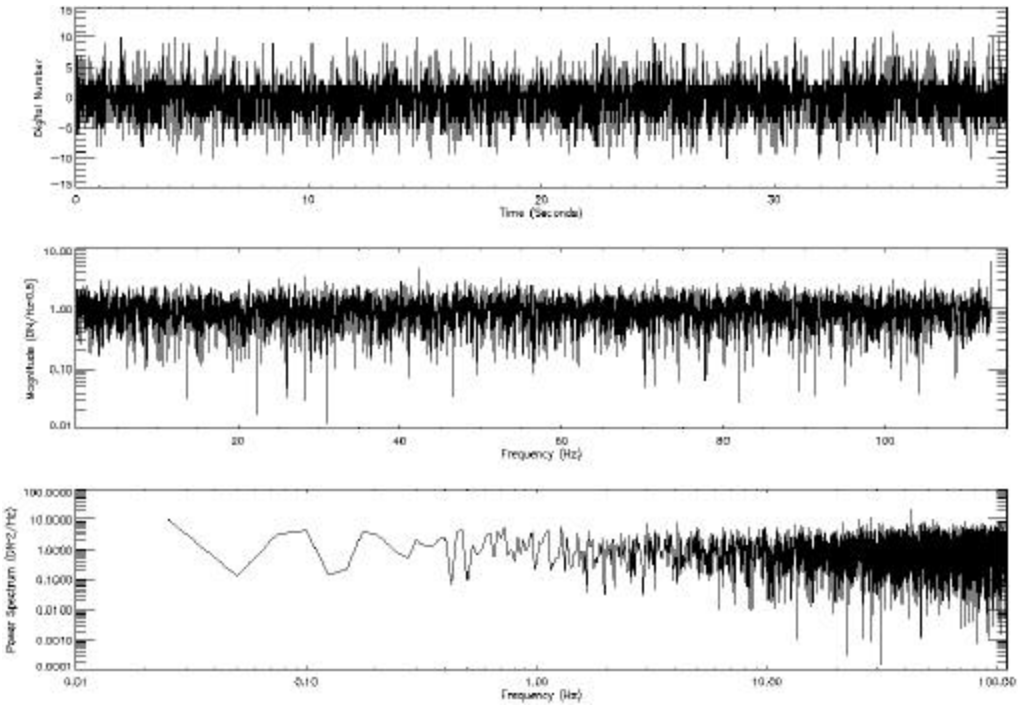

Figure 52: Fourier analysis of Band 5p, detector 372 (T=220 K).

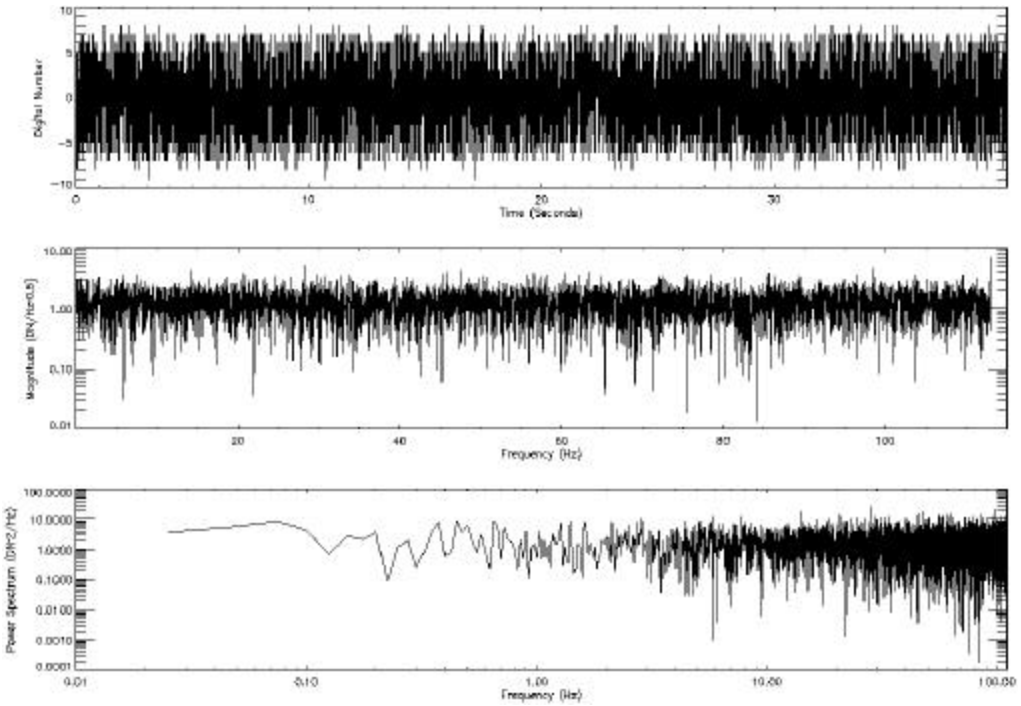

Figure 53: Fourier analysis of Band 5p, detector 636 (T=220 K).

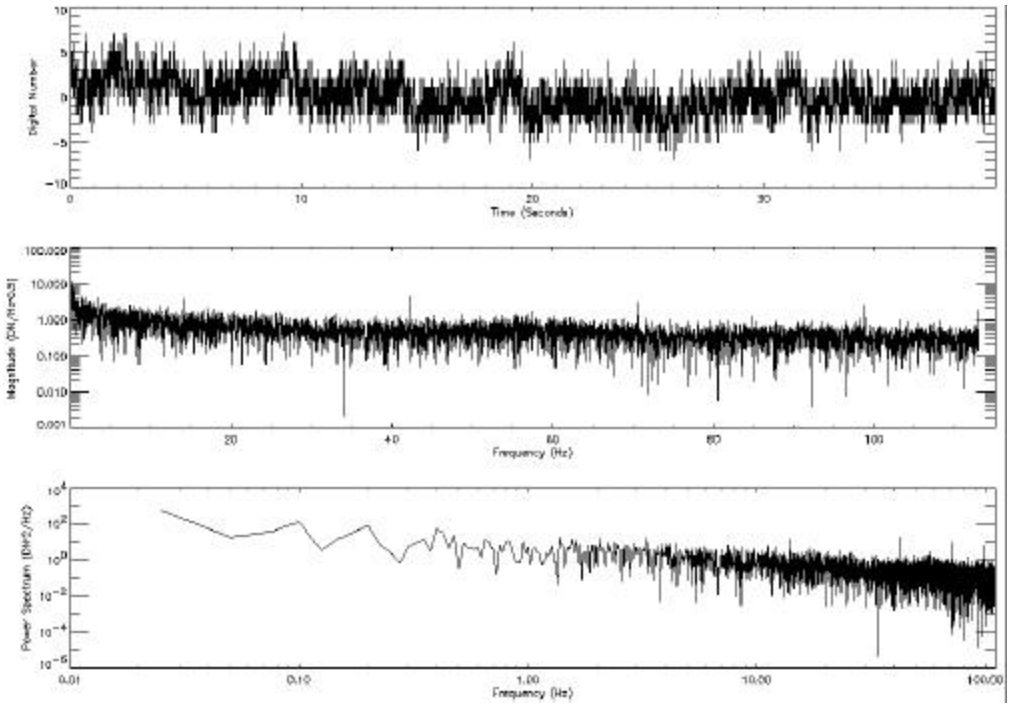

Figure 54: Fourier analysis of Band 5, detector 119 (T=220 K).

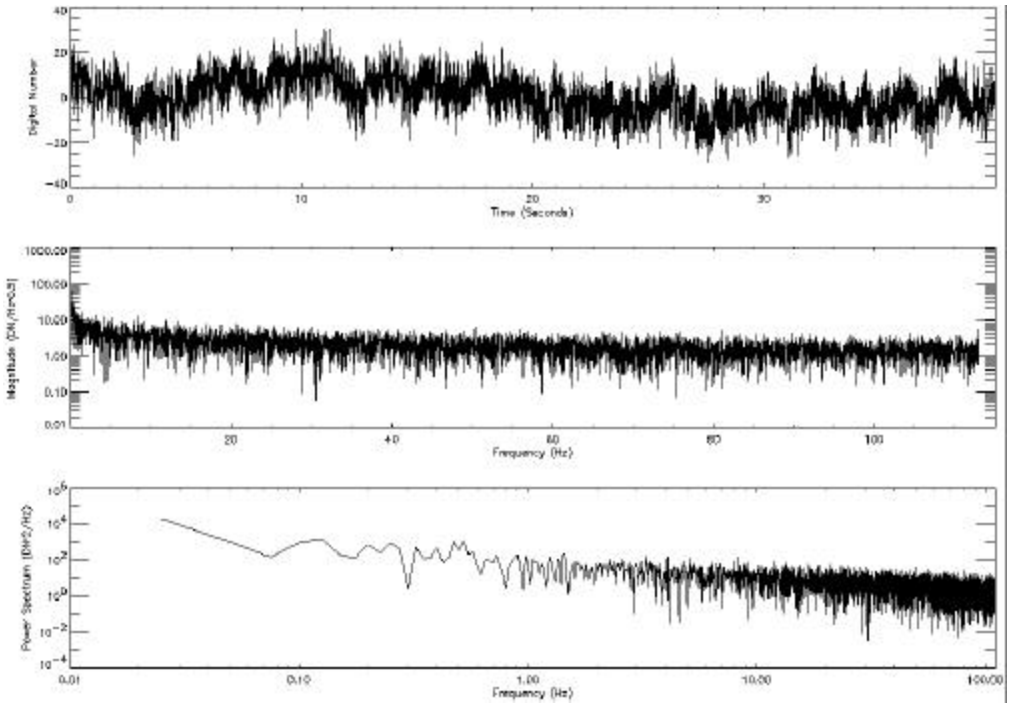

Figure 55: Fourier analysis of Band 5, detector 911 (T=220 K).

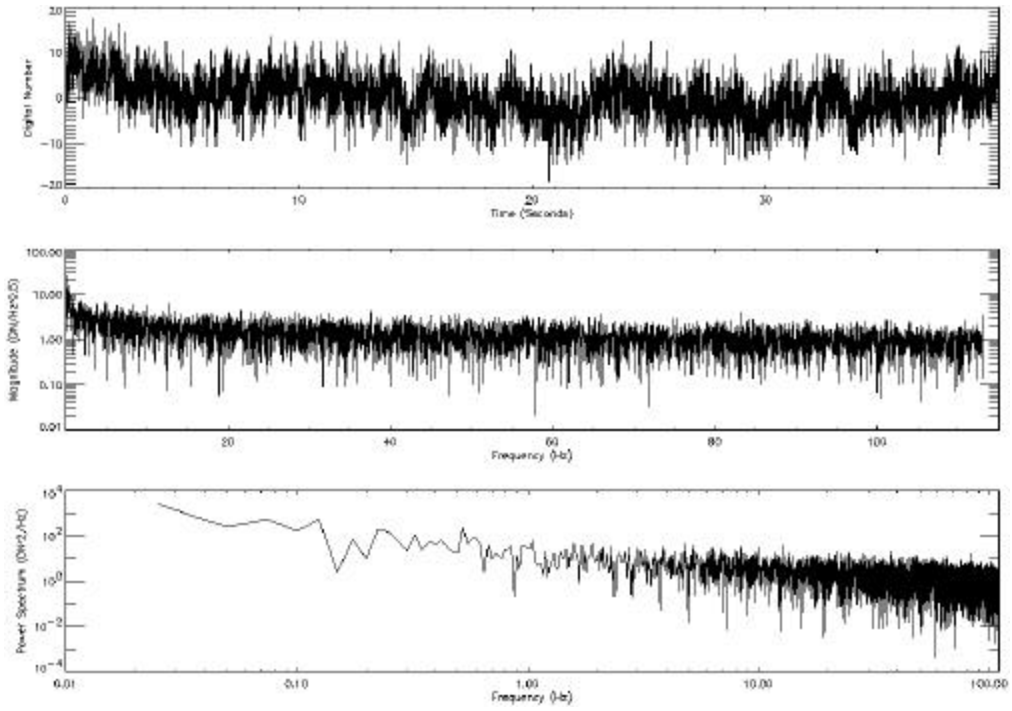

Figure 56: Fourier analysis of Band 5, detector 913 (T=220 K).

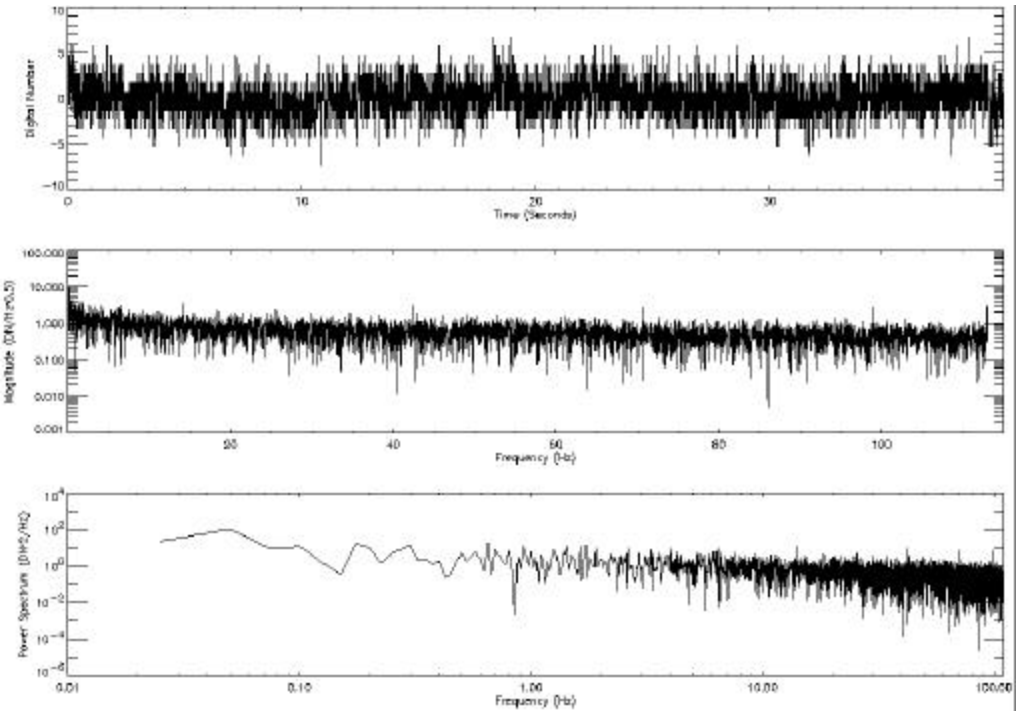

Figure 57: Fourier analysis of Band 7, detector 4 (T=220 K).

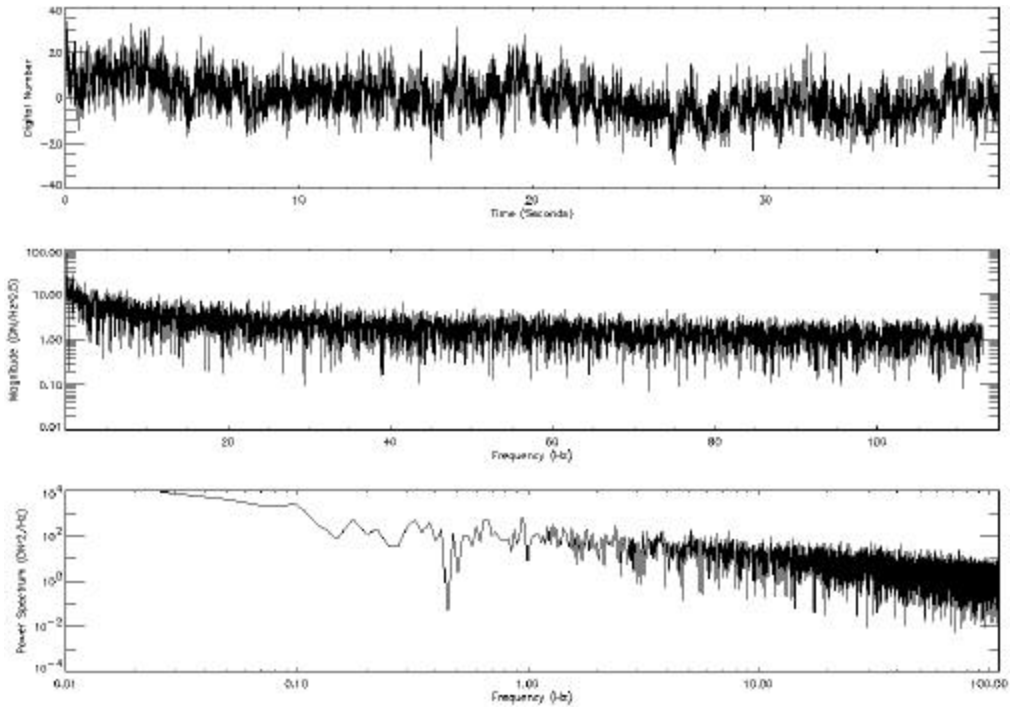

Figure 58: Fourier analysis of Band 7, detector 11 (T=220 K).

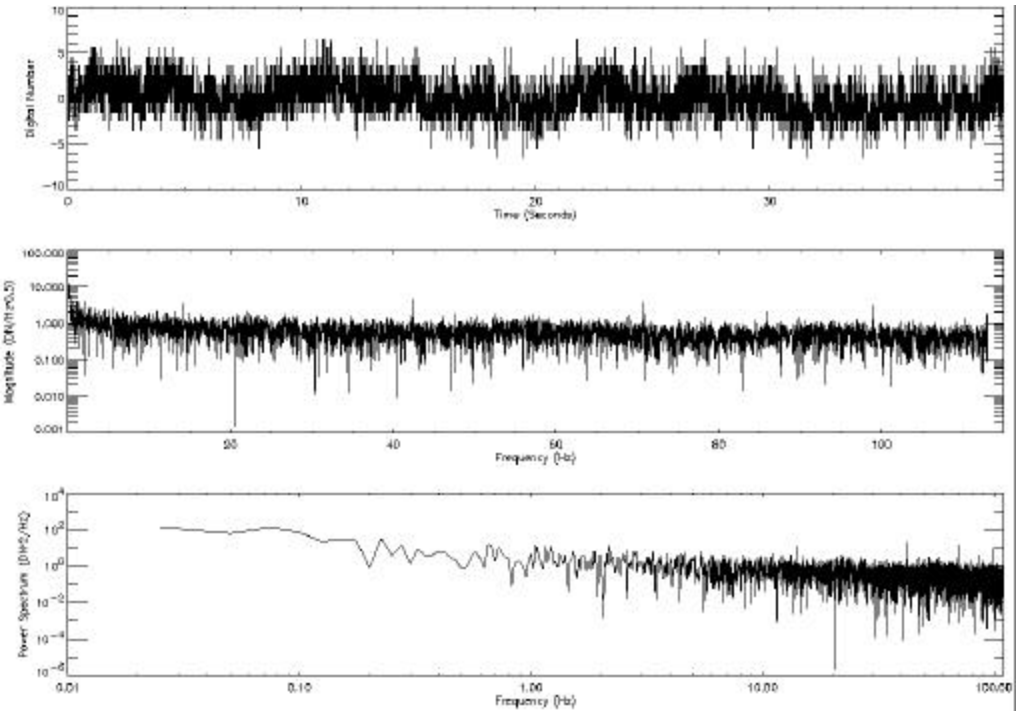

Figure 59: Fourier analysis of Band 7, detector 17 (T=220 K).

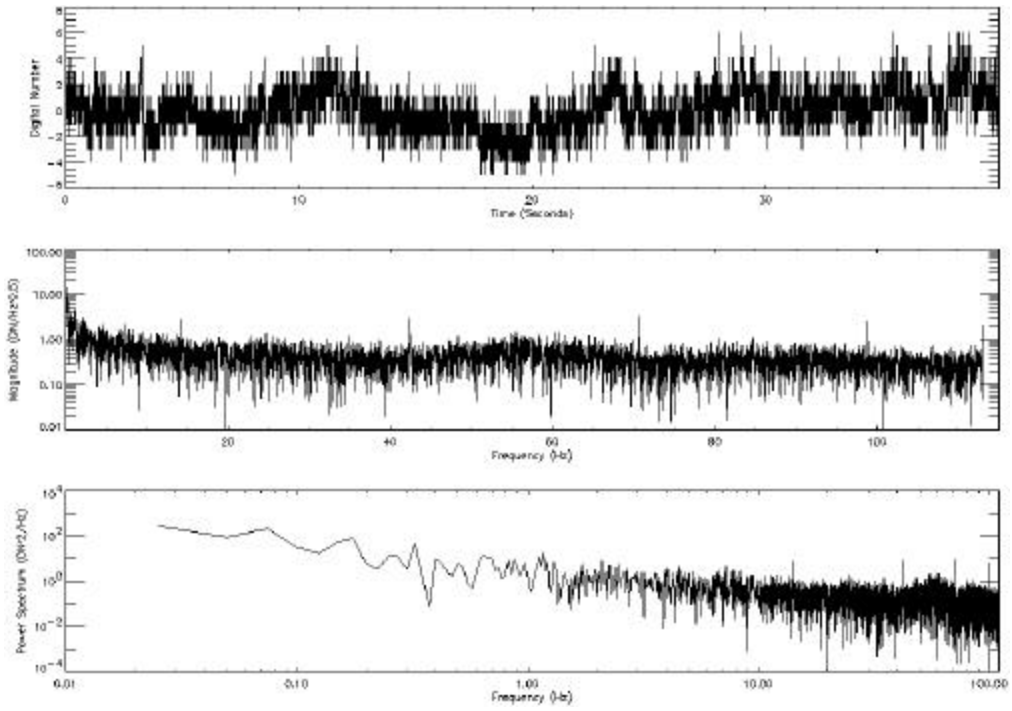

Figure 60: Fourier analysis of Band 7, detector 126 (T=220 K).

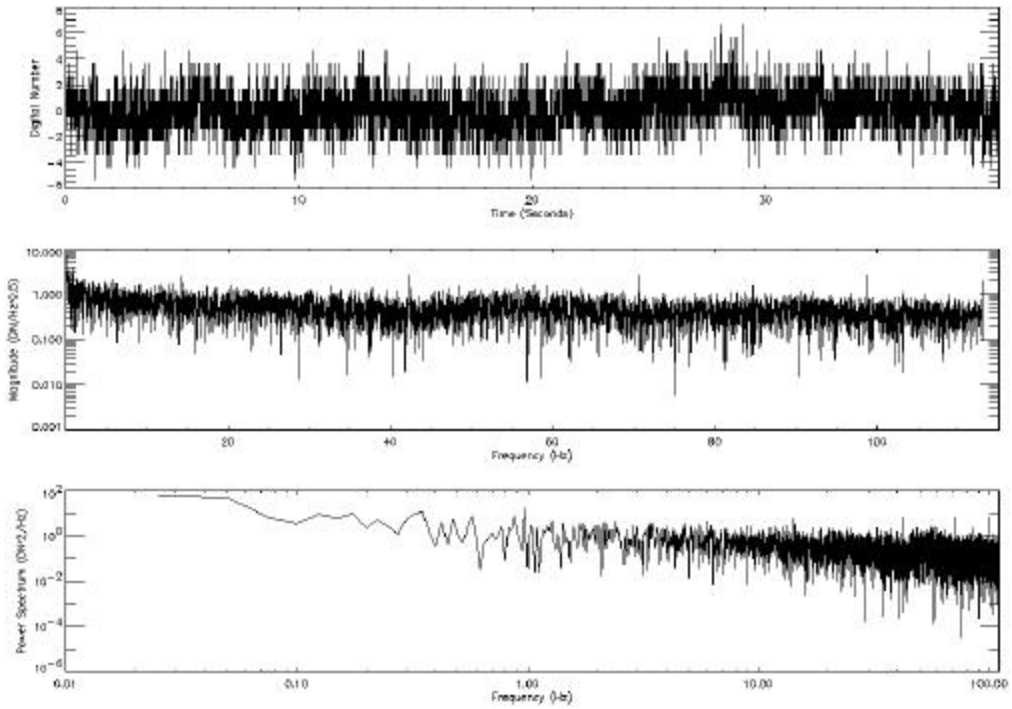

Figure 61: Fourier analysis of Band 7, detector 307 (T=220 K).

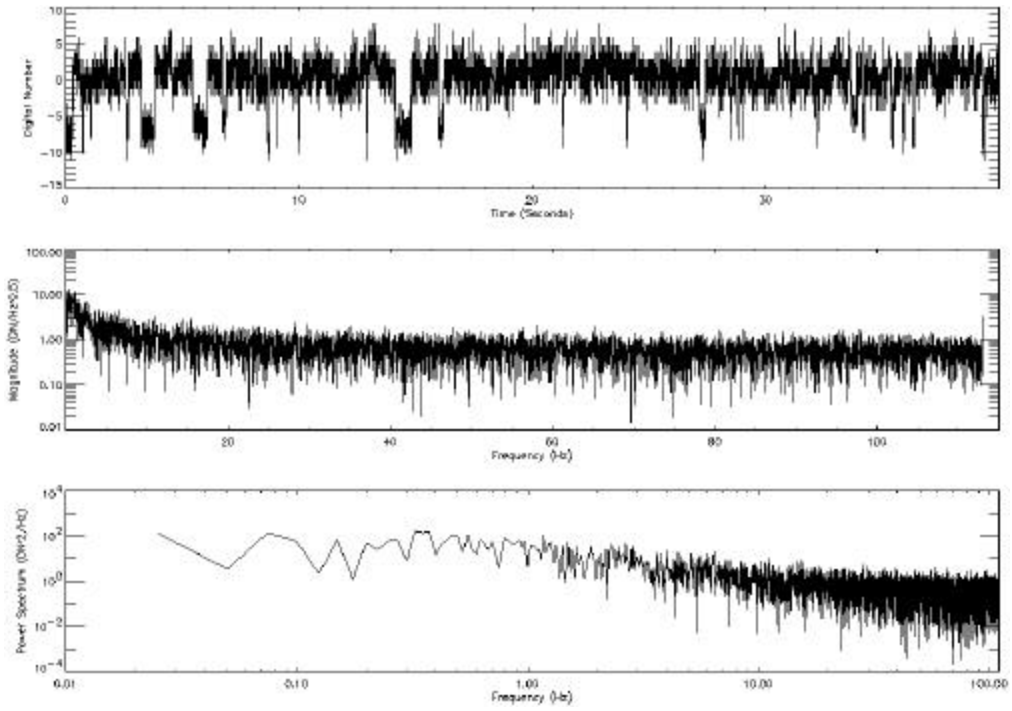

Figure 62: Fourier analysis of Band 7, detector 382 (T=220 K).

Table 7: Detectors with Marked Pseudo-Random Noise at 215 K

Band	Detector	Comment	A_0	A_1	A_2	S^*
5p	2	--	0.57	1.95	0.87	-0.0030
5p	82	Excess white noise	0.82	9.52	0.56	-0.0049
5p	92	Excess white noise	0.87	8.90	0.67	-0.0044
5p	99	Excess white noise	0.93	7.80	0.66	-0.0042
5p	365	Excess dark current, Excess white noise	12.01	7.11	0.66	-0.0617
5p	372	Excess white noise	1.36	5.87	0.53	0.0002
5p	636	Excess white noise	1.90	4.46	0.53	-0.0016
5	911	Excess dark current, Excess white noise	1.38	11.55	0.55	-0.0076
5	913	Excess dark current, Excess white noise	0.96	4.74	0.53	-0.0040
7	11	Excess white noise	1.10	16.98	0.54	-0.0082
7	382	Excess white noise	0.50	7.59	1.00	-0.0010

S^* = Slope used to normalize magnitude data before fit.

Table 8: Detectors with Marked Pseudo-Random Noise at 220 K

Band	Detector	Comment	A_0	A_1	A_2	S^*
5p	2	--	0.51	32.91	0.73	-0.0038
5p	82	Excess white noise	1.18	12.01	0.60	-0.0067
5p	83	--	0.53	5.37	0.48	-0.0028
5p	92	Excess white noise	1.04	9.04	0.71	-0.0049
5p	99	Excess white noise	0.95	35.54	0.43	-0.0055
5p	365	Excess Dark current Excess white noise	14.21	8.78	0.64	-0.0691
5p	372	Excess white noise , No 1/f component	1.61	5.20	0.53	-0.0004
5p	636	Excess white noise No 1/f component	1.79	5.13	0.53	0.0001
5	119	--	0.51	7.11	0.57	-0.0034
5	911	Excess dark current Excess white noise	1.93	6.59	0.66	-0.0093
5	913	Excess dark current Excess white noise	1.25	4.26	0.63	-0.0048
7	4	--	0.60	3.37	0.48	-0.0030
7	11	Excess white noise	1.30	36.67	0.53	-0.0100
7	17	--	0.68	1.70	0.73	-0.0028
7	126	--	0.54	2.28	0.94	-0.0026
7	307	--	0.53	1.51	0.55	-0.0020
7	382	Excess white noise	0.55	13.34	0.82	-0.0016

S^* = Slope used to normalize magnitude data before fit.

2.3 Repeatability

Focal planes with highly repeatable dark current and noise properties are very desirable. This repeatability simplifies the normalization of background signal and the prediction for future scenes' signal to noise ratios. The Advanced Land Imager repeatability has been characterized by measuring the dark current and noise of each detector for ten data sets spanning ten days. For each of these data, the focal plane was maintained at 220 K, and the nominal integration time (4.05 ms for multispectral detectors, 1.35 ms for panchromatic detectors) was used.

Plotted in Figures 63 and 64 are the overlaid differences between dark current for each band collected over a ten-day period during ground calibration at Lincoln Laboratory. The dark current was found to be repeatable to within ±2 digital numbers for all VNIR and panchromatic detectors. SWIR detectors are repeatable to within -20/+100 digital numbers. Of particular interest are the sensitivities of the SWIR bands on SCA 1 and the good repeatability of the hot spot centered on detector 1200 of bands 5p, 5 and 7.

Plotted in Figures 65 and 66 are the overlaid differences between mean white noise levels for data collected over a ten-day period during ground calibration. The mean noise levels were found to be repeatable to within 0.1 digital numbers for all bands. Fourteen ALI detectors demonstrating noise differences $> \pm 0.5$ digital numbers are listed in Table 9. All but two of these detectors have been previously flagged as having high dark current or excessive noise values.

The above results indicate the VNIR and panchromatic dark current values and all detector noise levels of the ALI are highly repeatable. However, SWIR dark current levels have shown up to 100 DN variability. It is therefore recommended that dark reference scenes should be used to determine actual dark current and

noise levels at the time of each earth scene such that small day-to-day variations will not add to the uncertainties of the measurements.

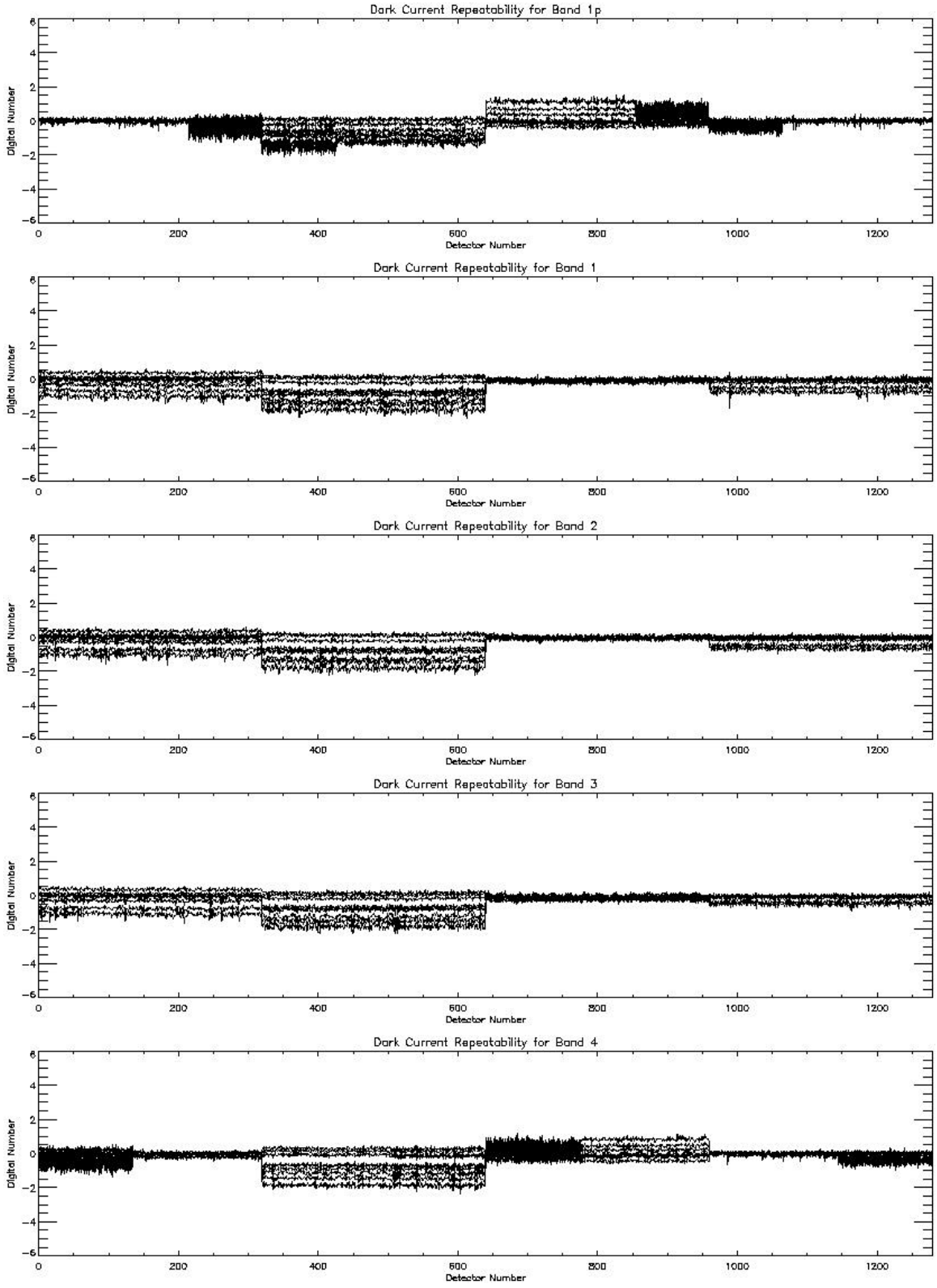

Figure 63: Bands 1p, 1, 2, 3, 4 dark current repeatability at 220 K.

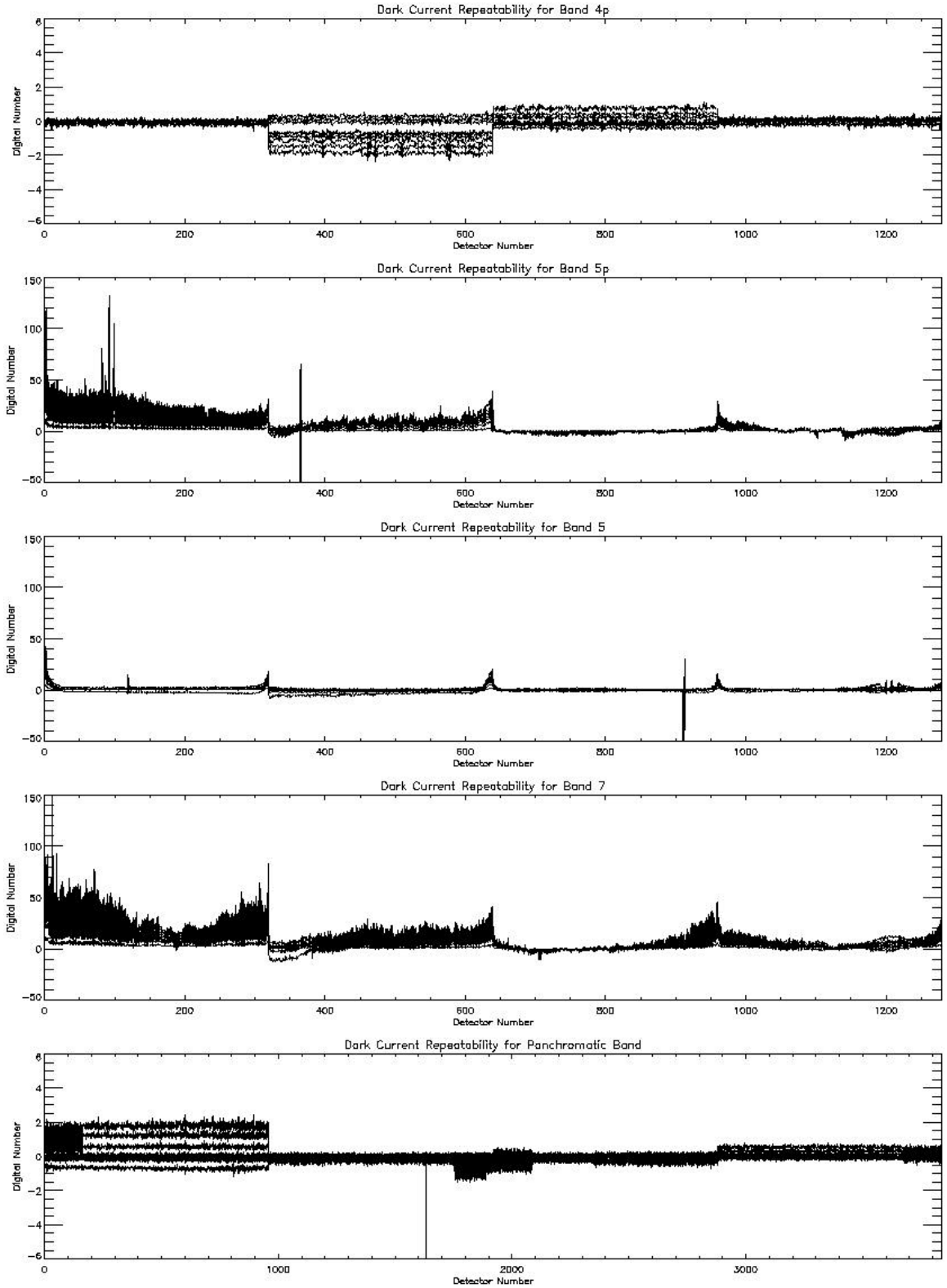

Figure 64: Bands 4p, 5p, 5, 7 and pan band dark current repeatability at 220 K.

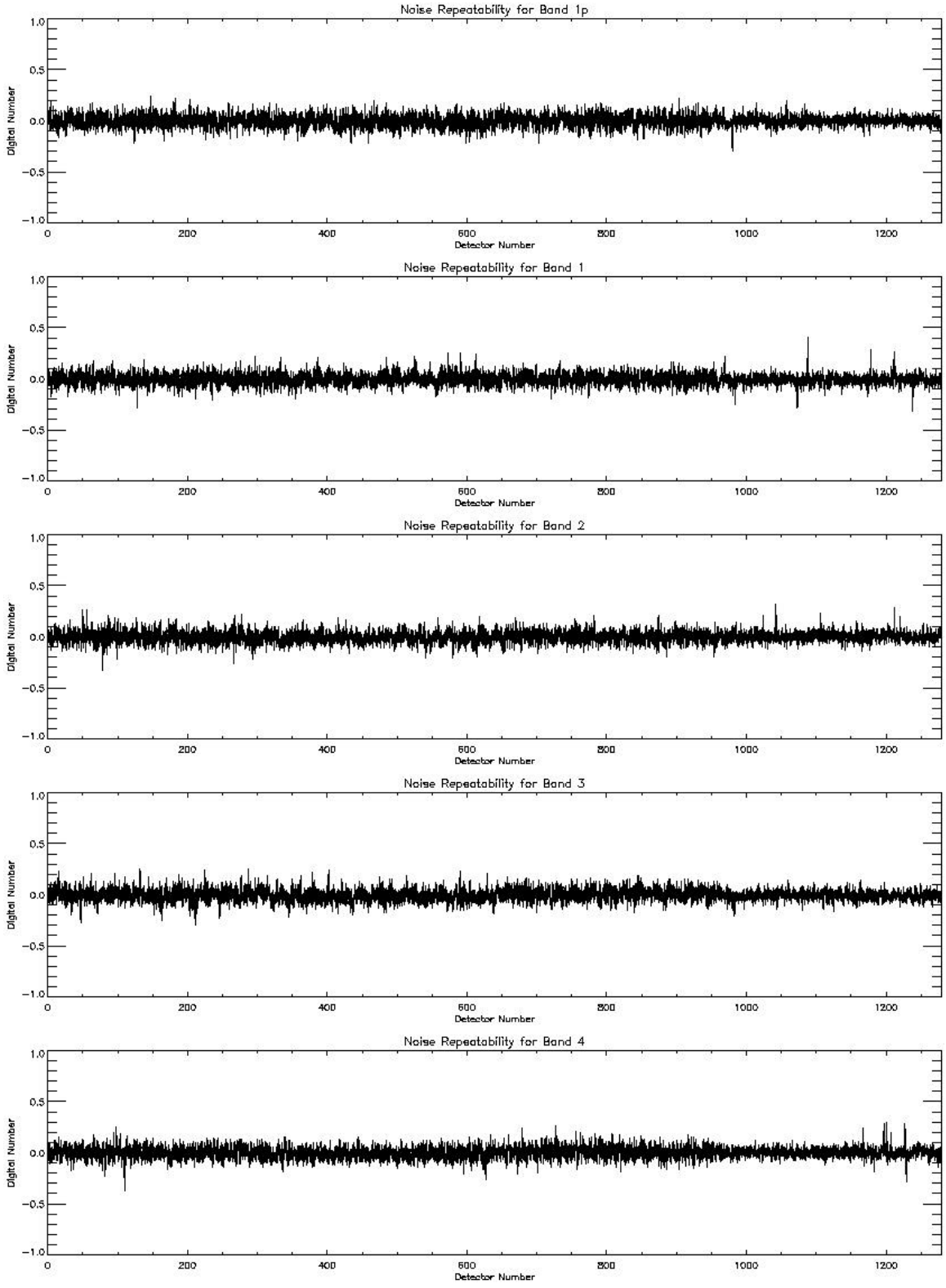

Figure 65: Bands 1p, 1, 2, 3, 4 noise repeatability at 220 K.

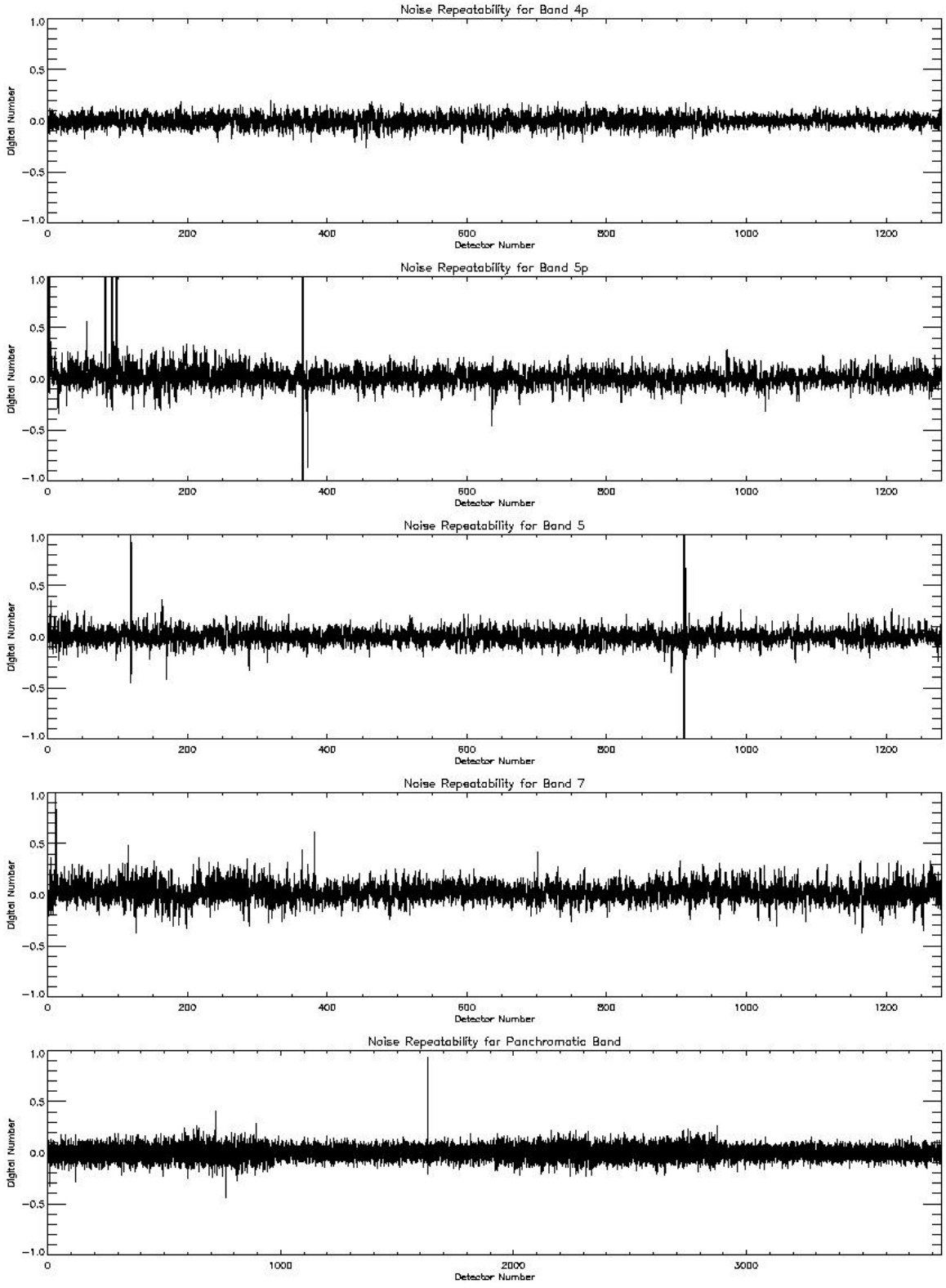

Figure 66: Bands 4p, 5p, 5, 7 and pan band noise repeatability at 220 K.

Table 9: Detectors with Variable Noise Levels at 220 K

Band	Detector	Comment
5p	2	Excess PRF*
5p	56	--
5p	82	Excess PRF, Excess white noise
5p	83	Excess PRF
5p	92	Excess PRF, Excess white noise
5p	99	Excess PRF, Excess white noise
5p	365	Excess dark current, Excess PRF, Excess White Noise
5p	372	Excess PRF, Excess white noise
5	119	Excess PRF
5	911	Excess dark current, Excess PRF, Excess White Noise
5	913	Excess dark current, Excess PRF, Excess White Noise
7	11	Excess PRF, Excess white noise
7	382	Excess PRF, Excess white noise
Pan	1631	Excess white noise

* PSR = Pseudo-Random Fluctuation.

2.4 Dark Current and Noise Characterization Summary

The dark current and noise characteristics for the EO-1 Advanced Land Imager have been characterized. Six inoperable detectors were identified indicating that 99.96% of the ALI focal plane is functional.

All SWIR detectors have a transient effect associated with the initial data collected following the focal plane turn-on. As a result, the first ten frames of the first dark image should be excluded from on-orbit dark current and noise analysis.

Ground calibration data indicate the VNIR and panchromatic dark current values and all detector noise levels of the ALI are highly repeatable. However, SWIR dark current levels have shown significant day-to-day variability. Additionally, the dark current is dependent on focal plane temperature, more particularly for the SWIR bands. It is therefore recommended that concurrent dark reference scenes should be used to determine actual dark current and noise levels at the time of each Earth scene.

The noise levels of the ALI focal plane are excellent (less than 1.2 digital number for the mean of all bands and sensor chip assemblies). Twenty-two detectors were identified as having higher than average noise values. All but one of these were SWIR detectors and were associated with high dark current or pseudo-random noise. The overall noise of the ALI is dominated by white noise with little contribution from coherent or pseudo-random fluctuation components.

Dark current and white noise figures of merit have been discussed and baseline values provided. These figures will be used to track the dark performance of the ALI throughout the EO-1 mission (e.g., the effects of charged particle damage on the detector lattice and focal plane electronics). It is recommended that a single one-minute dark scene be collected once every 14 days to characterize and track the dark current and noise of the Advanced Land Imager. Repeatability may be characterized by assessing the dark scenes obtained with each observation over a two-week period.

3 ANOMALOUS DETECTORS

This section provides a summary listing of all Advanced Land Imager detectors that exhibit anomalous behavior. Anomalous detectors have been selected based on the following criteria:

1. Inoperable detector
2. Excessive dark current
3. Excessive noise
4. Anomalous gain value
5. High cross-talk

Detectors identified for each of the above criteria are listed in subsequent sections. All data used to generate this list were taken with the focal plane at 220 K and the nominal integration times: 1.35 ms for panchromatic detectors and 4.05 ms for multispectral detectors. Some detectors may be listed in several sections (e.g., a high noise detector may be temporally unstable). It must also be noted that although detectors may be marked 'anomalous', most of the characteristics noted in this document are accounted for during instrument calibration. Only the inoperable detectors are definite problems that need to be addressed by nearest neighbor interpolation or other schemes during image reconstruction. However, in the interest of fully understanding the ALI instrument, it is important to list all interesting focal plane array characteristics.

3.1 Classification

3.1.1 Inoperable Detector

An inoperable detector is one that has zero dark current or zero gain ('dead') or is saturated at all times ('hot'). Six ALI detectors have been identified as inoperable and are listed in Table 10.

Table 10: Inoperable Detectors

Band	Detector	Comment
5p	374	HOT
5p	638	HOT
5	982	Gain = 0
5	1202	HOT
5	1204	HOT
5	1206	HOT

3.1.2 Excessive Dark Current

Detectors with dark current values greater than 1.25 times the mean dark current for that band and SCA are flagged as having excessive dark current. Nine ALI detectors have been identified as having excessive dark current and are listed in Table 11.

Table 11: Detectors with Marked Dark Current

Band	Detector	Comment
1	989	--
5p	365	Excess white noise, Excess PRF*
5p	374	Excess white noise, Inoperable
5p	638	Excess white noise, Inoperable
5	911	Excess white noise, Excess PRF
5	913	Excess white noise, Excess PRF
5	1202	Excess white noise, Inoperable
5	1204	Inoperable
5	1206	Excess white noise, Inoperable

* PSR = Pseudo-Random Fluctuation.

3.1.3 Excessive Noise

Detectors with noise values (standard deviation of dark current) greater than three times the mean noise value for that band and sensor chip assembly or detectors with more than 1 DN shift in dark current over a forty-second period have been flagged as having excessive noise. Twenty-two detectors have been noted as having excessive noise by the above criteria and are listed in Table 12. Fifteen ALI detectors have higher than average random (white) noise values, and sixteen ALI detectors have been noted as temporally unstable (low frequency pseudo-random fluctuations or high frequency pseudo-random fluctuations).

Table 12: Detectors with Marked Noise.

Band	Detector	Comment
5p	2	Excess PRF
5p	82	Excess white noise, Excess PRF
5p	83	Excess PRF
5p	92	Excess white noise, Excess PRF
5p	99	Excess white noise, Excess PRF
5p	365	Excess white noise, High dark current, Excess PRF
5p	372	Excess white noise
5p	374	Excess white noise, Inoperable, Excess dark current
5p	636	Excess white noise, Excess PRF
5p	638	Excess white noise, Inoperable, Excess dark current
5	119	Excess PRF
5	911	Excess white noise, Excess dark current, Excess PRF
5	913	Excess white noise, Excess dark current, Excess PRF
5	1202	Excess white noise, Inoperable, Excess dark current
5	1206	Excess white noise, Inoperable, Excess dark current
7	4	Excess PRF

7	11	Excess white noise, Excess PRF
7	17	Excess PRF
7	126	Excess PRF
7	307	Excess PRF
7	382	Excess white noise, Excess PRF
Pan	1631	Excess white noise

3.1.4 Anomalous Gain Value

An anomalous gain value will either lead to lower dynamic range of the detector (early saturation), if too high, or low signal to noise ratios over the range of scene radiances expected, if too low. Four ALI detectors are found to exhibit anomalous gain values and are listed in Table 13.

Table 13: Detectors with Anomalous Gain Values.

Band	Detector	Comment
5p	365	Gain too high
5	911	Gain too high
5	913	Gain too high
5	982	Gain = 0

3.1.5 High Cross-Talk or Leaky Detectors

Detectors with high cross-talk are problematic in that they add signal to adjacent detectors. Correcting for this effect may be difficult, especially for scenes with high spatial frequencies covering a large dynamic range. Two ALI detectors have been identified as being leaky, i.e., having high cross-talk characteristics, and are listed in Table 14.

Table 14: Detectors with Marked Cross Talk

Band	Detector
2	1149
3	864

3.2 Anomalous Detectors Summary

Six inoperable detectors were identified, indicating 99.96% of the ALI focal plane is functional. Twenty-one additional detectors have been observed with degraded performance due to such effects as noted dark current values and/or white, low frequency pseudo-random fluctuation, or high frequency pseudo-random fluctuation noise. The remaining 99.82% of the focal plane have excellent dark current stability and noise characteristics. Finally, a master list of anomalous detectors is provided in Table 15.

Table 15: Master Anomalous Detector List

Band	Detector	Inoperable	Excess Dark Current	Excess Noise		High Cross-Talk	Anomalous Gain
				White	PRF		
1	989		X				
2	1149					X	
3	864					X	
5p	2				X		
5p	82			X	X		
5p	83				X		
5p	92			X	X		
5p	99			X	X		
5p	365		X	X	X		X
5p	372			X			
5p	374	X	X	X			
5p	636			X	X		
5p	638	X	X	X			
5	119				X		
5	911		X	X	X		X
5	913		X	X	X		X
5	982	X					X
5	1202	X	X	X			
5	1204	X	X				
5	1206	X	X	X			
7	4				X		
7	11			X	X		
7	17				X		
7	126				X		
7	307				X		
7	382			X	X		
Pan	1631			X			

REFERENCES

1. J. A. Mendenhall et al., "Earth Observing-1 Advanced Land Imager: Instrument and Flight Operations Overview," MIT/LL Project Report EO-1-1, 23 June 2000.
2. D. E. Lencioni, C. J. Digenis, W. E. Bicknell, D. R. Hearn, J. A. Mendenhall, "Design and Performance of the EO-1 Advanced Land Imager," *SPIE Conference on Sensors, Systems, and Next Generation Satellites III*, Florence, Italy, 20 September 1999.
3. W. E. Bicknell, C. J. Digenis, S. E. Forman, D. E. Lencioni, "EO-1 Advanced Land Imager," *SPIE Conference on Earth Observing Systems IV*, Denver, Colorado, 18 July 1999.
4. C. J. Digenis, D. E. Lencioni, and W. E. Bicknell, "New Millennium EO-1 Advanced Land Imager," *SPIE Conference on Earth Observing Systems III*, San Diego, California, July 1998.
5. D. E. Lencioni and D. R. Hearn, "New Millennium EO-1 Advanced Land Imager," *International Symposium on Spectral Sensing Research*, San Diego, 13-19 December 1997.
6. J. A. Mendenhall, "Earth Observing-1 Advanced Land Imager: Leaky Detector Calibration and Correction," MIT/LL Project Report, in preparation.